THE COMBINED EFFECTS OF FREESTREAM TURBULENCE, PRESSURE GRADIENTS, AND SURFACE ROUGHNESS ON TURBINE AERODYNAMICS

THESIS

Christine P. Ellering, 2nd Lieutenant, USAF

AFIT/GAE/ENY/02-5

DEPARTMENT OF THE AIR FORCE
AIR UNIVERSITY

AIR FORCE INSTITUTE OF TECHNOLOGY

Wright-Patterson Air Force Base, Ohio

Report Documentation Page

Report Date	Report Type	Dates Covered (from... to)
26 Mar 02	Final	Aug 2000 - Mar 2002

Title and Subtitle The Combined Effects of Freestream Turbulence, Pressure Gradients, and Surface Roughness on Turbine Aerodynamics	**Contract Number**
	Grant Number
	Program Element Number
Author(s) 2nd Lt Christine P. Ellering, USAF	**Project Number**
	Task Number
	Work Unit Number
Performing Organization Name(s) and Address(es) Air Force Institute of Technology Graduate School of Engineering and Management (AFIT/EN) 2950 P Street, Bldg 640 WPAFB, OH 45433-7765	**Performing Organization Report Number** AFIT/GAE/ENY/02-5
Sponsoring/Monitoring Agency Name(s) and Address(es) Dr. Richard A. Wenglarz Department of Energy South Carolina Institute for Energy Studies (SCIES) Advanced Gas turbine Systems Research 386-2 College Ave. Clemson, SC 29634-5711	**Sponsor/Monitor's Acronym(s)**
	Sponsor/Monitor's Report Number(s)

Distribution/Availability Statement
Approved for public release, distribution unlimited

Supplementary Notes
The original document contains color images.

Abstract
This work used scaled facsimiles of real turbine blade surfaces to characterize correlations between turbine blade roughness, freestream turbulence, pressure gradients and skin friction (Cf). Addition of roughness caused Cf to increase: up to 300% for the roughest surface. Addition of freestream turbulence resulted in 125% increase for the same surface. The combined effects showed increases up to 380%. Although decreasing roughness, freestream turbulence, and Reynolds number resulted in less dramatic results, it was concluded that the Cf increases due to combined effects were consistently higher than their corresponding sum of the parts. The combined effects of roughness and pressure gradients yielded inconclusive results, however, limited observations seem to corroborate the trends seen during zero pressure gradient tests.

Subject Terms
Skin Friction, Roughness, Freestream Turbulence, Pressure Gradients, Bulk Drag, Heat Transfer

Report Classification unclassified	**Classification of this page** unclassified
Classification of Abstract unclassified	**Limitation of Abstract** UU
Number of Pages 99	

The views expressed in this thesis are those of the author and do not reflect the official policy or position of the Unites States Air Force, Department of Defense, or the U.S. Government.

AFIT/GAE/ENY/02-5

THE COMBINED EFFECTS OF FREESTREAM TURBULENCE, PRESSURE GRADIENTS, AND SURFACE ROUGHNESS ON TURBINE AERODYNAMICS

THESIS

Presented to the Faculty

Department of Aeronautics and Astronautics

Graduate School of Engineering and Management

Air Force Institute of Technology

Air University

Air Education and Training Command

in Partial Fulfillment of the Requirements for the

Degree of Master of Science in Aeronautical Engineering

Christine P. Ellering, BS

2nd Lieutenant, USAF

March 2002

AFIT/GAE/ENY/02-5

THE COMBINED EFFECTS OF FREESTREAM TURBULENCE, PRESSURE GRADIENTS, AND SURFACE ROUGHNESS ON TURBINE AERODYNAMICS

Christine P. Ellering, BS

2nd Lieutenant, USAF

Approved:

Jeffrey P. Bons (Chairman)	12 MAR 02 date
Milton E. Franke (Member)	12 Mar 2002 date
Paul I. King (Member)	12 Mar 02 date

Acknowledgments

I would like to extend my sincere gratitude to my thesis advisor, Major Jeffrey Bons, for his dedication to this project. Without his knowledge and expertise, this research project would have certainly proven more difficult. I would also like to thank Drs. Schichuan Ou and Richard Rivir for their vast generosity. Not only did they allow me to use the AFRL Propulsion Laboratory, they often times put their own research aside to assist me. A big thanks also goes to Captain Jess Drab. Without all of his hard work and dedication my thesis would not have been possible. I would also like to thank Russ Hastings, Andy Pitts, and Bill Nillson for the manufacturing and maintenance all of my testing apparatuses.

To my mom and dad, once again, without your incredible love and support I wouldn't be were I am today. Matt, your patience and understanding is truly unique. You are a blessing in my life and for that I am truly grateful. Lastly, but certainly not least, I would also like to thank the Suwalski family. Though you may not realize it, having a "family" nearby really does make life better.

Christine P. Ellering

Table of Contents

Page

List of Figures

Page

List of Tables

List of Symbols

A	area
B	constant ≈5.0
C_f	skin friction coefficient
F	force
H	momentum shape factor
Ku	kurtosis
k_s	sandgrain roughness height
L	length of trace
N	number of elements along a trace
P	pressure
R_a	average centerline roughness
Re	Reynolds number
R_q	root-mean-square roughness
R_t	maximum peak-to-height roughness
Sk	skewness
T	time interval
t	time
Tu	freestream turbulence
u,U	streamwise velocity component
υ	vertical velocity component
x	streamwise rectangular coordinate
y	deviation from mean height, vertical rectangular coordinate

Greek Symbols

β	Clauser parameter
δ	boundary layer thickness
δ*	displacement thickness
Π	Coles wake parameter
θ	momentum thickness
κ	von Karman constant ≈0.41
λ	Thwaites dimensionless parameter
ν	kinematic viscosity
μ	dynamic viscosity
ρ	density
τ	shear stress
υ*	wall-friction velocity

Superscripts

*	dimensionless quantity
+	inner variables
‘	fluctuations

Subscripts

w	wall
∞	freestream conditions
x	local conditions
δ	boundary layer
rms	root-mean-square
θ	momentum thickness
o	initial conditions
i	i^{th} element

Miscellaneous

$\bar{}$	average conditions

Abstract

A significant amount of research has been aimed toward turbine blade surface roughness, freestream turbulence, and pressure gradients and their associated efficiency losses. Typically, roughness studies use artificially created surfaces that are easily characterized by statistical parameters such as average centerline roughness, R_a, which is, in turn, often correlated to the well-defined equivalent sandgrain roughness, k_s. This research differs in that it uses scaled facsimiles of real turbine blade surfaces to characterize correlations between blade roughness, with the combined effects of freestream turbulence and pressure gradients, and skin friction coefficient (C_f). The models tested yielded R_a values ranging from 0.1 to 1.2 mm and were representative of eroded, fuel deposited, pitted, and thermal barrier coated (TBC) surfaces with spallation. For the eroded surfaces, the addition of roughness caused C_f increases up to 300% when compared to flat plate data. Addition of freestream turbulence caused increases up to 125%. The combined effects of roughness and turbulence yielded increases up to 380%. This is 55% larger than simply summing the two independent effects. Though other surfaces typically offered less dramatic results, it was concluded that the C_f increases due to combined effects were consistently higher than the corresponding sum of the parts. The results presented for the combined effects of roughness and pressure gradients were inconclusive due to errors in measurement. However, limited observations seem to corroborate the trends seen with zero pressure gradient.

THE COMBINED EFFECTS OF FREESTREAM TURBULENCE, PRESSURE GRADIENTS, AND SURFACE ROUGHNESS ON TURBINE AERODYNAMICS

I. Introduction

1.1 Background

When considering aerodynamic applications, such as turbomachinery, the reduction of skin friction drag (C_f) is of utmost importance. Consequently, factors such as surface roughness, freestream turbulence, and pressure gradients also find themselves playing a prevailing role as they ultimately dictate C_f and, in turn, a turbine's efficiency. Although the study of these factors has not fallen by the wayside over the past several decades of aerodynamic research, recent advances in turbine technology are now demanding more sophisticated and up-to-date means of analyzing and predicting surface drag.

A significant amount of research has been done on surface roughness, with the majority of it focusing on sandgrain roughness. But often times, the multifarious surfaces of a turbine blade cannot be successfully quantified by a single parameter, such as an equivalent sandgrain roughness. This, in turn, leaves the prospect of developing a correlation that does not involve the use of equivalent sandgrain roughness (Acharya, 1986:34-35).

In addition to surface roughness, freestream turbulence and pressure gradients also play a dominant role in turbine environments but, historically, the combined effect of these features with turbine roughness has been overlooked. Often times, freestream turbulence is seen as a complicating factor instead of a natural accompaniment to these turbomachinery systems. Because of this mindset, most experimental roughness research has been performed at low turbulence levels. As a result, low turbulence flow fields have set all the benchmarks in this area, while current gas turbine engines continue to run at up to 20-30% turbulence levels (Maciejewski, 1992:827).

1.2 Importance of Research

This project was designed to examine both the individual and combined effects of freestream turbulence, pressure gradients, and surface roughness on skin friction drag. Though much research has been done on surface roughness, the efforts have primarily focused on analytic correlations or artificial approximations of the blade surface. While the areas of pressure gradients and freestream turbulence have also undergone extensive research, their focus has primarily involved flat plate studies. This research deviates from past efforts in that it considers combinations of roughness, freestream turbulence, and pressure gradients. Additionally, the surfaces at hand are not the usual approximated roughness, but instead a scaled facsimile of actual turbine blade surfaces. Consequently, this research proves to be a vanguard to providing a better

understanding of the complex environment seen by an in-service turbine blade section.

1.3 Research Objectives

The objective of this research is to perform experiments that will yield results relating surface roughness, pressure gradients, and freestream turbulence to skin friction characteristics. The individual results will first be compared to other experimental results and then to empirical correlations. The combined effects of the aforementioned properties will then be studied.

1.4 Thesis Overview

This thesis is organized in a manner that will first provide the reader with insight of the topics at hand, then explain the methodology, and end in an analysis of the experimental results. The Theory chapter divulges the mathematical foundation behind each topic as the equations used for the data processing are derived. This provides great insight into what type of conditions the turbine blades may encounter. This chapter also includes a section on statistical parameters and how they can be applied to the surfaces being tested. Chapter 3 describes the method and materials employed during the testing process and guides the reader through the testing progression detailing the apparatuses used along the way. The experimental data and discussion is found in Chapter 4. This chapter provides the results obtained during testing and compares them to previously established analytic and empirical correlations.

Finally, Chapter 5 summarizes with significant conclusions and recommendations for future research in this area.

II. Theory

2.1 Surface Roughness Statistics

As previously noted, the surface roughness of real turbine blades can vary significantly. Because of this variation, it is both necessary and helpful to develop an analogous relationship between differing surfaces. In order to do so, several statistical parameters can be applied to characterize each surface. Some of the more common parameters used to describe surface roughness are average centerline roughness, R_a, root-mean-square roughness, R_q, and maximum peak-to-height roughness, R_t. Additional parameters may include surface skewness, Sk, and kurtosis, Ku.

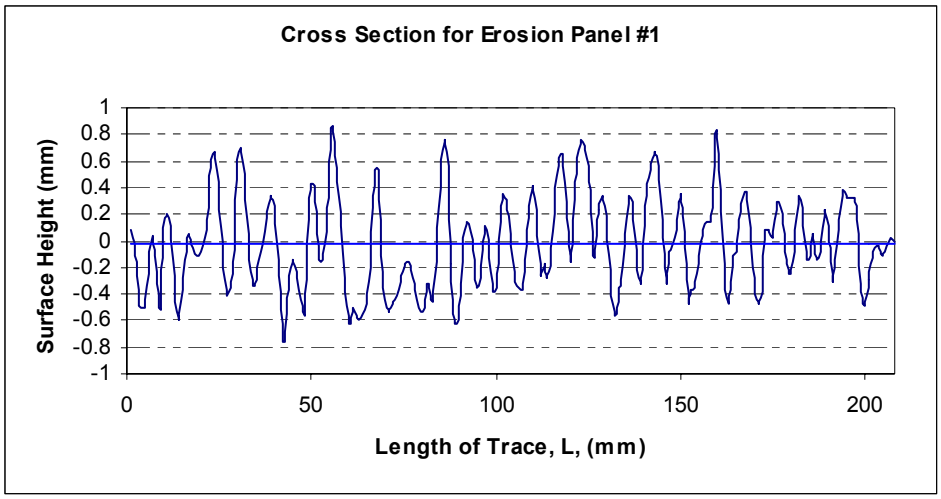

Figure 2.1 Roughness Trace from Erosion Panel #1

Average centerline roughness is typically used to describe machined surfaces (Bennett, 1989:39). It is measured along a line of length L, as shown in Figure 2.1, and is defined as the mean surface level such that equal areas of

surface lie above and below it. The mean surface level can mathematically be written as:

$$\sum_{i=1}^{N} y_i = 0 \tag{1}$$

Where N is the number of elements measured along the trace length L.

R_a is the measure of the variability in a given set of data and provides one with the average of the absolute deviations of the surface heights from their mean. R_a is mathematically given by:

$$R_a = \frac{1}{N}\sum_{i=1}^{N}|y_i| \tag{2}$$

The root-mean-square roughness is the most important statistical parameter and is typically used to describe the finish of optical surfaces (Bennett, 1989:38-39). It is defined as the square root of the average of the squares of the surface heights from their mean surface level and can be written as:

$$R_q = \sqrt{\frac{1}{N}\sum_{i=1}^{N} y_i^2} \tag{3}$$

Rms roughness, like R_a, is also measured along the trace length L, but is additionally dependent upon the surface area of the measurement and the distance between the elements. Consequently, there is no specific rms value for a given surface (Bennett, 1989:38).

For surfaces composed of small, consistent roughness elements, R_a and R_q will be very similar. Conversely, if the surface has a significant number of

large peaks or valleys, the second order terms in R_q dictate the calculation and R_q becomes larger than R_a (Bennett, 1989:39).

The maximum peak-to-height roughness, R_t, is simply that, a measure of the total size of the elements. It is mathematically written as:

$$R_t = y_{max} - y_{min} \tag{4}$$

where y_{max} is the largest positive deviation from the mean centerline and y_{min} is the largest negative deviation from the mean centerline.

Skewness, Sk, is a characterization of the degree of asymmetry of a surface about its mean centerline and is written as:

$$Sk = \frac{1}{R_q^3}\left[\frac{1}{N}\sum_{i=1}^{N} y_i^3\right] \tag{5}$$

The sign of skewness relates whether the deviations generally lie above or below the mean centerline. Thus, bumps on a surface will result in a positive skewness and pits or holes in the surface will, conversely, result in a negative skewness. It is also noteworthy that skewness, like rms, is greatly governed by its higher order term. As a result, Sk is more sensitive to deviations that lie farther from the mean centerline (Bennett, 1989:43).

Kurtosis is defined as the relative peakedness or flatness of a distribution compared with its normal distribution. A large kurtosis is representative of peaked distributions while a small kurtosis indicates a relatively flat distribution (Bennett, 1989:43). Kurtosis is defined as:

$$Ku = \frac{1}{R_q^4}\left[\frac{1}{N}\sum_{i=1}^{N} y_i^4\right] \tag{6}$$

2.2 The Velocity Boundary Layer

To introduce the concept of boundary layers, consider flow over the flat plate of Figure 2.2.

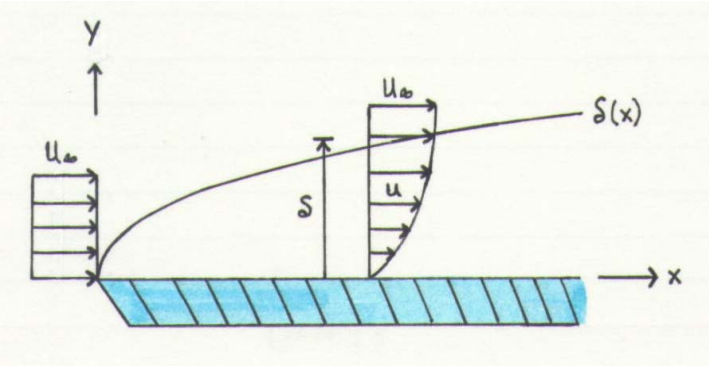

Figure 2.2 Boundary Layer Development Over a Flat Plate

As fluid particles come in contact with the surface of the plates, the viscous forces at hand cause them to assume zero velocity. These particles, in turn, slow the velocity of the particles in the adjoining layer. This process continues until, at a distance y=δ, the effect becomes negligible. This quantity, δ, is known as the boundary layer thickness and is defined as having a y value for which u=0.99u_∞. The symbol ∞ is used to designate conditions outside the boundary layer, otherwise known as the freestream.

The slowing of this fluid motion is of great significance because of its relationship with the wall shear stress, τ_w. The shear stress at the surface can then be used to determine the local skin friction coefficient:

$$C_f = \frac{\tau_w}{\frac{1}{2}\rho U_\infty^2} \tag{7}$$

where ρ is the fluid density and U_∞ is the freestream velocity.

The slowing of this fluid motion also results in a velocity gradient that transfers momentum through the fluid between the top and the bottom of the boundary layer. Shear stress is proportional to this velocity gradient and accounts for the fluid's dynamic viscosity, μ, or the fluid's ability to resist flow. Thus the shear stress may be evaluated from the velocity gradient at the wall by:

$$\tau_w = \mu \frac{d\bar{u}}{dy}\Big|_{y=0} \tag{8}$$

Solving Equation (7) for τ_w and setting it equal to Equation (8) yields:

$$\frac{c_f}{2}\frac{\rho U_\infty^2}{\mu} = \frac{d\bar{u}}{dy}\Big|_{y=0} \tag{9}$$

which directly relates the skin friction coefficient to the velocity gradient at the surface.

There are two types of boundary layers, laminar and turbulent, and it is crucial to determine which boundary layer is being dealt with as surface friction is strongly dependent on which condition exists. As shown in Figure 2.3 there are vast differences between the laminar and turbulent regions.

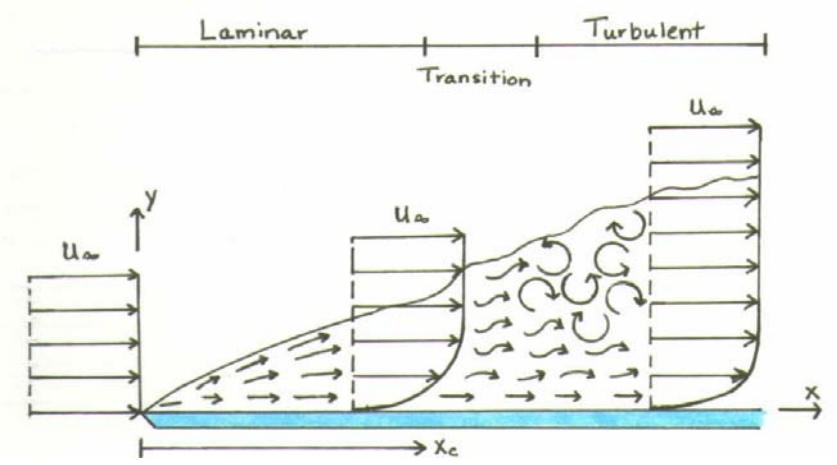

Figure 2.3 Boundary Layer Transition

The boundary layer is initially laminar. The fluid motion is well ordered and it is possible to identify streamlines, or lines along which constant velocity exist. At some distance from the leading edge, small disturbances become amplified and transition to turbulent flow begins. Eventually the boundary layer becomes fully turbulent. In this region, the boundary layer is highly irregular and is characterized by velocity fluctuations. It is these fluctuations that increase the transfer of momentum and energy and result in a significant increase in boundary layer thickness and, in turn, an increase surface friction.

As mentioned above, transition begins at some distance, x, from the leading edge of the surface in question. This location is dependent on the common non-dimensional flow parameter called Reynolds number which is written as:

$$\mathrm{Re}_x = \frac{\rho U_\infty x}{\mu} \tag{10}$$

Reynolds number, which defines the ratio of inertial to viscous forces can further be broken down as such:

$$\rho U_\infty \frac{\partial U_\infty}{\partial x} \tag{11}$$

$$\mu \frac{\partial^2 U_\infty}{\partial x^2} \tag{12}$$

Expressions (11) and (12) have units of force/volume and are representative of the inertial and viscous force terms found in the incompressible form of the Navier-Stokes equations. It is noteworthy that the ratio μ/ρ, also known as the kinematic viscosity, ν, is sometimes used in Equation (10) in place of ρ and μ.

Reynolds numbers having values greater than $1x10^6$, for a smooth plate with zero pressure gradient, generally indicate fully turbulent flow for external flow. The same is true for Reynolds numbers reaching 2,000 for pipe flow, where Re is based on the pipe diameter. "In-service turbine blades typically operate in flow with $1x10^6<Re_x<5x10^6$, depending upon blade size and rotational speed" (Drab: 2000,13). The panels used in the research for this thesis were thus subjected to a turbulent boundary layer.

A direct relationship between Re_x and C_f can now be established by substituting Equation (10) into Equation (9) and non-dimensionalizing to obtain:

$$\frac{c_{f_x}}{2}\mathrm{Re}_x = \frac{du^*}{dy^*}\Big|_{y^*=0} \qquad (13)$$

The dimensionless height and velocity used are defined as $y^* = y/x$ and $u^* = u/U_\infty$. With this equation it is now possible to determine a skin friction coefficient based solely on the velocity gradient and Reynolds number.

While a simple velocity profile would provide all the necessary information to calculate C_f, this method may, however, prove to be quite tedious. In order to obtain an accurate depiction of a large asymmetric surface, a vast number of velocity profiles would need to be taken. Moreover, obtaining an accurate reading at the wall would prove difficult even for the smallest of instruments (Drab, 2000:14). Fortunately, another method exists through the momentum integral relationship.

In addition to Reynolds number, surface roughness, turbulence levels, and pressure gradients can also affect transition. "The introduction of a roughness or

projection at the wall will generally cause earlier transition, because of the additional disturbances it feeds into the boundary layer" (White, 1991:385). In order to ensure fully turbulent flow, a trip wire was placed near the leading edge of the wind tunnel used in this study. Increasing the freestream turbulence levels by means of grids or jets will also result in earlier transition and thus a fuller velocity profile.

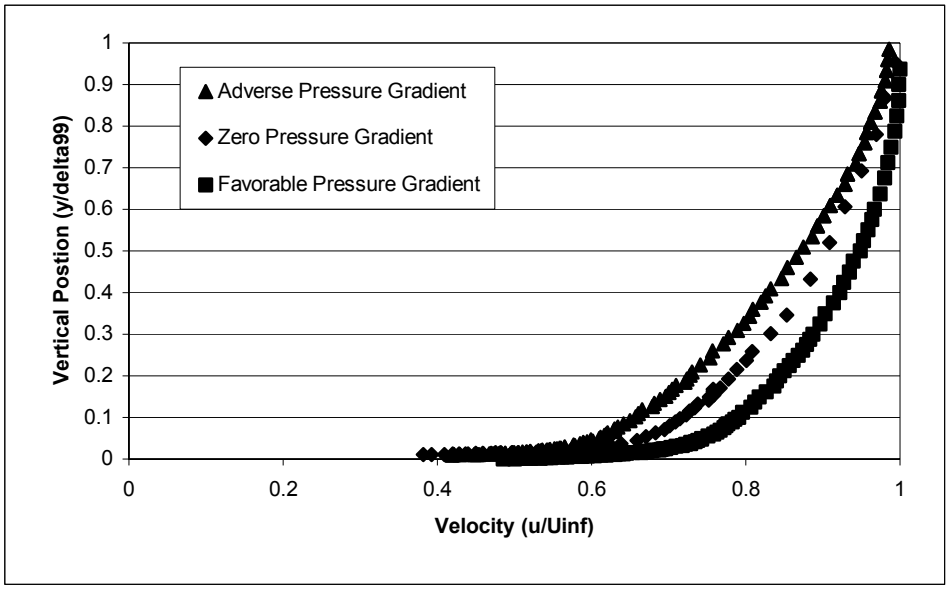

Figure 2.4 Velocity Profiles at Various Pressure Gradients

When a pressure gradient is introduced, the streamwise velocity varies with respect to x. For a favorable pressure gradient, freestream velocity increases along the streamwise direction and in turn causes the boundary layer to develop more rapidly. The opposite holds true for an adverse pressure gradient. An example is shown in Figure 2.4. The mathematics behind this theory will be presented in Section 2.5.

2.3 Boundary Layer Integral Method

Many flowfields, such as those found in a turbine, can be difficult to accurately characterize. But applying one or two very basic assumptions allows these complex flowfields to move into territory that is possible to study. Though these assumptions may sometimes oversimplify the typical turbine flowfield, they do, in turn, make mathematical representation easier. Additionally, these simplified equations provide for a wider range of application. Take the turbine flowfield for example. Assuming the flow to be two dimensional, incompressible, and steady, the boundary layer over the turbine can be represented by a simplified form of the continuity equation:

$$\frac{\partial \bar{u}}{\partial x} + \frac{\partial \bar{\upsilon}}{\partial y} = 0 \tag{14}$$

where x is the streamwise direction and y is the direction perpendicular to the surface, and u and υ are the respective mean velocities. Assuming a thin boundary layer, where $\partial/\partial x << \partial/\partial y$, the x-direction momentum equation:

$$\frac{\partial \bar{u}}{\partial t} + \bar{u}\frac{\partial \bar{u}}{\partial x} + \bar{\upsilon}\frac{\partial \bar{u}}{\partial y} = \left(\frac{\partial U_\infty}{\partial t} + U_\infty \frac{\partial U_\infty}{\partial x} \right) + \frac{1}{\rho}\frac{\partial \tau}{\partial y} \tag{15}$$

can be written as:

$$\bar{u}\frac{\partial \bar{u}}{\partial x} + \bar{\upsilon}\frac{\partial \bar{u}}{\partial y} = U_\infty \frac{dU_\infty}{dx} + \frac{1}{\rho}\frac{\partial \tau}{\partial y} \tag{16}$$

assuming steady flow conditions. τ in this case represents shear stress, thus making the above equation valid for turbulent flow (White, 1991:265). In order to obtain the momentum integral relation, the continuity equation is multiplied by u –

U_∞ and subtracted from the momentum Equation (16). The result is then integrated from the wall to infinity and is written as:

$$\frac{\tau_w}{\rho} = \frac{\partial}{\partial x}\int_0^\infty u(U_\infty - u)dy + \frac{\partial U_\infty}{\partial x}\int_0^\infty (U_\infty - u)dy - U_\infty v_w \tag{17}$$

This is the most general form of the momentum integral relation and is often called the Karman integral relation after T. von Karman who first developed this method in 1921 (White, 1991:265). When the integrals of $U_\infty - u$ and $u(U_\infty - u)$, the displacement and momentum thickness respectively, are substituted and the equation is divided through by U_∞^2, the momentum integral relation can be written as:

$$\frac{\tau_w}{\rho U_\infty^2} = \frac{C_f}{2} = \frac{\partial \theta}{\partial x} + (2\theta + \delta^*)\frac{1}{U_\infty}\frac{\partial U_\infty}{\partial x} - \frac{v_w}{U_\infty} \tag{18}$$

Assuming an impermeable wall, the equation can then be written as:

$$\frac{\tau_w}{\rho U_\infty^2} = \frac{C_f}{2} = \frac{d\theta}{dx} + (2 + H)\frac{\theta}{U_\infty}\frac{dU_\infty}{dx} \tag{19}$$

where:

$$\text{Momentum thickness} = \theta = \int_0^\infty \frac{u}{U_\infty}(1 - \frac{u}{U_\infty})dy \tag{20}$$

$$\text{Momentum shape factor} = H = \frac{\delta^*}{\theta} \tag{21}$$

$$\text{Displacement thickness} = \delta^* = \int_0^\infty (1 - \frac{u}{U_\infty})dy \tag{22}$$

This equation ultimately contains only three variables, θ, H, and C_{fc}, which for laminar flow can be solved without difficulty. But for turbulent flow, which is what

a real turbine typically experiences, the solution is much more difficult. As a result, there are many different correlations that have been proposed as plausible solutions to the above equation.

Although a true turbine environment experiences various pressure gradients, the effects of such will be discussed in Section 2.5. For now, consider flow having zero pressure gradient. The above momentum integral relation then simplifies to:

$$C_f = 2\frac{d\theta}{dx} \tag{23}$$

Having assumed a zero pressure gradient, it is substantiated that equilibrium flow exists. As a result, the velocity profile can be approximated by Coles wall-wake law (White, 1991:417-419):

$$u^+ = \frac{1}{\kappa}\ln(y^+) + B + \frac{2\Pi}{\kappa} f(\frac{y}{\delta}) \tag{24}$$

where κ and B are near-universal constants for turbulent flow past smooth, impermeable walls. u^+ and y^+ are inner variables defined as $u^+ = \bar{u}/\upsilon*$ and $y^+ = y\upsilon*/\nu$. The wall-friction velocity, $\upsilon*$, has units equivalent to velocity and is defined as $\upsilon* = \left(\frac{\tau_w}{\rho}\right)^{1/2}$ (White, 1991:412). Π is Coles wake parameter and is assigned a constant value of Π=0.45 for zero pressure gradient equilibrium flow (White, 1991:429). $f(y/\delta)$ is the wake function [$\approx \sin^2\left(\frac{\pi}{2}\frac{y}{\delta}\right)$] and is normalized

to equal zero at the wall and unity at the boundary layer edge. Evaluation of the wall-wake law at y=δ provides a friction relation between C_f and Re_δ of:

$$\left(\frac{2}{C_f}\right)^{1/2} = 2.44\left[\mathrm{Re}_\delta\left(\frac{C_f}{2}\right)^{1/2}\right] + 7.2 \tag{25}$$

Because the complex algebra involved in obtaining C_f as a function of Re_δ, White proposes the following power-law curve-fit from this empirical relation:

$$C_f \approx 0.020\,\mathrm{Re}_\delta^{-1/6} \tag{26}$$

using Prandtl's suggested relation of:

$$\mathrm{Re}_\delta \approx 0.16\,\mathrm{Re}_x^{6/7} \tag{27}$$

a direct relation between skin friction and Reynolds number was established:

$$C_f = 0.027\,\mathrm{Re}_x^{-1/7} \tag{28}$$

This simple power-law expression has been experimentally verified with turbulent flow, flat-plate data and is highly recommended by White for general use (White, 1991:430). It will additionally serve as a foundation to which the experimental data at hand will be compared. Mills' C_f-Re equation will also be used for comparison and is written as (Mills, 1992:429):

$$C_f = 0.026\,\mathrm{Re}_x^{-1/7} \tag{29}$$

Although the aforementioned method has proven to be reliable, another was suggested in 1962 by Kestin and Persen (White, 1991:430). In this method, it was assumed that the streamwise velocity in the boundary layer could be

correlated by inner variables u^+ and y^+ defined above. Then, by simple integration of the continuity equation, the normal velocity is obtained:

$$\bar{\upsilon} = -\frac{\nu}{\upsilon^*}\frac{d\upsilon^*}{dx}u^+ y^+ \tag{30}$$

Assuming $dU_\infty/dx=0$, these velocity assumptions were substituted into the momentum equation to yield:

$$\bar{u}\frac{\partial \bar{u}}{\partial x} + \bar{\upsilon}\frac{\partial \bar{u}}{\partial y} = \frac{1}{\rho}\frac{\partial \tau}{\partial y} \tag{31}$$

which can be expressed explicitly in terms of inner variables as:

$$\upsilon^*\frac{d\upsilon^*}{dx}u^{+^2} \approx \frac{\upsilon^*}{\mu}\frac{\partial \tau}{\partial y^+} \tag{32}$$

This equation can then be integrated across the boundary layer from $y^+=0\rightarrow\delta^+$ to yield a first-order differential equation for the distribution of the wall-friction velocity, υ^* or, equivalently, τ_w:

$$\tau_w = \rho\upsilon^{*^2} = -\mu\frac{d\upsilon^*}{dx}G(\lambda) \tag{33}$$

where $G = \int_0^{\delta^+} u^{+^2} dy^+$. Upon substitution of Thwaites dimensionless parameter, $\lambda=U_\infty/\nu^*$, the result can again be integrated to produce:

$$\frac{U_\infty}{\nu} = G(\lambda)\frac{d\lambda}{dx} \tag{34}$$

which can be related to Re_x by simply introducing a multiplicative factor of x. While integration of this is somewhat complex, its result is very accurate.

Fortunately, in 1969, White noted that G, if kept within range, was well approximated by the exponential:

$$G(\lambda) = 8.0e^{0.48\lambda} \tag{35}$$

This exponential, when introduced into Equation (34) and integrated, yielded the following formula for a flat plate:

$$C_f = \frac{0.455}{\ln^2(0.06\,\mathrm{Re}_x)} \tag{36}$$

This simpler expression is reported to be within $\pm 1\%$ of Kestin and Perstin's complex integral, and is essentially suggested as an "exact" relation for flat-plate turbulent skin friction (White, 1991:432). This relation, in addition to Equations (28) and (29), will also serve as a basis for data comparison.

2.4 Turbulence Effects

It was stated earlier that turbulent flow is inherently unsteady and can be characterized by the existence of random fluctuations. In fact, White characterizes turbulence as "a spatially varying mean flow with superimposed three-dimensional random fluctuations which are self-sustaining and enhance mixing, diffusion, entrainment, and dissipation: (White, 1991:396). Though this statement seems overly complex, it is, in fact, ironically will suited for the complexity of turbulent flow. Also, it is because of this, that complete analysis and quantification of turbulent flow will most likely never be achieved (White, 1991:394).

Although turbulence is admittedly unpredictable in theory, its statistical properties are supposedly thought reproducible (Mathieu, 2000:10). Thus it would be advantageous to consider practical modeling ideas for given mean statistical properties of turbulent flow. Take for example the trace, taken by a hotwire, of velocity fluctuations with time.

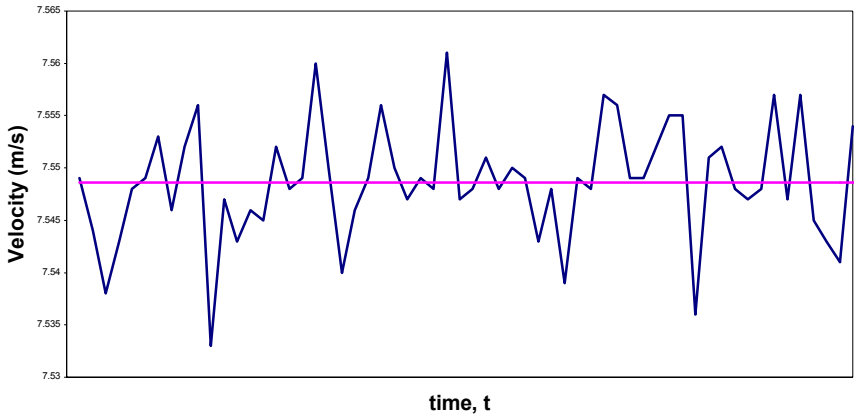

Figure 2.5 Turbulent Velocity Fluctuations Over Time

If this trace represents the velocity, u(t), at a given location, then the time average of u, or the mean flow velocity, is defined as:

$$\bar{u} = \frac{1}{T}\int_{t_0}^{t_o+T} u dt \tag{37}$$

where T is a time interval that is larger than any significant period of the fluctuations in velocity (White, 1991:398). It is then possible to define the actual velocity fluctuation, u', as:

$$u' = u - \bar{u} \tag{38}$$

In order to characterize the magnitude of the fluctuations its mean-square value is implemented:

$$\overline{u'^2} = \frac{1}{T}\int_{t_o}^{t_o+T} u'^2\, dt \tag{39}$$

This, thereby, defines the root-mean-square value of u' as:

$$u'_{rms} = \left(\overline{u'^2}\right)^{1/2} \tag{40}$$

This value, in turn, is used to calculate the turbulence intensity of the flow. Although turbulent fluctuations occur in all directions, it is assumed that both υ' and w' can be neglected (White, 1991:399; Schlichting, 1979:475). The resulting equation is often specified as a percentage and is mathematically written as:

$$Tu = \frac{u'_{rms}}{U_\infty} \tag{41}$$

2.5 Pressure Gradient Effects

Again, consider the flow over a turbine section. More specifically, consider the flow over a single turbine blade. Unlike flow over a flat plate, a turbine blade has varying pressure gradients along its surface. Because of this, it is necessary to investigate the effects of pressure gradients on skin friction drag.

A variety of methods have been developed to investigate the effects of pressure gradients on turbulent boundary layers. One such method is an extension of the previously noted Karman integral relation. Like before, this integral method is one in which ordinary differential equations are averaged across the boundary layer (White, 1991:449). Beginning, again, with the integral momentum equation:

$$\frac{\tau_w}{\rho U_\infty^2} = \frac{C_f}{2} = \frac{d\theta}{dx} + (2+H)\frac{\theta}{U_\infty}\frac{dU_\infty}{dx} \tag{42}$$

Assuming $U_\infty(x)$ is known, the equation is left with the three unknowns θ, H, and C_f. In order to solve this equation additional equations are needed. One such equation is provided by Coles wall-wake law:

$$\lambda = \frac{2 + 3.179\Pi + 1.5\Pi^2}{\kappa(1+\Pi)}\frac{H}{H+1} \tag{43}$$

$$\mathrm{Re}_\theta = \frac{1+\Pi}{\kappa H}^{(k\lambda - kB - 2\Pi)} \tag{44}$$

where λ, H, Π, κ, B are as defined in Equations (34), (21), and (24) respectively. If these equations are manipulated such that Π is eliminated, a relation between C_f, H, and $Re\theta$ can be obtained. White approximates this with an explicit relation for C_f (H, Re_θ) that is within $\pm$3% of the exact expression over a practical range of C_f.

$$C_f = \frac{0.3e^{-1.33H}}{(\log_{10}\mathrm{Re}_\theta)^{1.74+0.31H}} \tag{45}$$

In an effort to complete the method, an approximate correlation between Coles wake parameter Π and the Clauser parameter β is used: The correlation is:

$$\beta = -0.4 + 0.76\Pi + 0.42\Pi^2 \tag{46}$$

This correlation, as stated by White, is often the desired “third relation”, but it results in additional relationships between Π and β and C_f, H, and $Re\theta$ (White, 1991:451). The resulting solution now becomes this: Π is related to C_f and H by Equation (43) and β is found by its definition:

$$\beta = \frac{\delta^*}{\tau_w}\frac{dp_\infty}{dx} = -\lambda^2 H \frac{\theta}{U_\infty}\frac{dU_\infty}{dx} \tag{47}$$

With the above equations it is now possible to calculate C_f for a given pressure gradient. Predictions for both the favorable and adverse pressure gradients were calculated using a Runge-Kutta method similar to that presented by White.

2.6 Roughness Effects

As additional surface roughness is introduced to a system, the structure of the boundary layer near the wall is altered causing an increase in skin friction drag. Presuming the surface has a uniform average roughness height k, an inner variable approach similar to that used in Section 2.3 can be used to determine the skin friction coefficient, C_f. Assuming the sand-grain correlation, represented by:

$$\Delta B_{sandgrains} = \frac{1}{\kappa}\ln(1+0.3k^+) \tag{48}$$

applies to the local boundary layer, the inner variable u^+ can then be written as:

$$u^+ = \frac{1}{\kappa}\ln(y^+) + B - \frac{1}{\kappa}\ln(1+0.3k^+) \tag{49}$$

where $k^+ = k\upsilon^*/\nu$, which is further defined by Equation (24), and Karman's constant, which is the same for all roughness, is $\kappa = 0.41$ (White, 426). Substituting Equation (49) into the Equation (32) yields the following:

$$\upsilon^* \frac{d\upsilon^*}{dx}\left[u^{+^2} - \frac{0.3k^+}{\kappa(1+0.3k^+)}\left(u^+ - \frac{1}{\kappa}\right)\right] = \frac{\upsilon^*}{\mu}\frac{\partial\tau}{\partial y^+} \tag{50}$$

This equation, when integrated twice and non-dimensionalized, yields:

$$\mathrm{Re}_x = 1.73(1+0.3k^+)e^Z\left[Z^2 - 4Z + 6 - \frac{0.3k^+}{1+0.3k^+}(Z-1)\right] \quad (51)$$

where: $Z = \kappa\lambda$ (52)

and $\lambda = \left(\frac{2}{Cf}\right)^{1/2}$ (53)

This result is valid for all uniform sand-grain roughness in turbulent flat-plate flow, but it may not, however, yield accurate predictions for roughness elements such as spheres or rivets (White, 1991:434).

With increases in Re_x, k^+ becomes extremely large, and eventually the dependence of C_f on Re_x dies out. At this point the flow becomes fully rough and C_f can be approximated by:

$$Cf = \left[1.4 + 3.7\log_{10}\left(\frac{x}{k_s}\right)\right]^{-2} \text{ for } \frac{x}{k} > \frac{\mathrm{Re}_x}{1000} \quad (54)$$

White's suggested Equation (54) is also in good agreement with the corresponding equation recommended by Schlichting (Schlichting, 1979:654).

$$Cf = \left[2.87 + 1.58\log_{10}\left(\frac{x}{k_s}\right)\right]^{-2.5} \quad (55)$$

Both Equation (54) and Equation (55) will be used as means for data comparison.

Several formulas were used to correlate equivalent sandgrain roughness to the roughness data presented in Section 2.1. Specifically, the measured R_a values for each surface were used to determine corresponding k_s values. The first correlation used was the result of research performed by Bammert and

Sandstede. This equation, which is cautioned to contain a margin of error up to 50%, is applicable for machined surfaces and is mathematically written as (Acharya, 1986:34):

$$k_s = 2.19Ra^{0.877} \tag{56}$$

Using profilometer traces of test sandpapers, Koch and Smith obtained the relation (Acharya, 1986:34):

$$k_s = 6.2Ra \tag{57}$$

Both of these equations will be used in Section 4.2.3 of the data analysis.

Though the above equations provide means by which to relate actual roughness data to an equivalent sand grain roughness, a large degree of uncertainty still lies in the use of these correlations. In order to more accurately predict equivalent roughness correlations, individual experiments should be performed for each surface considered.

III. Methods and Materials

3.1 Turbine Blade Roughness Measurement

Although Section 3.1, in its entirety, was not actually performed as part of this thesis, its information proves valuable and is therefore presented in order to complete the picture for the research at hand. The information provided in the following sections was taken from the thesis presented by Jess W. Drab, which may be located if further detail is required (Drab, 2001:27-34).

As a result of the efforts put forth by numerous corporations, nearly 100 turbine blades were obtained for study. The service life of these blades varied over a range of 40 to 22,000 hours. Accordingly, the blade surfaces also varied significantly. The types of surfaces were categorized as 1) erosion, 2) deposits, and 3) corrosion/pitting, which include thermal barrier coating (TBC) spallation.

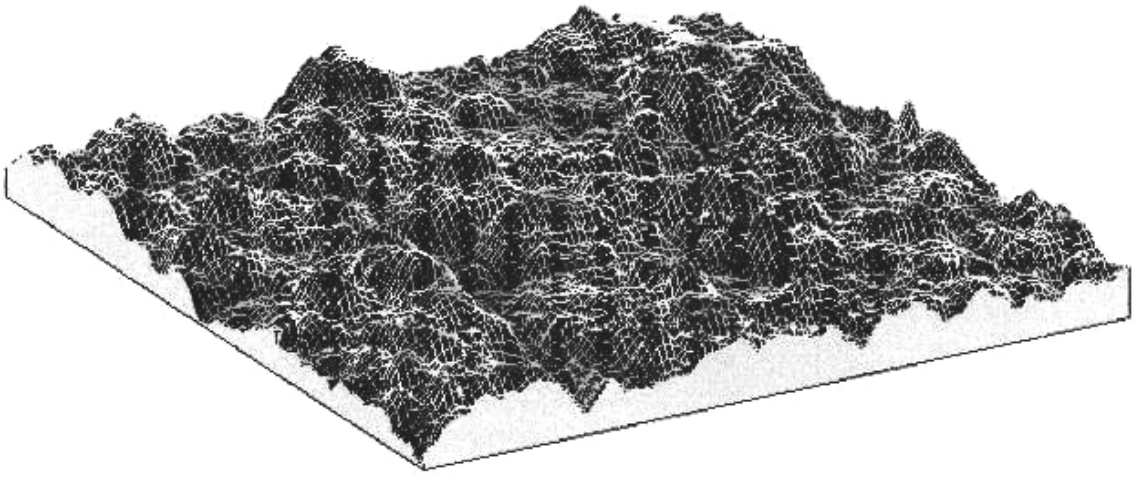

Figure 3.1 Erosion Surface (Vertical Scale Magnified 4.2 Times)

A general roughening of the turbine blade, due to prolonged use or hostile operating environments, resulted in the eroded surface shown in Figure 3.1. The surface was typically characterized as having peaks above and valleys below the mean surface level. The resulting R_a values varied between 10-18 μm. This type of surface occurred erratically on the turbine blades and was found to exhibit a gritty feel due to the steep roughness elements.

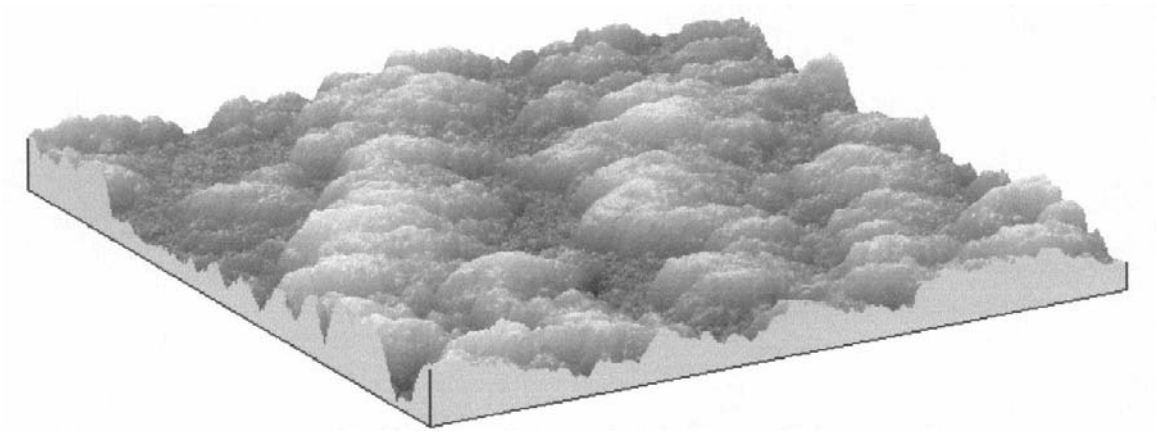

Figure 3.2 Fuel Deposit Surface (Vertical Scale Magnified 2.4 Times)

Areas of dark brown discoloration and rounded elevations often characterized fuel deposited surfaces, Figure 3.2. The deposits, unlike the eroded surfaces, were typically raised above the mean surface level of the blade. The resulting R_a values ranged from 10-14 μm. This characterization was commonly found on the pressure side of the blade or downstream of the cooling holes on the suction side.

Corroded and pitted surfaces were illustrated by deep and sudden indentations of the blade surface, and occurred on both bare metal and TBC blades. The corroded surfaces were commonly found where superheated fuel-

air mixtures had attacked weak areas of the blade's surface. Small canyons, measuring depths of 250 μm and widths of 5 cm, often found along the upper and lower lines of surface cooling holes depicted this. The resulting R_a values for corroded areas reached up to 25 μm. Gouges and chips caused by foreign debris striking the blade represented the pitted surfaces found along the leading and trailing edges. The pitted surfaces occurred more frequently than corrosion and brought about R_a values of 8-10 μm.

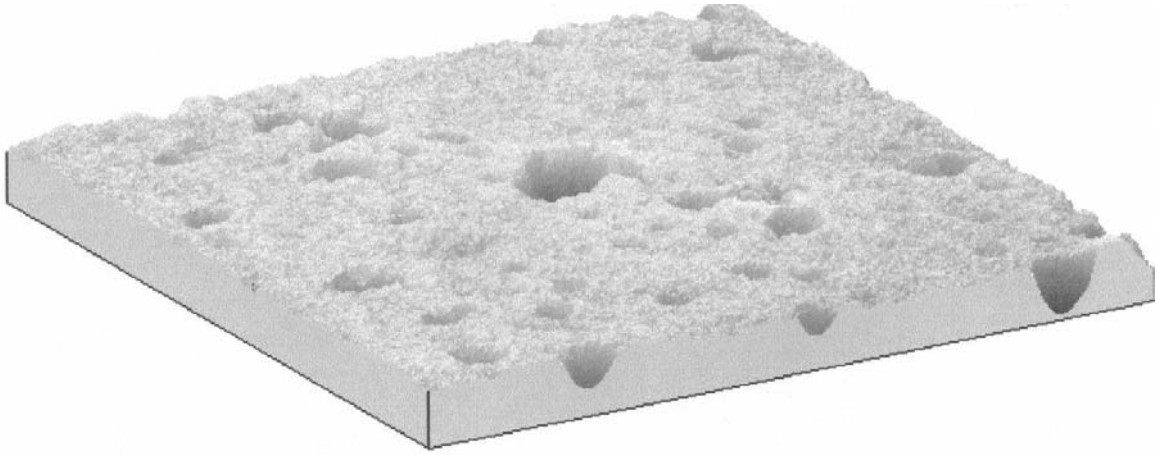

Figure 3.3 Pitted Surface (Vertical Scale Magnified 9.1 Times)

3.1.1 Profilometer Apparatus

A Taylor-Hobson Form TalySurf Series 2 profilometer was used to obtain the three-dimensional surface roughness data. The device used a 1.5 μm-radius conical tip on a 10 cm-long stylus to acquire the surface data, which was then sent to the TalySurf software analysis program. The 10 cm stylus provided a 2 mm vertical range with a resolution of 0.032 μm.

3.1.2 Roughness Measurement Procedure

In order to achieve a quality representation of the surface roughness, the blades were visually scanned and a roughness area was chosen. Due to the stylus requirements, the area was then checked to ensure its maximum vertical deviation did not exceed 2 mm. While this requirement did not pose a problem for flat blade surfaces, it did require greater care for the selections lying on cambered surfaces. Once the selection was complete, the area's physical boundary information and the number of 2-D traces were entered into the TalySurf software. In order to create a 3-D surface, multiple 2-D traces were taken at 5-40 μm spacings. With this information, the profilometer independently controlled the profiling of the chosen surface.

Upon completion of the profile, the raw vertical data, which contained the curvature of the blade, was input in the TalySurf Talymap 3-D software. The software applied a higher order polynomial surface fitting routine that isolated and removed the blade curvature from the raw data. Using the flat plate boundary layer thickness-to-Reynolds number correlation of Equation (27), a boundary layer thickness estimate for the actual turbine blade was obtained. The remaining roughness data was then scaled so that it resulted in the same turbine blade boundary layer thickness-to-roughness height ratio. The scaling factors are annotated in Figures 3.1-3.3.

3.1.3 Plastic Printer Apparatus

A Genisys Xs 3-D printer, made by Stratasys Inc, produced the various roughness coupons using a computer-generated CAD file representative of the real surface. The manufacturing process consisted of a spring-loaded cassette that pushed wafers of plastic polymer into a pump where it was melted. The plastic was then pushed though the 0.33 mm (0.013 in), 180°C (355°F) tip onto the 71°C (160°F) platen floor. The printer tip would move along the x-axis while the floor would move along the y and z-axes. The coupons were built up by layers from the floor and took approximately 4 ½ hours to complete. Each coupon was 14 cm x 12 cm and was manufactured so it would later fit into a congruent 28 cm x 36 cm surface.

3.2 Skin Friction Coefficient Measurement

With the skin friction testing already underway, the efforts at hand focused on developing an accurate, time efficient, and repeatable method for obtaining the desired data. The two previous methods chosen by Drab were a momentum deficit method and a bulk drag method. While the momentum deficit method was proven sounder in theory, the bulk drag method seemed extremely promising. This method, with some refining, yielded the potential to accurately obtain skin friction data at a much faster rate.

3.2.1Wind Tunnel Configuration

The boundary layer wind tunnel used for the experiments was located in the AFRL/PRTT Aero-Thermal Research Facility. The tunnel was fabricated from one inch Plexiglass and included an adjustable ceiling for investigating pressure gradients. The inner tunnel dimensions, for zero pressure gradient, were 38.1 cm wide x 22.86 cm tall (15 in x 9 in). Supporting the tunnel floor was a four-inch length of plywood lowered onto metal rails. The bottoms of the tunnel walls were lined with foam weather stripping to ensure an airtight seal during operation.

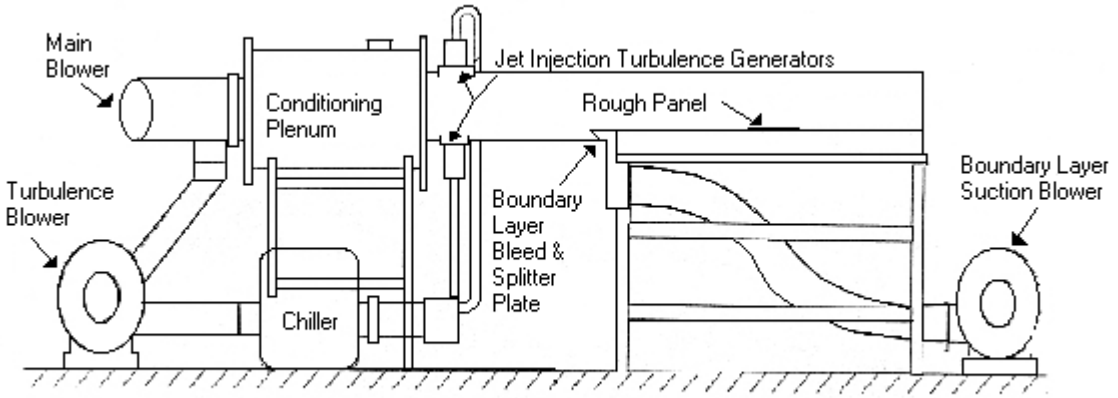

Figure 3.4 Diagram of Tunnel Schematic

A single blower pulled air from inside the bay, feeding it through a heating/chilling element, and then into the tunnel. An addition tunnel, running parallel with the test section, was also available to divert the air when necessary. The flow velocity, with the entire flow going through the test section, measured roughly 11 m/s (36 ft/s). With both tunnels open, the flow measured approximately 5 m/s (16.4 ft/s). The air entering the tunnel encountered a splitter

plate with an attached vacuum that suctioned off the lower portion of the flow. This ensured that a new boundary layer started at the leading edge of the tunnel. Additionally, a tripwire located 2.54 cm (1 in) downstream guaranteed fully turbulent flow. The leading edge of the test section was located approximately 104 cm (41 in) downstream of the splitter plate.

A set of freestream turbulence jets were located approximately 60 cm (23.6 in) upstream of the splitter plate. The jets were operated independently of the tunnel, and when running, produced freestream turbulence levels of approximately 11%. A square mesh grid, producing turbulence levels around 5-6% could also be installed roughly 10 cm (3.9 in) upstream of the leading edge.

3.2.2 Hanging Plate Apparatus

The hanging plate apparatus, shown in Figure 3.5, was comprised of three main parts: 1) support rig, 2) stationary plate, and 3) free-swinging plate. The support rig consisted of two braces that mounted to the sidewalls of the tunnel. Additionally, two narrow aluminum members, measuring roughly 43.2 x 5.1 x 1.27 cm (17 x 2 x ½ in) were bolted to the braces for cross support.

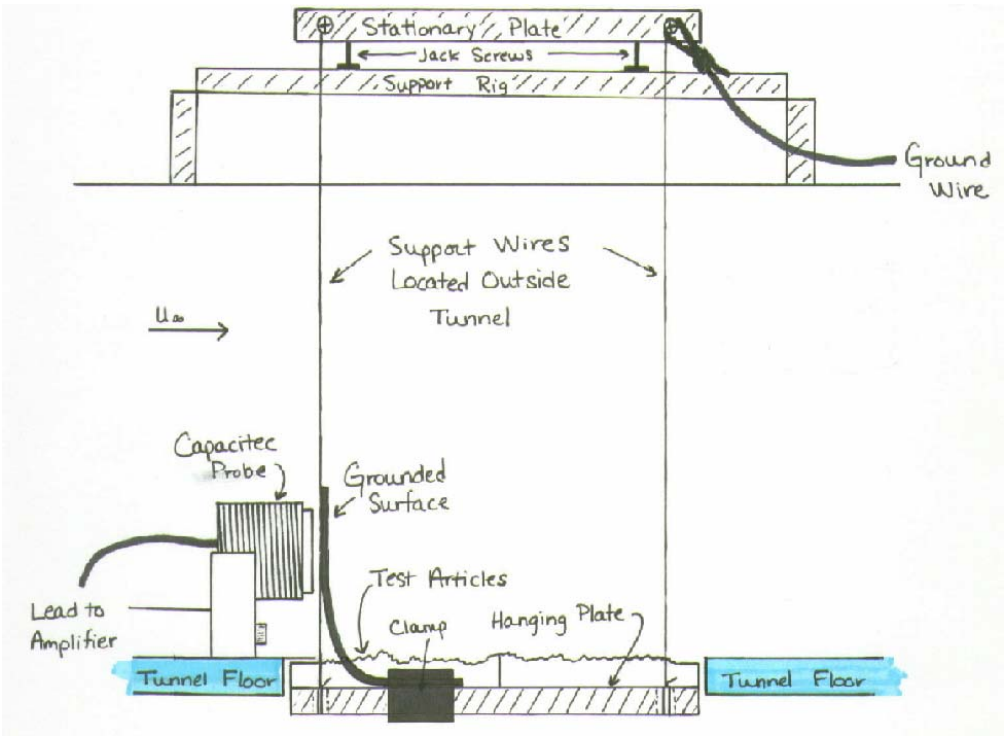

Figure 3.5 Hanging Plate Apparatus

The stationary plate, made also of aluminum, measured 66 x 27.6 x 0.635 cm (26 x 10 $^{7}/_{8}$ x ¼ in) and contained three tapped screw holes at various locations. Jackscrews were placed in the holes which, in turn, allowed the plate to sit atop the two cross supports. Moreover, the screws allowed for quick and easy leveling of the stationary plate. Two elongated semi-circular sections were cut out from each end of the plate and nylon-lined nuts were attached in front of each cut. The respective screws, used for suspending the free-swinging plate, had small holes drilled through the head in order to secure the wire and the first 0.635 cm (½ in) of the shaft was smooth, thus avoiding any binding of the wire. It is noteworthy that using nylon-lined nuts eliminates the possibility of the screw slipping.

The free-swinging plate, measuring 60.9 x 27.6 x 0.635 cm (24 x 10 $^{7}/_{8}$ x ¼ in), provided the floor upon which the roughness samples would rest. Four 0.635 cm (¼ in) holes were drilled at each corresponding suspension-screw location. The support wire, chosen for its durability and thermal resistance, was tied securely at each hole allowing the plate to swing freely from its stationary partner above. The wire length was adjusted so that the plate was level and the leading edge of the roughness samples aligned with the edge of the tunnel floor. To make certain that no airflow would be seen by this boundary, a 0.00254 cm (0.001 in) thick shim was secured as shown in Figure 3.6.

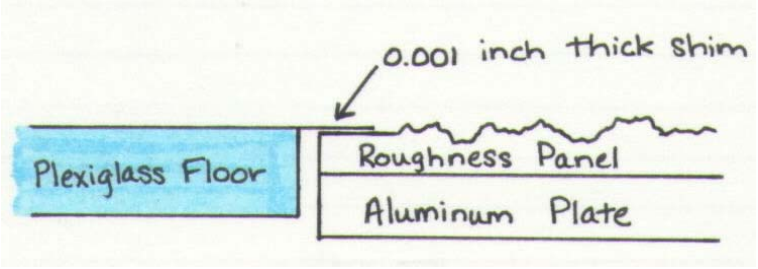

Figure 3.6 Diagram of Leading Edge Boundary

3.2.3 Capacitec Apparatus

The device used for measuring the displacement of the hanging plate was a Capacitec non-contact displacement probe and Series 4000 Capacitec amplifier and rack. When properly assembled, the amplifier would produce an analog voltage proportional to the distance between the capacitive probe and the electrically conductive surface connected to a ground. The underlying principle is that capacitive reactance is proportional to the spacing of a parallel-plate capacitor, or simply, the probe and the grounded surface. For these

experiments, the grounded surface was affixed to the free-swinging plate as shown in Figure 3.7.

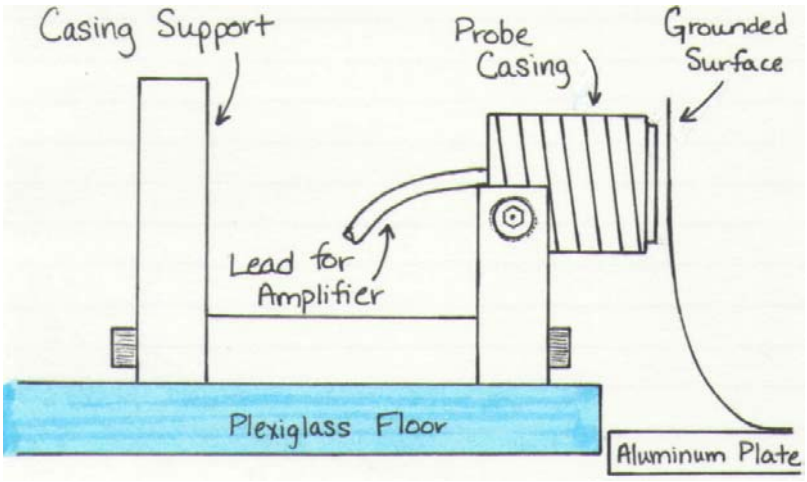

Figure 3.7 Capacitec Apparatus

The probe used for the experiments measured 1.27 cm (0.500 in) O.D. and was enclosed in a 2.54 cm (1.000 in) O.D. casing. The probe provided a linear measurable range of 0.9525 cm (0.375 in) and had an operating temperature range of –37.7°C (-100°F) to 260°C (500°F). The Capacitec 4100-S amplifier was a basic single channel amplifier card with a 2.54 cm (1.0 in) rack mountable front panel. The panel offered screwdriver implemented offset and gain controls and had a full-scale linearity of ±2% with 0.01% repeatability. The Capacitec 4004 rack enclosure, used in conjunction with the amplifier, contained four channels and had an individual 0-10Vdc analog output. A ±20 Vdc power supply powered the unit.

3.2.4 Pressure Measurements

Drag-balance measurements, such as the ones being obtained, can be subject to errors due to the pressure differences involving the leading and trailing edge of the hanging plate. In order to correct for this difference, three pressure ports were placed in the stationary Plexiglass walls adjacent to both the leading and trailing edge walls. The ports were located at the center and roughly 8.89 cm (3.5 in) from center along opposite cross-stream directions. The three ports from each edge were combined and fed into a pressure transducer having a 0-0.4" H_2O range. The transducer slope was calibrated with a dead-weight pressure tester to be 0.08 "H_2O/Vdc. The use of these values will be covered in more detail in Section 3.2.7.

3.2.5 Calibration of the Hanging Plate

The calibration of the hanging plate was also simple in nature. A durable polyester thread was attached to the trailing edge of the free-swinging plate as seen in Figure 3.8. The thread was drawn across a pulley system located outside the tunnel and a mesh bag was tied to the end. A voltage reading was taken before and after attaching the thread. The displacement measured after attaching the thread was due to the weight of the vertical thread length and the mesh bag. Small masses were then weighed and added to the bag one at a time. Voltage readings were taken following each addition. The calibration was complete once the plate reached a displacement equivalent to that of the largest rough panel displacement. The displacement (Vdc) was then plotted against the

mass (gm). A linear equation fitted to the data points provided a corresponding slope. The average slope for all plate calibrations was 0.102524 Vdc/gm with less then 2½% precision error among calibrations. The use of this slope in the data reduction process will be covered in detail in Section 3.2.7.

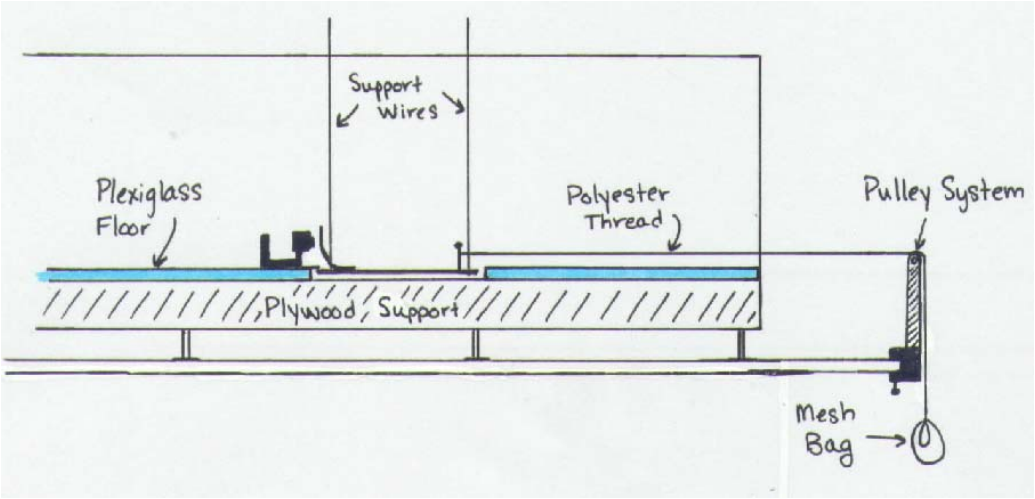

Figure 3.8 Schematic of Hanging Plate Calibration

3.2.6 Bulk Drag Procedure

Using a single blower, the flow was started through the adjacent tunnel. With the use of the aforementioned chiller, the flow was cooled to match the ambient temperature of the room, thus eliminating any possible bias due to temperature fluctuations. All electronic devices were thoroughly warmed up to avoid potential noise. Once steady state conditions were achieved, the LabView program designed to record the data was started.

The program required user inputs for relative humidity, atmospheric pressure, freestream distance x, and sample rate. The program took A samples at B samples/minute. For each sample, the program recorded the temperatures

from each thermocouple, the velocity from the hotwire, and the output voltage from both the pressure transducer and the Capacitec probe. In addition, the program calculated percent turbulence, Reynolds number, and density for each reading.

The objectives of this research were multifaceted, thus requiring numerous test variations. Tests focusing on freestream turbulence levels required data for zero flow, flow with low freestream turbulence, flow with grid turbulence, and flow with jet turbulence. Consequently, the subsequent pattern was followed: off, on, off, on w/grid, off, on, on w/jets (one minute), on, off. Periods labeled as off indicate that the flow was being directed, in its entirety, through the adjacent tunnel. The turbulence grid was installed/uninstalled during the off periods before and after respectively. All patterns were performed in two-minute intervals with the exception being noted above. Upon completion, the LabView program was stopped. This procedure was repeated for both high and low velocities. An example of the turbulent flow data is located in Appendix A.

Tests focusing on pressure gradient effects were more simplistic and only required data for zero flow, low velocity flow (both tunnels open), and high velocity flow. The pattern used for testing followed this sequence: off, low velocity, high velocity, low velocity, high velocity, off. Again, all positions were recorded in two-minute intervals.

Upon completion of each sequence, the hanging plate was braced against the leading edge wall for exchange of the roughness panels. A small section of the tunnel ceiling was removed and, being careful not to touch the suspension

wires, the panels were switched. With the new panels properly situated, the ceiling was replaced and the hanging plate released. The desired sequence was then repeated. This process was performed until all the roughness panels had been tested. To facilitate experimentally sound comparisons, each set of data was run at one time. This ensured that, at a minimum, that set of data was performed under the same conditions.

3.2.7 Data Reduction

The raw data files were edited using Microsoft Excel. Average values for U_∞, Tu, Re_x, ρ, and the Capacitec and pressure transducer voltages were calculated for each of the required flow settings discussed in Section 3.2.6. The actual voltage changes for both displacement and pressure were calculated by subtracting away the zero flow value as shown below:

$$Actual_{SettingX} = \mathrm{Re}\,corded_{SettingX} - \mathrm{Re}\,corded_{ZeroFlow} \tag{58}$$

Example calculations can be located at the end of Appendix A. These values, in conjunction with the other averages, were then used to determine the shear and pressure forces acting on the plate. The net force was determined using the following equation:

$$F_{Net_{SettingX}}(N) = \frac{CapacitecActual_{SettingX}(Vdc)}{HangingPlateSlope(Vdc/gm)} \frac{9.81(m/s^2)}{1000 gm/kg} \tag{59}$$

The pressure force acting on the leading edge of the plate was calculated using the equation:

$$F_{\Pr essure_{SettingX}}(N) = \Pr essureActual_{SettingX}(Vdc) \times 0.08\left(\frac{H_2O}{Vdc}\right) \times 249\left(\frac{Pa}{H_2O}\right) \times A_{side} \qquad (60)$$

The shear force on the plate can then be found by subtracting Equation (60) from (59).

$$F_{Shear} = F_{Net} - F_{\Pr essure} \qquad (61)$$

Dividing Equation (61) by the surface area yielded τ_{shear}:

$$\bar{\tau}_{shear} = \frac{F_{Shear}}{A_{Surface}} \qquad (62)$$

This result was then substituted into Equation (7) to obtain the actual skin friction coefficients.

When all of the drag data was taken, a pressure adjustment was determined based on the flat plate subset of data. The pressure adjustment accounted for a non-uniform pressure distribution over the leading and trailing edge gaps. The adjustment was determined by locating the maximum and minimum C_f values among the entire subset of flat plate data. The difference between the two values was then minimized by adjusting the pressure voltage percentage. For example, if 100% (1.0 x PressureActual) of the pressure voltage was used, the data yielded a spread of roughly 10% whereas using an adjustment of 70% (0.70 x PressureActual) decreased the spread to approximately 2%. The optimum pressure adjustment was found using Excel's solver tool. This adjustment ultimately changes Equation (60) to:

$$F_{\Pr essure_{SettingX}}(N) = 0.70 \Pr essureActual_{SettingX}(Vdc) \times 0.08\left(\frac{H_2O}{Vdc}\right) \times 249\left(\frac{Pa}{H_2O}\right) \times A_{side} \qquad (60\text{-b})$$

3.3 Convective Heat Transfer Method

Additional data was gathered using the transient method described in detail in Section 3.3 of Drab's thesis (Drab, 2001:44-48). The only notable difference was the change in x from x=0.96 m to x=1.25 m (49.125 in). This data was processed using the same method, developed by Drab, and used to corroborate the C_f data gathered.

IV. Results and Analysis

4.1 Statistical Roughness Results

The statistical parameters described in Section 2.1 were applied to each surface file. The scaled results, expressed in millimeters, are summarized in Table 4.1.

Table 4.1 Surface Roughness Statistics

Panel	Scaling Factor	Ra	Rq	Rt	Sk	Ku	Alpha
TBCop	25	0.286	0.352	2.29	0.03	2.73	
Pitted	28.5	0.134	0.211	3.48	-0.88	7.83	7.7
TBC	28.1	0.804	1.008	8.16	-0.69	6.47	
Erosion #1	62.7	0.445	0.561	5.04	0.35	5.51	24.0
Fuel Deposit	34.25	1.157	1.389	7.36	0.17	1.27	24.7
Erosion #2	57.7	0.493	0.619	4.23	0.05	4.95	23.7
KS Erosion #2	N/A	0.447	0.528	2.00	0.86	3.75	

The results show an average centerline roughness of 0.134 mm for the pitted surface. The eroded panels produced the next highest values of 0.445 mm, 0.447 mm, and 0.493 mm. TBCop followed with R_a = 0.286 mm. Finally, TBC and the fuel deposited panels yielded the highest values with R_a= 0.804 mm and R_a = 1.157 mm respectively. Note that the average R_a value is extremely small compared to the typical boundary layer thickness of 19-24 mm.

As noted in Section 2.1, surfaces comprised of small consistent roughness elements yield similar R_a and R_q values. This appears to be the case for all of the eroded surfaces. With smaller R_t values and mild kurtosis levels, these statistical parameters accurately define the typical eroded surface. Also

noteworthy, is the negative skewness in both the pitted and TBC surfaces. Combined with prominent R_t values, these numbers indicate large steep valleys where the ceramic coating was likely chipped away. These surfaces also yielded the highest kurtosis levels, which is yet another indication of severe surface variations. The extremely small kurtosis levels for the fuel deposited and TBCop surfaces indicate a relatively smooth or gradually curving surface. Combined with positive skewness and substantial R_a, R_q, and R_t values, the fuel deposited surface is one with large flowing features. In contrast, with minimal roughness statistics and very little skewness, the TBCop surface is one with only slight features.

In order to establish a basis for comparison, smooth panels were also made. They were created using the same manufacturing process as the rough panels, but due to the printer's tip size, the upper surface contained small variations of approximately 0.125 mm. Although not perfectly flat, the surface was considered hydraulically smooth and was thus suitable for providing a comparative reference (Drab, 2001:50). Additionally, KS Erosion #2 panels, designed to match the k_s value of the Erosion #2 panels, were created. The panels consisted of cones, 2 mm in height, positioned evenly across the surface in 5 mm increments.

4.2 Bulk Drag Results

The aim of this research was to explore the effects of surface roughness, freestream turbulence and pressure gradients on skin friction drag. Because

these topics together were of such great extent, each area was explored individually before combined effects were studied. In order to ensure that the data being collected was worthwhile, smooth plate flow was first investigated. Using known flow conditions, the flat plates were tested and the results compared to reputable empirical correlations. This, in turn, allowed the procedure to be applied to the rough surfaces with a considerable amount of confidence.

4.2.1 Flat Plate Results

As previously stated, ensuring worthwhile results for smooth, flat plate flow was an absolute necessity. This not only made certain that the tunnel flow was acting properly, but that the bulk drag setup, Capacitec device, and pressure transducer were also consistent and reliable. Upon gathering sufficient flat plate data, the results were compared to several sources. While Schlichting provides numerous flat plate, zero incidence, turbulent flow skin friction correlations such as Prandtl, Prandtl-Schlichting, and Schultz-Grunow, only a select few were chosen for the comparison at hand (Schlichting, 1979:639). Plotted in Figure 4.1 is the resulting data along with the White, Prandtl, and Mills curves, which are represented by Equations (36), (28), and (29) respectively (White, 1991:430-432).

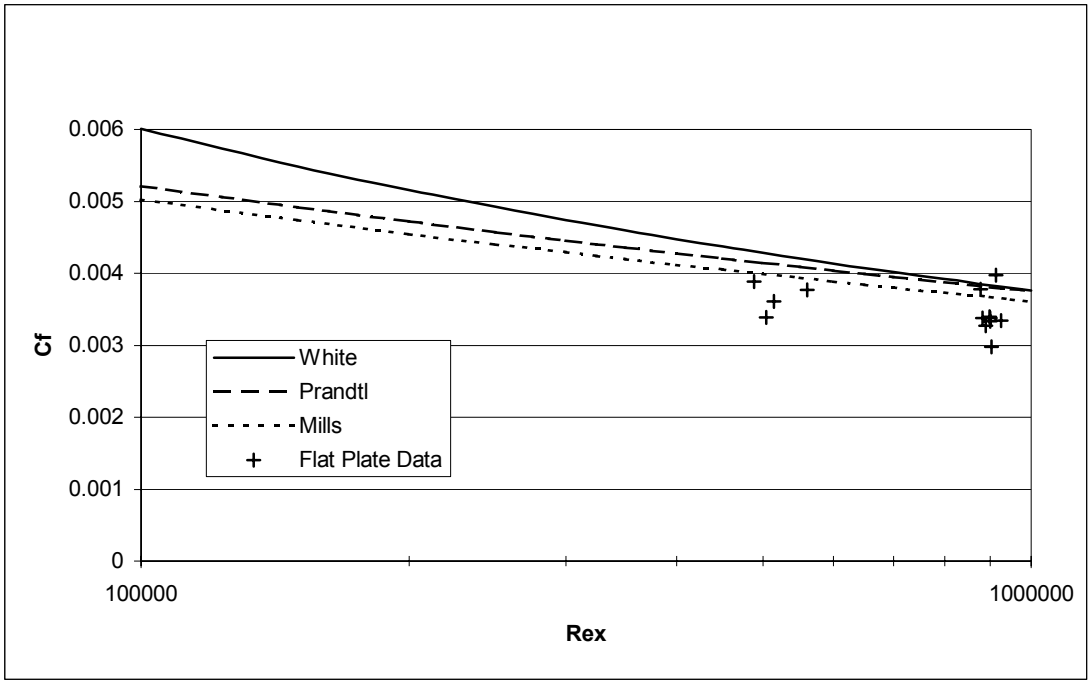

Figure 4.1 Flat Plate Results vs. Empirical Correlations

As shown in Figure 4.1, the raw data is slightly varied, but the majority lies within 5% of the empirical correlations, the closest being the Mills equation. In order to decrease the variation in the data, the pressure modification method, described in Section 3.2.6, was applied. An optimal pressure adjustment of 70% was applied and the results are displayed in Figure 4.2.

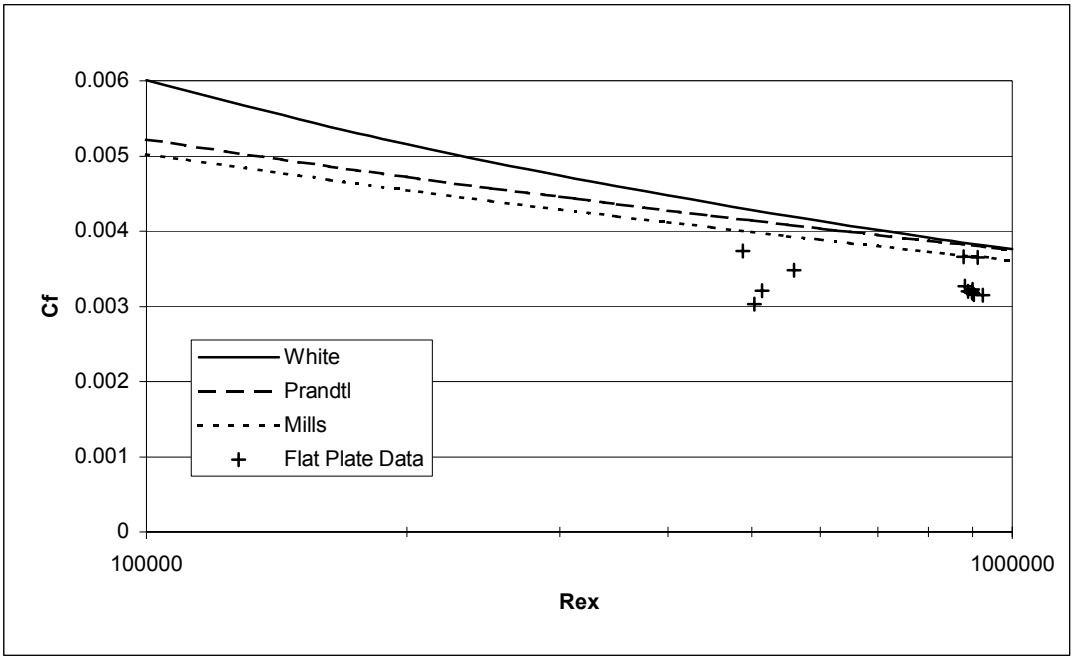

Figure 4.2 Modified Flat Plate Results vs. Empirical Correlations

Although the adjustment caused the data to move slightly away from the curves, the converged data was still within 10% of the predicted values. As a result the 70% adjustment was used throughout the remainder of the zero pressure gradient tests.

In an effort to qualify the data, an error analysis was performed using methods presented by Wheeler and Ganji (1996). The complete results are shown in Appendix C, but a brief summary follows. For a zero-pressure-gradient condition and low Reynolds number, the smooth plates yielded a precision error of ±10.5% while the rough plates averaged a precision error of± 2.8%. A high Reynolds number and zero pressure gradient setting resulted in a flat plate precision error of ±12.5% and a rough plate average precision error of ±4.0%. A bias error analysis was also performed on the zero pressure gradient, flat plate

data. The resulting bias error was ±7.0% for both Re_x=500,000 and Re_x=900,000. The error sources, their uncertainties, and the respective changes to the skin friction coefficient are also tabulated in Appendix C.

4.2.2 Flat Plate with Freestream Turbulence

Two turbulence devices were used to simulate the differing freestream turbulence levels seen by a turbine section. A square mesh grid and turbulence jets, both located upstream of the leading edge, were used to create freestream turbulence levels of approximately 5% and 11% over the roughness section. As discussed in Section 2.4, it was expected that as turbulence levels increased the resulting skin friction coefficient would also increase. The data obtained during the tests supported this theory and the average values are presented in Figure 4.3. Here C_f is normalized by a value with low (1%) turbulence labeled as C_{fo}.

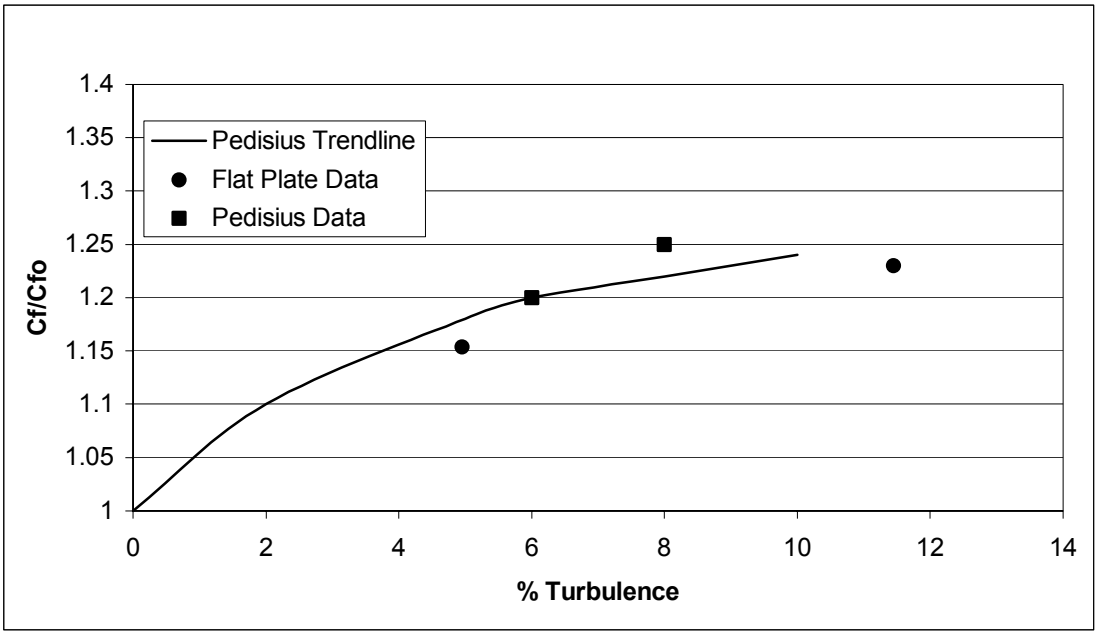

Figure 4.3 Variations in Flat Plate Skin Friction (C_f) with Freestream Turbulence

Also depicted in Figure 4.3 is the combined work of Pedisius, Kazimekas, and Slanciauskas (1979). In an experimental study of turbulent boundary layer characteristics for $Re_x \leq 3x10^6$, and Tu ≤10%, they also found that there was an increase in skin friction corresponding increases in Tu. Specifically, when turbulence levels were increased from 6% to 8% the resulting C_f value increased from 1.20 to 1.25 (Pedisius et al., 1979:125). Although Figure 4.3 does not contain the actual data obtained during those experiments, the resulting trend line alone corroborates the experimental data at hand. When compared to the works of Pedisius et al., the average data consistently measured roughly 2% lower. It should also be noted that without including the aforementioned pressure adjustment of 70%, the data is extremely spread out and considerably lower than the displayed trend lines.

4.2.3 Effects of Surface Roughness

Bulk drag measurements were taken using the procedure detailed in Section 3.2.6. Displacement and pressure values were recorded for freestream turbulence levels of 1%, 5%, and 11%. This section will cover only 1% turbulence, as the combined effects will be discussed in the next section. The average skin friction coefficients for 1% turbulence are plotted in Figure 4.4.

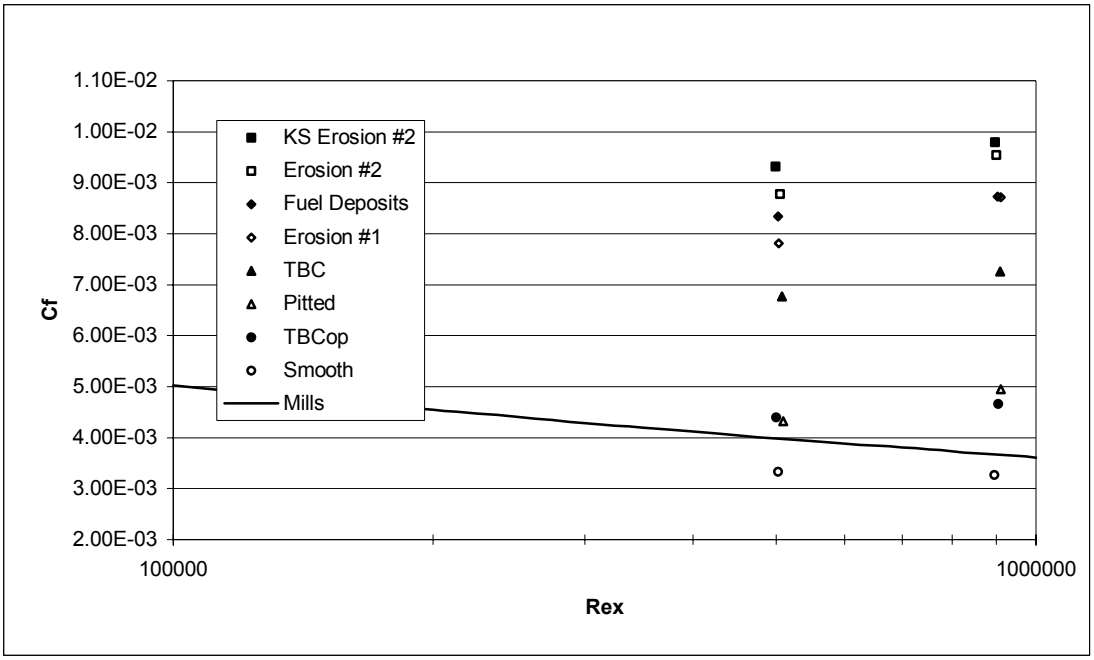

Figure 4.4 Variations in Skin Friction (C_f) with Roughness

Because of the inherent fluctuations accompanying the hanging plate apparatus, the various C_f values for each surface varied slightly from one another. This occurred more often among the rougher plates and is attributed to the larger surface variations. The smoother panels, or those containing more valleys than peaks, were found to have very similar C_f values for each test. The percent variation for each surface is defined by it respective precision error and is located in Appendix C. An average C_f for each surface, along with its relative flat-plate percentage, is listed in Table 4.2. Also included are the comparable percentages recorded during the previous research performed by Drab using a more primitive hanging balance method (Drab, 2001:54).

Table 4.2 Measured Skin Friction Coefficients

Panel	Average Cf		Percent Relative to Flat Plate		Percentages from Drab
	Re=500,000	Re=900,000	Re=500,000	Re=900,000	
Smooth	3.33E-03	3.27E-03	100%	100%	100%
TBCop	4.40E-03	4.66E-03	132%	143%	N/A
Pitted	4.32E-03	4.95E-03	130%	151%	176%
TBC	6.77E-03	7.26E-03	203%	222%	N/A
Erosion #1	7.82E-03	8.71E-03	235%	267%	307%
Fuel Deposits	8.34E-03	8.72E-03	251%	267%	300%
Erosion #2	8.78E-03	9.55E-03	264%	292%	355%
KS Erosion #2	9.32E-03	9.80E-03	280%	300%	N/A

According to Table 4.2, both sets of rough panel data follow the same trend. On the low end of the scale are the TBCop and pitted panels. The mid range includes the TBC panel. Next in line are the erosion #1 and fuel deposit panels, which in both cases exhibit very similar results. The high end of the scale is closed off with the erosion #2 and KS erosion #2 panels.

In comparing this trend to the corresponding surfaces, some simple conclusions emerge. Panels that display minimal kurtosis and skewness values, such as TBCop, result in the smallest drag increase. The subsequent trend appears to be largely dependent on unique combinations of surface statistics. Surfaces with negative skewness values, seemingly regardless of kurtosis, result in moderate increases in skin friction drag. The largest increases in drag were found to occur in panels with positive skewness and moderate kurtosis values.

When the data was broken down by Reynolds number another tendency materialized. Although the trend among the panels remained consistent, Table 4.2 shows that the overall percentages for each roughness panel were greater for the Re_x =900,000 case. This trend is to be expected and is accounted for in

Equations (7) and (10). The increases, however, are exaggerated among rougher surfaces. While this effect should be mitigated with the use of Equation (7) also, it is evident that something is not accounted for and there is additional momentum present. It is this additional momentum that allows the flow to penetrate deeper into the surface valleys, which consequently results in an increase in skin friction drag. Thus, for identical changes in $Re_{x,}$ surfaces with fewer valleys result in smaller changes in comparison to surfaces containing numerous valleys.

When compared to the research performed by Drab, it was found that the current data, in its entirety, yielded significantly lower skin friction values. Though the techniques used for each experiment were nearly identical, there were two outstanding differences that could be responsible for the differences among the resulting values.

The first distinction was the possible effects of temperature fluctuations. According to Drab, the data was taken when the tunnel reached a steady temperature of approximately 27°C (80°F) (Drab, 2001:44). Although further increases in temperature were gradual after the initial warm-up period, the impact on the system could still be significant. Foremost, any increase in temperature would result in an increase in flow velocity. Consequently, skin friction drag would increase over the period of the test. In addition, any increases in temperature could cause thermal expansion in the wire supporting the hanging plate (Drab, 2001:54). This would almost certainly impact the consistency of the panel displacement.

In an effort to eliminate thermal sources of error, two precautions were taken. First, a chilling element was used to keep the flow at ambient temperature, approximately 21°C (70°F). This ensured that the flow over the test section remained constant for the duration of the test and that the support wires saw no temperature fluctuations. Second, the wire selected to support the plate had an improved thermal expansion coefficient, thus diminishing errors due to thermal effects.

The second distinction, and most likely the primary cause for the notable differences, was accounting for the pressure difference between the leading and trailing edges. In nearly all the bulk drag tests, the leading edge was found to yield a higher pressure than the trailing edge. As a result, the measured displacement included the effects of both shear and pressure forces. As in the case of Drab's research, not accounting for the pressure forces would result in erroneously high skin friction data as shown in Table 4.2.

As briefly mentioned in Section 1.2, the majority of past research on the effects of roughened surfaces involved sandgrain roughness. Eventually, correlations between surface statistics, such as R_a, and equivalent sandgrain roughness were developed. These equations were presented in Section 2.6, but are repeated below for convenience:

Bammert/Sandstede: $k_s = 2.19 R_a^{\,0.877}$ (56)

Koch/Smith: $k_s = 6.2 R_a$ (57)

Although these equations may not be perfectly suited for this data, they do, nonetheless, allow for reasonable comparison against other published results. It is cautioned, however, that the margin of error may be substantial (Acharya, 1986:34).

Using the predetermined R_a values, a k_s was found for each surface. The corresponding C_f values were then obtained using Equations (54) and (55). Both the predicted and actual C_f values are plotted in Figure 4.5 below.

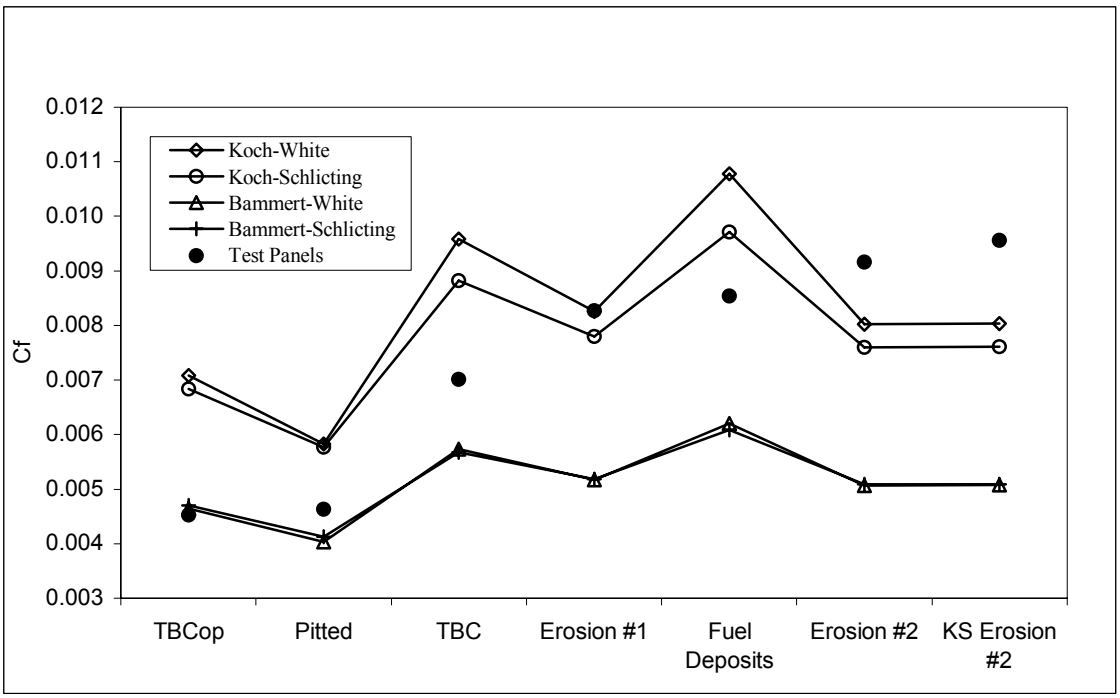

Figure 4.5 C_f Data vs. Sandgrain Roughness Predictions

According to the chart, Bammert's correlation, which was developed for machined surfaces, is well suited to the likes of the TBCop plates. Interestingly, of all the rough panels, TBCop is the most representative of a machined surface, as its features could easily characterize the slight markings left during machining. Both the pitted and TBC panels fell between the predicted curves. This is of no

surprise considering that these panels are rougher than typical machined surfaces but not as rough as sandgrain surfaces. It should also be noted that the primary features of the panels are valleys, which may not achieve the same shear drag as a surface dominated by peaks. The eroded surfaces tended to exhibit a gritty texture similar to that of extremely rough sandpaper. This would logically place the experimental data close to the predicted value presented by Koch and Smith, which was developed through profilometer traces of test sandpapers (Acharya, 1986:34). This prediction was supported by the findings of the erosion #1 panel. Although, the erosion #2 panel exhibited similar features, it is concluded that the roughness elements of this surface were typically greater than the sandgrain elements tested by Koch and Smith. Through trial and error, it was found that by increasing the multiplier in Koch and Smith's equation by 50%, the predicted values well approximated the experimental values for the erosion #2 and KS erosion #2 panels.

In an attempt to determine more appropriate k_s for the rough panels, a reverse strategy was applied. Each surface's k_s value was adjusted, using Equation (54), to perfectly match the C_f to the experimental data. These adjusted k_s values were then correlated against each of the surface statistics discussed in Section 2.1. The resulting plots are located in Appendix D. Based on the plots, it was determined that none of the parameters, on an individual level, yielded any significant trends. Skewness and kurtosis seemingly have a prevailing role in shaping k_s, as their coefficients of determination are much more significant, but they surely cannot be the sole factors in its determination. Based on the

resulting data, no single statistic is able to accurately predict k_s. Thus, the correlations based on R_a alone (Equations (56) and (57)) should not be used.

The slope angle, α, presented by Acharya (1986) as an important roughness parameter, was also found for several surfaces and its rms deviation plotted against k_s. This yielded a fairly reliable trend (R^2=0.8179) and with further study could possibly lead to a consistent correlation to equivalent sandgrain roughness. A more recent parameter, developed by Sigal and Danberg, uses both the spacing and shape of roughness elements to determine k_s. It is mathematically defined as:

$$\Lambda_s = \frac{S}{S_f}\left(\frac{A_s}{A_f}\right)^{1.6} \tag{63}$$

where S is the surface area without roughness, S_f is the total frontal area of the sample's roughness elements, A_s is the windward wetted surface area of an element, and A_f is the frontal area of an element. Though this parameter was not applied to the surfaces at hand, both Bons et al. (2001) and Bogard et al. (1998) have implemented it with success in similar experiments. In consideration, it may prove worthwhile to implement the calculation method similar to that used by Bons et al. (2001).

4.2.4 Combined Effects of Turbulence and Roughness

With the individual results of surface roughness and turbulence complete, the focus now turns to the results due to combined effects. As noted earlier, data was recorded for each roughness panel under multiple turbulence levels. The

data was then compared against the average flat plate, 1% turbulence value of C_f=0.00333 for Re_x=500,000 and Cf=0.00327 for Re_x=900,000. The results are summarized in Table 4.3.

Table 4.3 Skin Friction Ratios for Combined Roughness and Turbulence Effects

	Rex=500,000		Rex=900,000	
Panel	**Tu=5%**	**Tu=11%**	**Tu=5%**	**Tu=11%**
Smooth	1.38	1.37	1.16	1.21
TBCop	1.58	1.61	1.69	1.80
Pitted	1.57	1.64	1.82	1.90
TBC			2.67	2.85
Erosion #1	2.90	2.99	3.21	3.40
Fuel Deposits	3.14	3.22	3.19	3.37
Erosion #2	3.43	3.43	3.47	3.69
KS Erosion #2	3.45	3.48	3.58	3.80

According to the table, increasing turbulence levels results in an increase in skin friction drag regardless of the surface type. However, it does appear that the same increase in freestream turbulence will result in a greater increase in skin friction drag at higher Reynolds numbers. It should also be noted that the above results follow the same trend discovered during inspection of the surface roughness results.

In an effort to better understand the combined effects of surface roughness and turbulence, an attempt was made to verify whether or not the addition of the individual results would yield the same results as the measured data. The calculated results were found using values listed in Tables 4.2 and 4.3 with the equation below:

$$\frac{Rough_{Tu=1\%}}{Smooth_{Tu=1\%}} + \frac{Smooth_{Tu=P\%}}{Smooth_{Tu=1\%}} - 1 = \frac{Rough_{Tu=P\%}}{Smooth_{Tu=1\%}} \qquad (62)$$

These values were compared against the measured values for the combined effects and plotted according to Reynolds number in Figures 4.6 below.

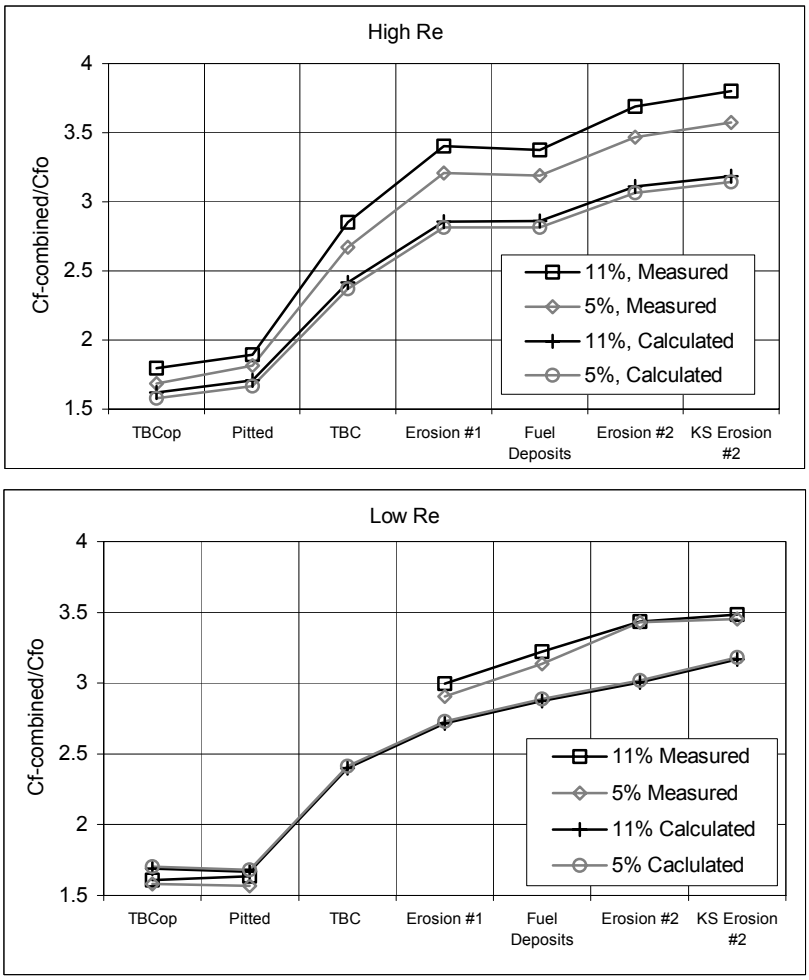

Figure 4.6 Calculated vs. Measured Results Due to Combined Effects (a) High Re_x (b) Low Re_x

As seen above, both the measured and calculated results follow similar trends. The measured values, however, appear larger than their calculated counterparts in each of the cases. For sake of ease, the surfaces are broken into minor and major roughness groups, where the minor roughness group consists of TBCop and pitted panels and the major roughness group contains all others. At the high Reynolds number and 5% freestream turbulence, the minor

roughness group yields measured values roughly 7.2% higher than the calculated values, while the major group yields values averaging 11.8% higher. Increasing freestream turbulence to 11% further exacerbates these differences and results in minor roughness increases of 9.7% and major roughness increases of 15.7%. The effects of freestream turbulence are not as significant at low Reynolds number. This is shown in plot two of Figure 4.6. Consequently, the measured values at the low Reynolds number, for both turbulence levels, are approximately 9.4% higher than the corresponding calculated values. This can only support the conclusion that the combined effects of surface roughness and turbulence are more severe that the sum of the two alone. This plot also supports the previous statement that increases in turbulence are even more detrimental to skin friction drag at higher Reynolds numbers.

4.2.5 Pressure Gradient Effects

Upon completion of the zero pressure gradient tests, the effects of favorable and adverse pressure gradients were investigated. By adjusting the tunnel ceiling, it was possible to create flow resembling that found in both nozzles and diffusers. The first aspect to be covered will be the favorable pressure gradient effect of a nozzle.

As depicted in Figure 2.4, a favorable pressure gradient results in a fuller velocity profile due to an increase in momentum. Consequently, the resulting C_f values should theoretically be greater than their zero pressure gradient counterparts. In an attempt to validate this theory, each surface was tested, by

the same means and setup as before, at both high and low Reynolds numbers. Following the data reduction, it was determined that the appropriate pressure adjustment was on the order of 105%. The average skin friction values for each surface under favorable pressure gradient conditions are plotted in Figure 4.7.

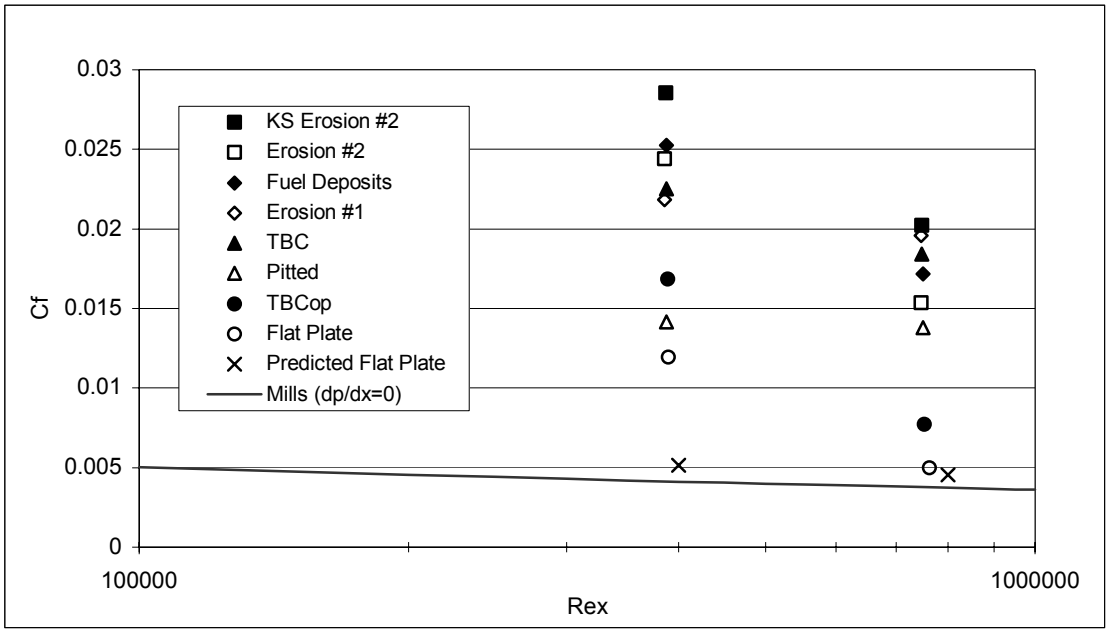

Figure 4.7 C_f Variations Under Favorable Pressure Gradient Conditions

As predicted, the skin friction values for the favorable pressure gradient were significantly higher than those for the zero pressure gradient. It was also found that introducing a pressure gradient to the test section dramatically reduced the fluctuations associated with the hanging plate. This conveniently reduced the deviation among the data subsets.

Using the method described in Section 2.5, the predicted skin friction coefficients for the smooth plate were C_f=0.00455 for the high Re_x and C_f=0.00514 for the low Re_x. When comparing these values to the actual data, it was evident that something was not accounted for. One possible source of error

is the pressure measurements on the leading and trailing edges. Although the pressure adjustment acts to converge the flat plate data, it is possible that the actual pressures present are not accurately measured. This could pose a problem if the pressures measured underestimate the actual pressure, because the resulting C_f would then overestimate the actual values.

Though the favorable pressure gradient results are likely problematic, it was reassuring, nonetheless, to see similar roughness trends. As displayed in Figure 4.8, smoother surfaces typically resulted in slighter increases while the rougher surfaces yielded the larger increases.

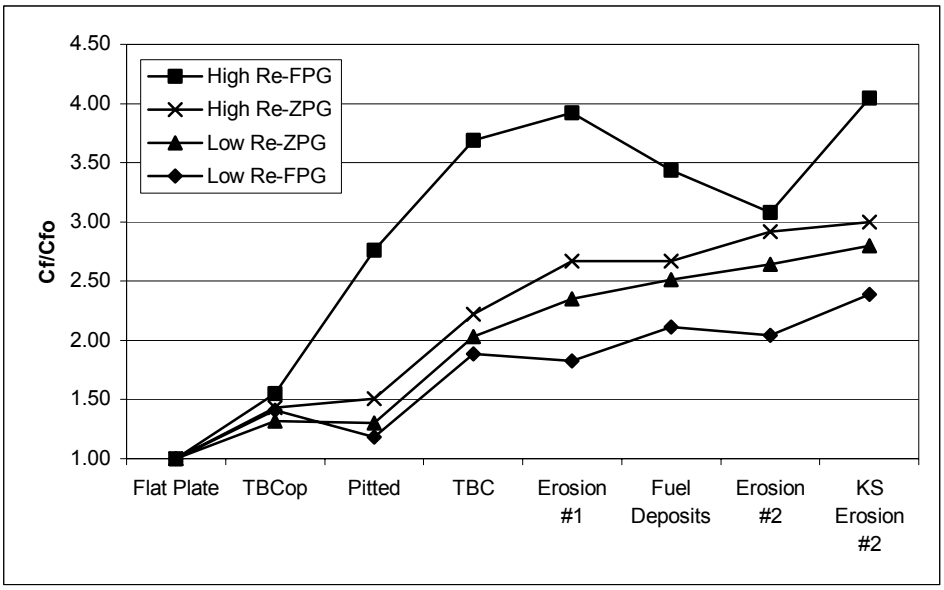

Figure 4.8 C_f Ratio Comparisons for Zero and Favorable Pressure Gradients

In an attempt to come full circle, adverse pressure gradient measurements were also taken. Contrary to the nozzle configuration, one would expect the skin friction drag through a diffuser to decrease with respect to the zero pressure gradient setting. This, however, was not the case for the data gathered. While

an attempt will be made to apply some sort of logic to the data, any suggested relationships or conclusions should be accepted with a great deal of reservation. Upon completion of the data reduction, a pressure adjustment of 77% was applied. The results are shown in Figure 4.9.

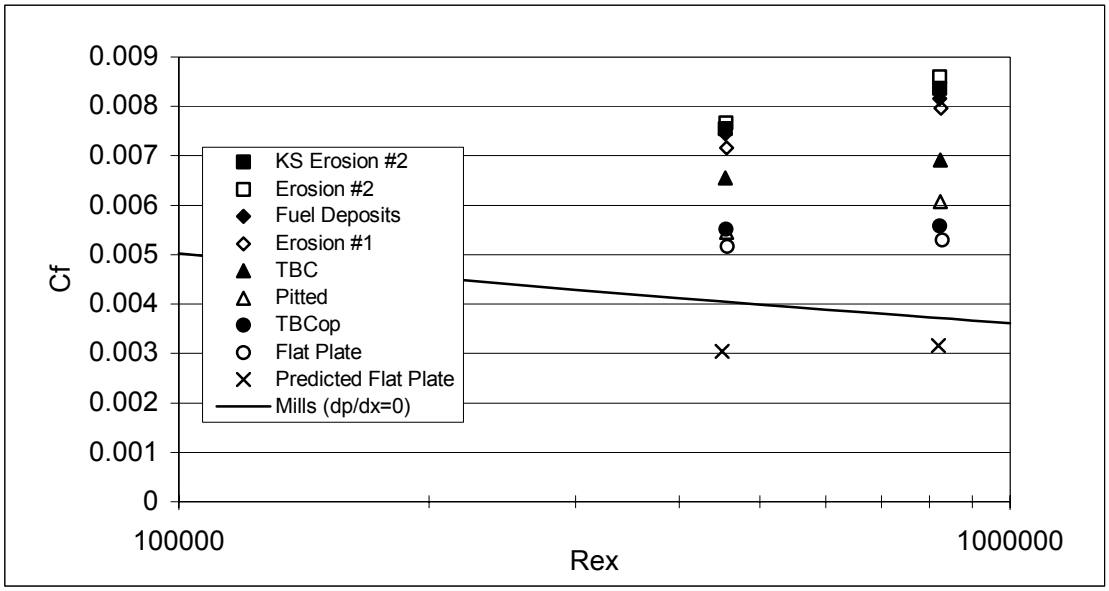

Figure 4.9 C_f Variations Under Adverse Pressure Gradient Conditions

As already alluded, the actual results did not even approximate the predicted values. In fact, the smooth data obtained were over 1½ times that of the predicted values. The predicted skin friction values, determined used the method described in Section 2.5, were C_f=0.003162 for the high Re_x and C_f=0.003041 for the low Re_x. Interestingly though, when the pressure adjustment was reduced by half, the data displayed a considerable shift towards the predicted curves as shown in Figure 4.10.

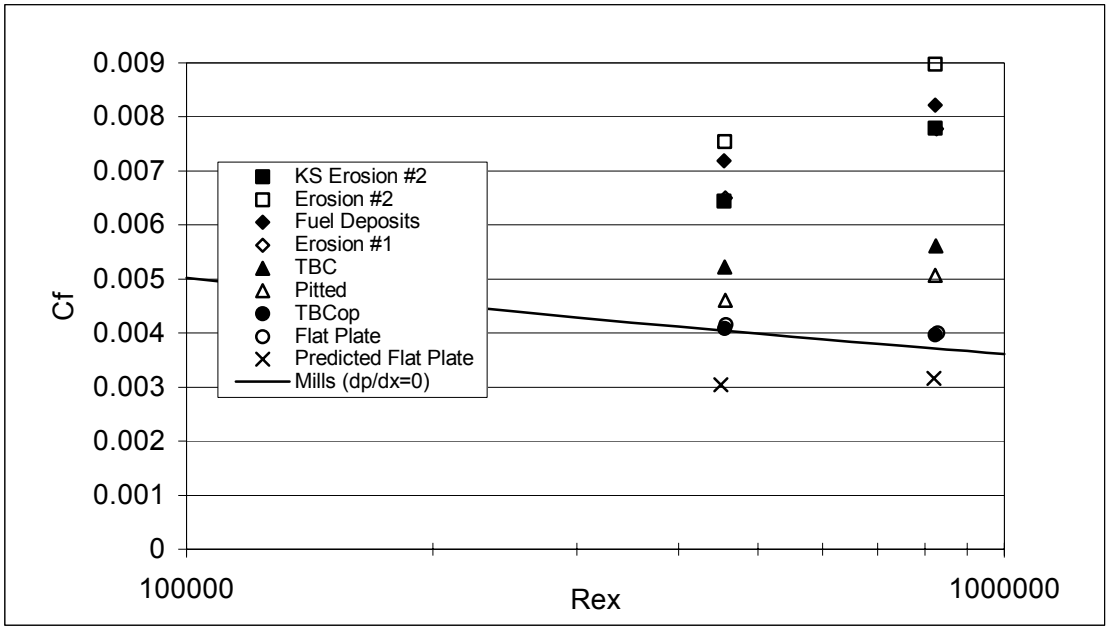

Figure 4.10 Adjusted C_f Variations Under Adverse Pressure Gradient Conditions

In comparing Figures 4.9 and 4.10 it is interesting to note that the decrease in the pressure adjustment had a stronger impact on the smoother panels. From this it could be thought that smoother surfaces are more dependent upon pressure forces, whereas rougher surfaces greatly rely on shear forces.

When attempting to find a cause for the unusual results, it was also found that the pressure being recorded was greatly dependent upon the trailing edge gap. Although the displacement of the plate remained fairly consistent, the pressure readings varied with respect to the trailing edge gap. Although a definite explanation has yet to be determined, it was deduced that the pressure ports, under certain conditions, could possibly be exposed to some of the dynamic pressure from the flow. Because this was only possible on the trailing edge, the pressure delta recorded was typically more negative than usual. This,

in turn, caused the overall pressure recorded to increase, thus yielding higher than normal C_f values.

Although the conditions under which the panels were tested did not accurately represent the true conditions of an adverse pressure gradient, the trend among the roughness panels seem to support some of the conclusions drawn from the zero pressure gradient data. As shown in Figure 4.11, the trend among the roughness panels was exactly the same as those found earlier. This was again reassuring as it supported the established roughness trend. The percentage increases, though, when compared to the zero pressure gradient results, were not as sharp.

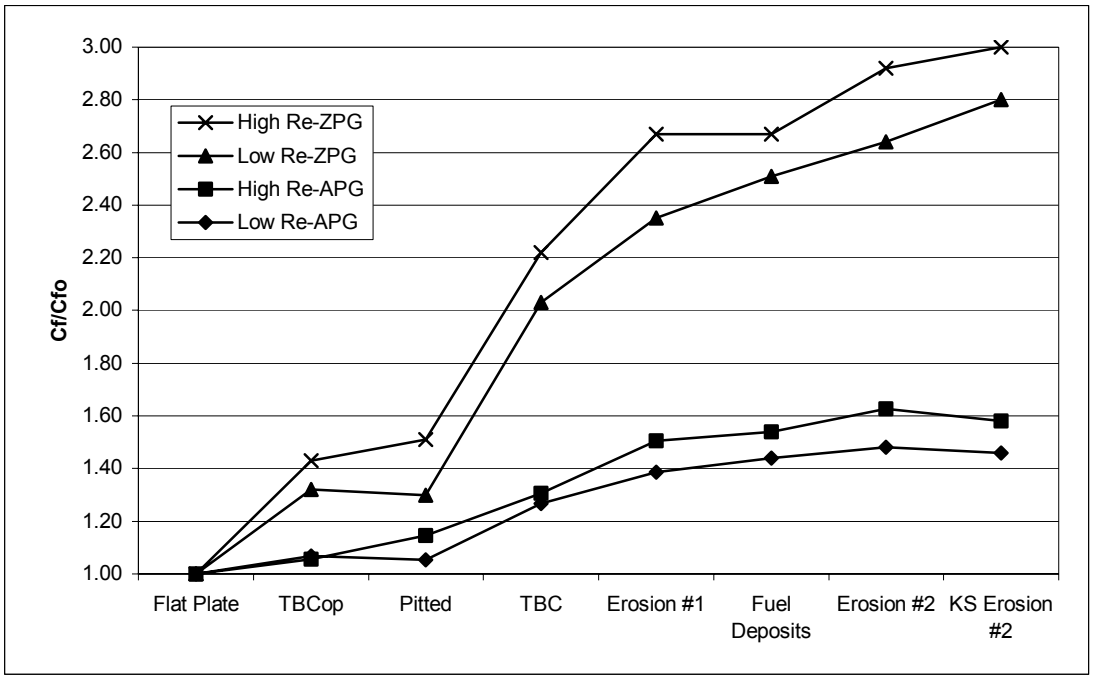

Figure 4.11 C_f Ratio Comparisons for Zero and Adverse Pressure Gradients

4.3 Heat Transfer Results

Using the method described in chapter three, heat transfer data was taken in an attempt to corroborate the bulk drag data. Using a Microsoft Excel program established during Drab's research, the Stanton numbers for the flat plate and TBC surface at each of the aforementioned pressure gradients was determined. The results, plotted against Reynolds number are shown in Figure 4.12.

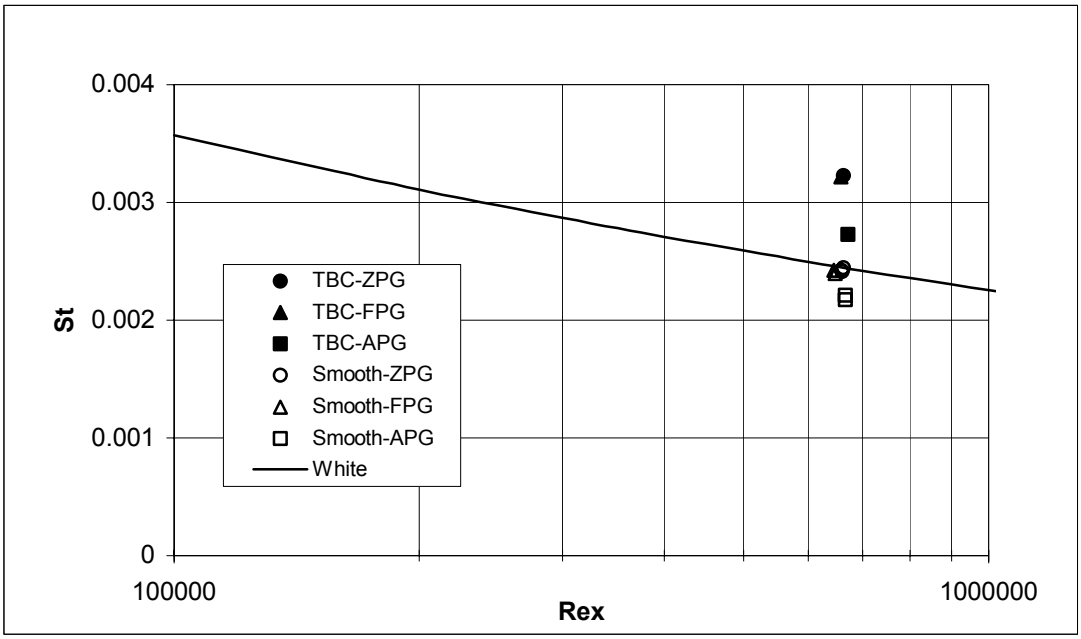

Figure 4.12 Combined Stanton Number Results

As expected, the Stanton results for the flat plate with zero pressure gradient placed precisely where predicted with St=0.00243. The corresponding TBC results averaged 133% higher with St=0.00323. For the diffuser configuration, the flat plate results dropped as anticipated to St=0.00219 with the TBC values lying approximately 124% higher at St=0.00273. The favorable pressure gradient results, instead of increasing, landed at approximately the same position as the zero pressure gradient data. It was thought that the hole

used for the infrared camera could possible skew the data. After taking a velocity profile with the hole both open and covered, it was determined that the hole in the tunnel ceiling was, most likely, the cause for the inaccurate results. In order to eliminate this effect, another method of taking infrared camera images would need to be explored.

V. Conclusions and Recommendations

5.1 Conclusions

This investigation was encouraged by the need to better understand the effects of freestream turbulence, pressure gradients, and surface roughness on the shear drag associated with turbine blading. Using facsimiles of real turbine blade surfaces, roughness statistics and skin friction coefficients were fashioned. The roughness statistics were further related to the well-researched sandgrain roughness through empirical correlations. Shear drag tests were taken using various combinations of the aforementioned effects. The various conclusions emerging from the experiments follow.

As discussed in chapter 4, the statistical descriptors associated with a given surface can provide great insight toward the surface's physical appearance. The average centerline roughness, R_a, commonly associated with equivalent sandgrain roughness, is often used to predict C_f, but, as noted by both Acharya et al. (1986:34) and Bogard et al. (1998:337), appears inadequate in the specification of skin friction effects. While the majority of the statistical descriptors yielded insignificant relationships when compared to k_s, skewness, kurtosis, and α_{rms}, however, appear to have a prevailing role in predicting skin friction coefficients, as panels having larger kurtosis generally resulted in greater increases in shear drag. It was also found that increasing Reynolds number exacerbates the effects of roughness.

As expected, increases in freestream turbulence resulted in increases in shear drag. When combined with roughness, the effect was worsened. This was, again, further aggravated with increases in Reynolds number. When the combined effect of freestream turbulence and surface roughness was compared to the sum of individual effects, it was found that the combined measurements yielded consistently higher skin friction values than the corresponding sum of the parts. At the high Reynolds number and 5% freestream turbulence, the measured results yielded values 7.2% to 11.8% higher. Increasing freestream turbulence to 11% resulted in increases of 9.7% to 15.7%. The measured values at the low Reynolds number, for both turbulence levels, were approximately 9.4% higher than the corresponding calculated values.

Though the pressure gradient tests are suspect due to the measure pressure effects, the following qualitative comments are offered. When a favorable pressure gradient was introduced, roughness effects were amplified. Conversely, introduction of an adverse pressure gradient resulted in decreasing roughness effects. Both pressure gradients, however, gave way to the exacerbation seen at higher Reynolds numbers. In performing the pressure gradient tests, it was also found that smoother surfaces were typically dominated by the pressure forces seen at the leading and trailing edges, whereas rougher surfaces were generally subject to the shear forces.

5.2 Recommendations

It was shown in the preceding chapter that adjusting the percentage associated with the pressure readings greatly affected the resulting skin friction coefficient for the case of non-zero pressure gradient. In order to better understand this phenomenon, a more accurate system of reading pressures along the leading and trailing edges should be developed. This could be accomplished by simply adding more pressure ports along these boundaries. Doing so would, in turn, provide the capability to measure the actual pressure distribution along the surface. Consequently, a more accurate average pressure could then be determined. This would hopefully eliminate the need for the pressure adjustment used throughout the previous data reduction.

During the final stage of the research it was found that the pressure recorded at the trailing edge port was dependent upon the corresponding gap. This development was never encountered during the two previous phases. For this reason, it would be advantageous to recreate the earlier configurations and test the dependency of the pressure on the trailing edge gap.

In an effort to eliminate the aforementioned difficulties with the trailing edge pressure, a trailing edge shim, similar to that of the leading edge, could be attached. By mounting a shim to the trailing edge of the hanging plate, the possibility of flow entering the gap could be eliminated altogether. There is, however, an inherent difficulty therein due to the position of the hanging plate with respect to the tunnel floor. As shown in Figure 3.5, the trailing edge of the plate is seated below the tunnel floor thus requiring the floor to be lowered

approximately 0.003. Consequently, the affect of lowering the tunnel floor would need to be studied.

If the aforementioned problems could effectively be eliminated, it would then be possible to research the true effects of adverse and favorable pressure gradients. If accurate reliable results could be obtained on the combined effects of roughness and pressure gradients it would greatly benefit the understanding turbine performance and efficiency.

Appendix A: Example of Skin Friction Data

Capacitec	Voltage	TC-1	TC-2	TC-3	Velocity	Tu	Rex	Transducer	Voltage	Density
1.353	1.353	68.495	68.817	68.502	0.164	2.64	12525.3	0.098	0.098	1.178
1.354	1.354	68.128	68.627	68.48	0.166	2.576	12639.6	0.098	0.098	1.178
1.354	1.354	68.251	68.67	68.506	0.164	2.618	12505.5	0.098	0.098	1.178
1.354	1.354	68.317	68.637	68.515	0.162	2.625	12401.2	0.098	0.098	1.178
1.353	1.354	68.429	68.711	68.522	0.162	2.696	12332.6	0.098	0.098	1.178
1.353	1.354	68.407	68.75	68.529	0.16	2.61	12240.6	0.098	0.098	1.178
1.353	1.354	68.443	68.648	68.508	0.162	3.129	12393.6	0.098	0.098	1.178
1.354	1.354	68.403	68.603	68.469	0.165	2.77	12584.2	0.098	0.098	1.178
1.353	1.354	68.481	68.574	68.468	0.166	2.699	12649.6	0.099	0.098	1.178
1.354	1.354	68.345	68.617	68.476	0.164	2.856	12502.8	0.099	0.098	1.178
1.354	1.354	68.334	68.697	68.437	0.159	2.604	12117.7	0.099	0.098	1.178
1.354	1.354	68.273	68.757	68.481	0.158	2.648	12080.2	0.098	0.098	1.178
1.353	1.354	68.483	68.893	68.502	0.16	2.597	12169.5	0.098	0.098	1.177
1.353	1.354	68.238	68.94	68.429	0.16	2.641	12198.2	0.098	0.098	1.177
1.355	1.354	68.177	69.063	68.438	0.161	2.667	12249.2	0.098	0.098	1.177
1.354	1.354	68.244	69.28	68.378	0.162	2.656	12306.8	0.099	0.098	1.176
1.355	1.354	68.179	69.442	68.41	0.162	2.623	12333.4	0.099	0.098	1.176
1.354	1.354	68.24	69.499	68.454	0.162	2.611	12339.7	0.099	0.098	1.176
1.353	1.354	68.338	69.435	68.537	0.162	2.621	12329.0	0.099	0.098	1.176
1.354	1.354	68.301	69.389	68.488	0.162	2.61	12300.3	0.099	0.098	1.176
1.353	1.354	68.203	69.3	68.465	0.161	2.614	12271.0	0.099	0.098	1.176
1.354	1.354	68.201	69.135	68.515	0.162	2.717	12383.1	0.098	0.098	1.177
1.354	1.354	68.49	69.213	68.636	0.163	2.649	12423.1	0.099	0.098	1.177
1.352	1.354	68.398	69.165	68.544	NaN	NaN	NaN	0.098	0.098	1.177
1.353	1.354	68.353	69.051	68.461	0.16	2.729	12230.8	0.099	0.098	1.177
1.352	1.354	68.218	69.046	68.435	0.161	2.791	12274.1	0.098	0.098	1.177
1.352	1.354	68.559	68.91	68.446	0.165	2.818	12620.3	0.099	0.098	1.177
1.353	1.354	68.583	68.849	68.448	0.167	2.782	12750.9	0.099	0.098	1.177
1.354	1.354	68.464	68.798	68.422	0.165	2.718	12618.7	0.098	0.098	1.178
1.354	1.354	68.42	68.704	68.425	0.165	2.773	12601.3	0.098	0.098	1.178
1.354	1.354	68.319	68.727	68.467	0.164	2.735	12537.6	0.098	0.098	1.178
1.355	1.354	68.294	68.744	68.458	0.163	2.797	12415.2	0.099	0.098	1.178
1.353	1.354	68.443	68.744	68.442	0.161	2.812	12291.8	0.098	0.098	1.178
1.354	1.354	68.361	68.764	68.447	0.162	2.76	12342.2	0.098	0.098	1.178
1.353	1.354	68.267	68.726	68.466	0.165	3.019	12622.6	0.098	0.098	1.178
1.353	1.354	68.289	68.466	68.395	0.171	2.748	13070.6	0.098	0.098	1.178
1.353	1.354	68.289	68.54	68.428	0.166	2.849	12684.6	0.098	0.098	1.178
1.353	1.354	68.286	68.53	68.49	0.167	3.125	12727.9	0.098	0.098	1.178
1.354	1.354	68.481	68.438	68.542	0.177	3.447	13495.6	0.098	0.098	1.178
1.412	1.356	68.602	68.334	68.552	1.37	102.58	104704.4	0.116	0.099	1.179
1.635	1.365	68.352	68.002	68.503	7.056	7.509	539964.9	0.129	0.1	1.18
1.662	1.375	68.311	67.772	68.465	7.557	1.633	578784.7	0.099	0.1	1.18
2.241	1.405	68.299	67.634	68.477	12.83	1.594	983124.3	0.149	0.102	1.18
2.28	1.436	68.362	67.635	68.49	12.838	1.76	983730.8	0.111	0.102	1.18
2.159	1.462	68.445	67.622	68.481	11.972	1.125	917385.5	0.112	0.103	1.181
2.162	1.489	68.423	67.534	68.494	11.969	2.337	917496.3	0.111	0.103	1.181
2.153	1.516	68.313	67.496	68.513	11.955	1.094	916536.3	0.109	0.103	1.181
2.156	1.543	68.294	67.432	68.495	11.968	1.026	917712.1	0.108	0.104	1.181
2.159	1.57	68.299	67.382	68.513	11.964	1.119	917554.1	0.11	0.104	1.181
2.156	1.596	68.297	67.416	68.538	11.964	1.034	917439.8	0.11	0.104	1.181
2.157	1.623	68.35	67.395	68.521	11.943	1.088	915927.0	0.109	0.105	1.181
2.164	1.65	68.479	67.407	68.558	11.972	1.175	918087.1	0.112	0.105	1.181
2.161	1.677	68.518	67.444	68.524	11.976	1.131	918322.1	0.11	0.106	1.181
2.161	1.704	68.53	67.379	68.526	11.959	1.017	917222.8	0.109	0.106	1.181
2.159	1.731	68.521	67.394	68.519	11.974	1.059	918351.5	0.109	0.106	1.181
2.161	1.758	68.405	67.356	68.556	11.986	1.073	919367	0.11	0.107	1.181
2.156	1.785	68.335	67.35	68.556	11.958	1.068	917235.3	0.109	0.107	1.181
2.157	1.811	68.206	67.297	68.46	11.938	1.134	915839.6	0.11	0.107	1.181
2.159	1.838	68.324	67.326	68.493	11.967	1.128	918024.0	0.11	0.108	1.181
2.154	1.865	68.329	67.379	68.504	11.951	1.077	916630.7	0.111	0.108	1.181
2.158	1.892	68.226	67.347	68.485	11.959	1.101	917293.8	0.112	0.109	1.181
2.157	1.918	68.33	67.403	68.525	11.962	1.04	917373.1	0.11	0.109	1.181
2.157	1.945	68.16	67.337	68.49	11.953	1.015	916912.0	0.108	0.109	1.181

2.158	1.972	68.326	67.356	68.518	11.958	1.151	917187.1	0.109	0.11	1.181
2.155	1.999	68.412	67.356	68.597	11.948	1.036	916429.3	0.111	0.11	1.181
2.163	2.026	68.32	67.398	68.551	11.975	1.172	918358.2	0.111	0.111	1.181
2.16	2.053	68.453	67.38	68.554	11.959	1.222	917206.2	0.112	0.111	1.181
2.158	2.079	68.425	67.388	68.541	11.952	1.029	916627.5	0.109	0.111	1.181
2.162	2.106	68.511	67.351	68.497	11.962	1.149	917558.6	0.112	0.112	1.181
2.158	2.131	68.533	67.342	68.529	11.958	1.057	917292.5	0.111	0.112	1.181
2.165	2.149	68.462	67.309	68.56	11.966	1.043	917976	0.111	0.111	1.181
2.156	2.165	68.488	67.364	68.573	11.955	1.149	916968.8	0.109	0.111	1.181
2.162	2.163	68.43	67.372	68.558	11.962	1.035	917448.8	0.111	0.11	1.181
2.16	2.159	68.381	67.356	68.459	11.961	1.068	917425.5	0.11	0.11	1.181
2.163	2.159	68.323	67.323	68.494	11.971	1.061	918332.2	0.111	0.11	1.181
2.161	2.159	68.314	67.282	68.514	11.952	1.163	917026.6	0.111	0.11	1.181
2.157	2.159	68.433	67.273	68.562	11.941	3.301	916180.7	0.111	0.11	1.181
2.161	2.159	68.422	67.361	68.517	11.959	1.08	917253.2	0.111	0.11	1.181
2.155	2.159	68.416	67.323	68.446	11.943	1.057	916139.7	0.108	0.11	1.181
2.157	2.159	68.24	67.251	68.465	11.955	1.053	917357.5	0.111	0.11	1.181
2.157	2.159	68.444	67.311	68.533	11.951	1.04	916855.9	0.108	0.11	1.181
2.158	2.159	68.409	67.319	68.534	11.953	1.064	916936.6	0.11	0.11	1.181
2.158	2.159	68.421	67.271	68.553	11.96	1.126	917649.9	0.109	0.11	1.181
2.158	2.159	68.443	67.36	68.493	11.958	1.08	917181.0	0.11	0.11	1.181
2.164	2.159	68.347	67.324	68.495	11.966	1.078	917961.5	0.112	0.11	1.181
2.162	2.159	68.41	67.284	68.527	11.967	1.085	918157	0.11	0.11	1.181
2.164	2.159	68.45	67.312	68.568	11.965	1.099	917862	0.11	0.11	1.181
2.159	2.159	68.469	67.36	68.582	11.97	1.11	918155.5	0.11	0.11	1.181
2.164	2.159	68.603	67.375	68.53	11.955	1.125	916918.0	0.11	0.11	1.181
2.157	2.159	68.545	67.295	68.51	11.955	1.072	917192.5	0.11	0.11	1.181
2.161	2.16	68.482	67.311	68.513	11.97	1.135	918251.8	0.111	0.11	1.181
2.159	2.16	68.502	67.264	68.52	11.949	1.108	916846.8	0.113	0.11	1.181
2.166	2.16	68.558	67.33	68.59	11.971	1.23	918262.2	0.111	0.11	1.181
2.159	2.16	68.538	67.353	68.57	11.968	1.1	918022.0	0.112	0.111	1.181
2.156	2.16	68.5	67.347	68.539	11.95	1.058	916588.8	0.11	0.111	1.181
2.156	2.16	68.54	67.298	68.53	11.96	1.073	917514.8	0.11	0.111	1.181
1.736	2.146	68.556	67.274	68.581	8.291	26.983	636091	0.141	0.112	1.181
1.631	2.128	68.557	67.306	68.527	6.649	1.197	510089.3	0.096	0.111	1.181
1.537	2.107	68.581	67.272	68.533	6.655	1.262	510635.3	0.095	0.111	1.181
1.606	2.089	68.57	67.338	68.573	6.643	1.256	509602.8	0.096	0.11	1.181
1.572	2.069	68.451	67.246	68.546	6.65	1.191	510280	0.095	0.11	1.181
1.585	2.05	68.523	67.422	68.548	6.65	1.251	509990.3	0.096	0.109	1.181
1.581	2.031	68.502	67.394	68.601	6.644	1.273	509510.7	0.096	0.109	1.181
1.585	2.012	68.537	67.504	68.566	6.659	1.199	510512.9	0.096	0.108	1.181
1.583	1.992	68.522	67.489	68.546	6.648	1.205	509658.3	0.096	0.108	1.181
1.583	1.973	68.646	67.501	68.574	NaN	NaN	NaN	0.096	0.107	1.181
1.582	1.954	68.593	67.522	68.607	6.657	1.236	510313.4	0.097	0.107	1.181
1.583	1.934	68.544	67.496	68.578	6.66	1.213	510609.0	0.095	0.106	1.181
1.583	1.915	68.467	67.52	68.527	6.652	1.186	509938.3	0.096	0.106	1.181
1.584	1.896	68.696	67.693	68.605	6.684	1.256	512067.8	0.097	0.105	1.18
1.583	1.877	68.532	67.586	68.544	6.666	1.246	510861.5	0.097	0.105	1.181
1.582	1.858	68.455	67.549	68.563	6.643	1.22	509193.2	0.096	0.104	1.181
1.584	1.839	68.434	67.639	68.526	6.671	1.198	511177.5	0.096	0.104	1.18
1.585	1.82	68.435	67.59	68.561	6.673	1.264	511432.2	0.097	0.103	1.181
1.584	1.8	68.553	67.603	68.612	6.655	1.151	510026.6	0.096	0.103	1.181
1.583	1.781	68.572	67.598	68.683	6.651	1.211	509708.6	0.097	0.102	1.181
1.583	1.762	68.586	67.659	68.682	6.659	1.184	510210	0.096	0.102	1.18
1.583	1.743	68.554	67.657	68.57	6.66	1.215	510280.6	0.096	0.102	1.18
1.582	1.723	68.527	67.638	68.567	6.678	1.207	511739.7	0.095	0.101	1.18
1.583	1.704	68.531	67.696	68.54	6.665	1.206	510573.0	0.095	0.101	1.18
1.585	1.685	68.548	67.662	68.533	6.667	1.219	510850.2	0.096	0.1	1.18
1.581	1.666	68.585	67.618	68.595	6.643	1.214	509100.4	0.096	0.1	1.181
1.584	1.646	68.504	67.635	68.545	6.678	1.218	511683.5	0.097	0.099	1.18
1.58	1.627	68.581	67.614	68.554	6.637	1.175	508597.9	0.095	0.099	1.181
1.585	1.608	68.675	67.636	68.578	6.658	1.21	510182.1	0.096	0.098	1.18
1.587	1.589	68.777	67.641	68.667	6.67	1.195	511126.9	0.097	0.098	1.18
1.584	1.584	68.709	67.683	68.662	6.67	1.187	511016.5	0.094	0.096	1.18
1.582	1.582	68.629	67.688	68.581	NaN	NaN	NaN	0.096	0.096	1.18
1.58	1.584	68.66	67.627	68.585	6.663	1.192	510548.3	0.097	0.096	1.181
1.58	1.583	68.84	67.699	68.613	6.638	1.207	508537.9	0.095	0.096	1.18
1.582	1.583	68.706	67.634	68.581	6.657	1.227	510070.5	0.094	0.096	1.18

1.582	1.583	68.912	67.803	68.653	6.67	1.248	510788	0.095	0.096	1.18
1.58	1.583	68.776	67.755	68.624	NaN	NaN	NaN	0.095	0.096	1.18
1.582	1.583	68.761	67.7	68.564	6.657	1.241	509974.1	0.095	0.096	1.18
1.584	1.583	68.828	67.71	68.61	6.653	1.208	509632.0	0.097	0.096	1.18
1.582	1.583	68.811	67.745	68.643	6.653	1.202	509631.1	0.095	0.096	1.18
1.58	1.583	68.779	67.786	68.58	6.655	1.192	509694.4	0.096	0.096	1.18
1.582	1.583	68.785	67.801	68.53	6.672	1.149	510973.2	0.096	0.096	1.18
1.582	1.583	68.847	67.75	68.57	6.661	1.205	510209.4	0.096	0.096	1.18
1.584	1.583	68.825	67.776	68.529	6.663	1.285	510334.7	0.096	0.096	1.18
1.583	1.583	68.815	67.749	68.497	6.658	1.166	510002.0	0.095	0.096	1.18
1.579	1.583	68.683	67.75	68.542	6.653	1.256	509564.2	0.096	0.096	1.18
1.582	1.583	68.849	67.801	68.591	6.669	1.176	510685.4	0.096	0.096	1.18
1.583	1.582	68.735	67.78	68.581	6.664	1.191	510347.0	0.096	0.096	1.18
1.581	1.582	68.57	67.737	68.592	6.657	1.208	509952.5	0.095	0.096	1.18
1.581	1.582	68.668	67.733	68.62	6.66	1.217	510183.1	0.095	0.096	1.18
1.582	1.582	68.859	67.779	68.632	6.607	1.788	505978.5	0.096	0.096	1.18
1.505	1.58	68.752	67.828	68.579	2.665	67.069	204052.1	0.156	0.098	1.18
1.398	1.574	68.589	68.078	68.556	1.589	14.159	121555.3	0.154	0.1	1.179
1.398	1.567	68.619	68.202	68.554	1.64	10.331	125437.3	0.147	0.101	1.179
1.376	1.56	68.634	68.253	68.55	1.419	17.995	108533.5	0.128	0.102	1.179
1.366	1.553	68.573	68.312	68.56	0.771	14.873	58936.5	0.106	0.103	1.179
1.361	1.546	68.601	68.194	68.608	0.505	15.63	38592.5	0.101	0.103	1.179
1.358	1.538	68.813	68.4	68.682	0.406	9.227	30994.0	0.099	0.103	1.179
1.357	1.531	68.793	68.361	68.619	0.353	9.45	26945.5	0.098	0.103	1.179
1.357	1.523	68.723	68.332	68.583	0.31	13.031	23672.8	0.099	0.103	1.179
1.356	1.516	68.737	68.309	68.586	0.252	7.379	19245.3	0.099	0.103	1.179
1.358	1.508	68.75	68.291	68.615	0.218	8.043	16662.8	0.098	0.103	1.179
1.357	1.501	68.806	68.309	68.652	0.188	9.985	14354.9	0.098	0.103	1.179
1.358	1.493	68.808	68.305	68.633	0.184	4.571	14032.8	0.098	0.103	1.179
1.358	1.486	68.859	68.297	68.596	0.182	4.204	13946.7	0.099	0.104	1.179
1.358	1.478	68.931	68.242	68.604	0.18	2.759	13731.9	0.098	0.104	1.179
1.357	1.471	69.03	68.303	68.669	0.164	2.891	12519.8	0.1	0.104	1.179
1.358	1.463	69.036	68.573	68.724	0.161	2.775	12287.8	0.099	0.104	1.178
1.356	1.456	68.964	68.786	68.642	0.163	2.8	12467.1	0.097	0.104	1.178
1.358	1.448	68.832	68.704	68.597	0.164	2.767	12514.6	0.099	0.104	1.178
1.358	1.441	68.639	68.616	68.544	0.163	2.689	12478.4	0.098	0.104	1.178
1.357	1.433	68.829	68.744	68.603	0.163	2.706	12436.4	0.099	0.104	1.178
1.358	1.426	68.772	68.932	68.571	0.163	2.784	12420.2	0.098	0.104	1.177
1.356	1.418	68.808	69.177	68.584	0.163	2.726	12413.5	0.098	0.104	1.177
1.356	1.411	68.899	69.257	68.641	0.163	2.741	12420.3	0.099	0.105	1.176
1.356	1.403	68.864	69.327	68.595	0.163	2.719	12442.6	0.098	0.105	1.176
1.356	1.396	68.771	69.316	68.583	0.163	2.752	12434.2	0.098	0.105	1.176
1.357	1.388	68.937	69.411	68.616	0.163	2.688	12435.9	0.098	0.105	1.176
1.359	1.381	68.603	69.324	68.56	0.163	2.759	12412.3	0.098	0.105	1.176
1.357	1.373	68.801	69.354	68.548	0.163	2.735	12431.2	0.098	0.105	1.176
1.358	1.366	68.768	69.224	68.521	0.163	2.747	12453.6	0.099	0.105	1.177
1.357	1.361	68.756	69.18	68.602	0.164	2.75	12504.7	0.098	0.103	1.177
1.355	1.359	68.728	69.256	68.594	0.164	2.751	12468.6	0.098	0.101	1.176
1.358	1.358	68.607	69.328	68.547	0.163	2.747	12432.8	0.098	0.1	1.176
1.358	1.358	68.67	69.376	68.585	0.163	2.713	12428.4	0.098	0.099	1.176
1.358	1.357	68.665	69.409	68.598	0.163	2.754	12419.3	0.099	0.098	1.176
1.355	1.357	68.616	69.343	68.599	0.163	2.755	12400.2	0.099	0.098	1.176
1.355	1.357	68.603	69.436	68.611	0.163	2.738	12412.8	0.099	0.098	1.176
1.356	1.357	68.662	69.374	68.577	0.163	2.745	12381.2	0.097	0.098	1.176
1.357	1.357	68.742	69.471	68.645	0.163	2.76	12384.0	0.098	0.098	1.176
1.357	1.357	68.765	69.555	68.645	0.163	2.688	12388.5	0.099	0.098	1.176
1.359	1.357	68.702	69.785	68.662	0.163	2.704	12403.9	0.099	0.098	1.175
1.357	1.357	68.572	69.817	68.625	0.163	2.743	12393.8	0.099	0.098	1.175
1.355	1.357	68.796	70.016	68.61	0.164	2.721	12432.3	0.099	0.098	1.175
1.355	1.357	68.599	69.864	68.579	0.163	2.688	12424.1	0.097	0.098	1.175
1.356	1.357	68.806	69.738	68.641	0.163	2.747	12386.6	0.098	0.098	1.175
1.357	1.357	68.782	69.883	68.634	0.164	2.696	12441.2	0.099	0.098	1.175
1.356	1.357	68.67	70.013	68.666	0.164	2.719	12463.6	0.099	0.098	1.175
1.357	1.357	68.593	70.003	68.596	0.164	2.695	12458.8	0.099	0.098	1.175
1.359	1.357	68.573	69.992	68.638	0.164	2.777	12481.4	0.099	0.098	1.175
1.358	1.357	68.654	70.032	68.638	0.164	2.758	12463.3	0.098	0.098	1.175
1.357	1.357	68.666	70.053	68.65	0.164	2.725	12459.5	0.098	0.098	1.175
1.357	1.357	68.569	69.814	68.618	0.163	2.726	12384.8	0.099	0.098	1.175

1.357	1.357	68.47	69.844	68.584	0.163	2.724	12369.0	0.098	0.098	1.175
1.356	1.357	68.522	69.88	68.576	0.163	2.747	12381.6	0.097	0.098	1.175
1.358	1.357	68.515	69.874	68.573	0.163	2.741	12392.3	0.099	0.098	1.175
1.357	1.357	68.612	69.891	68.581	0.163	2.73	12384.6	0.098	0.098	1.175
1.357	1.357	68.756	69.907	68.59	0.163	2.748	12373.5	0.098	0.098	1.175
1.357	1.357	68.603	69.727	68.612	0.162	2.731	12336.3	0.098	0.098	1.175
1.358	1.357	68.54	69.596	68.628	0.162	2.753	12297.9	0.098	0.098	1.176
1.36	1.357	68.497	69.625	68.616	0.162	2.736	12318.2	0.099	0.098	1.176
1.359	1.357	68.5	69.533	68.654	0.163	2.763	12371.3	0.099	0.098	1.176
1.358	1.357	68.511	69.631	68.586	0.162	2.767	12331.6	0.098	0.098	1.176
1.357	1.357	68.457	69.847	68.591	0.163	2.704	12429.7	0.099	0.098	1.175
1.357	1.357	68.314	69.876	68.492	0.163	2.728	12388.6	0.1	0.099	1.175
1.357	1.357	68.433	69.903	68.612	0.163	2.769	12384.1	0.099	0.099	1.175
1.355	1.357	68.578	69.732	68.633	0.163	2.682	12369.2	0.098	0.099	1.175
1.356	1.357	68.568	69.454	68.529	0.164	2.893	12515.5	0.098	0.099	1.176
1.356	1.357	68.512	69.126	68.587	0.175	3.787	13303.4	0.099	0.099	1.177
1.356	1.357	68.584	68.901	68.585	0.195	3.486	14884.7	0.097	0.099	1.177
1.355	1.357	68.851	68.774	68.637	0.203	2.597	15466.2	0.098	0.098	1.178
1.357	1.357	68.773	68.657	68.586	0.205	4.117	15666.8	0.098	0.098	1.178
1.357	1.357	68.676	68.539	68.568	0.18	5.311	13725.1	0.098	0.098	1.178
1.356	1.357	69.127	68.655	68.566	0.17	3.1	12969.4	0.098	0.098	1.178
1.356	1.357	68.84	68.574	68.524	0.167	3.889	12770.3	0.098	0.098	1.178
1.5	1.362	68.935	68.207	68.537	2.873	72.2	219730.3	0.139	0.1	1.179
1.653	1.372	68.731	67.8	68.505	6.865	5.566	525756.3	0.113	0.1	1.18
1.653	1.382	68.779	67.715	68.567	6.912	5.477	529475.1	0.098	0.1	1.18
2.255	1.411	68.878	67.756	68.573	12.001	6.773	919211.2	0.17	0.103	1.18
2.245	1.441	68.565	67.66	68.567	12.009	5.903	920168.3	0.105	0.103	1.18
2.264	1.471	68.381	67.602	68.525	11.338	4.948	868894.8	0.108	0.103	1.181
2.205	1.499	68.218	67.603	68.537	11.33	5.053	868261.7	0.106	0.103	1.181
2.236	1.529	68.281	67.534	68.526	11.328	4.83	868369.7	0.105	0.104	1.181
2.224	1.558	68.307	67.52	68.588	11.366	5.068	871284.9	0.105	0.104	1.181
2.229	1.587	68.403	67.519	68.634	11.296	4.974	865924.1	0.108	0.104	1.181
2.224	1.616	68.408	67.498	68.652	11.355	4.762	870523.1	0.105	0.104	1.181
2.224	1.645	68.24	67.461	68.613	11.309	4.876	867118.8	0.101	0.104	1.181
2.216	1.673	68.235	67.45	68.6	11.316	5.127	867717	0.108	0.105	1.181
2.217	1.702	68.289	67.514	68.597	11.351	5.211	870197.6	0.106	0.105	1.181
2.229	1.731	68.227	67.487	68.557	11.373	5.188	871919.3	0.105	0.105	1.181
2.228	1.76	68.299	67.446	68.621	11.326	4.873	868476.4	0.106	0.105	1.181
2.222	1.789	68.398	67.495	68.619	11.371	5.138	871735.1	0.105	0.106	1.181
2.225	1.818	68.35	67.47	68.576	11.361	5.06	871038.7	0.105	0.106	1.181
2.223	1.846	68.345	67.467	68.585	11.349	5.25	870123.8	0.104	0.106	1.181
2.225	1.875	68.528	67.573	68.625	11.352	5.382	870020.5	0.105	0.106	1.181
2.23	1.904	68.403	67.437	68.613	11.342	5.23	869685.1	0.106	0.107	1.181
2.225	1.933	68.467	67.478	68.642	11.338	5.138	869303.1	0.105	0.107	1.181
2.228	1.962	68.465	67.404	68.613	11.406	5.087	874729.3	0.106	0.107	1.181
2.239	1.992	68.429	67.482	68.641	11.386	5.049	872949.3	0.107	0.107	1.181
2.222	2.021	68.412	67.449	68.604	11.404	4.887	874436.4	0.105	0.108	1.181
2.228	2.05	68.434	67.464	68.618	11.403	4.825	874322.5	0.105	0.108	1.181
2.224	2.079	68.396	67.484	68.622	11.347	5.09	869939.9	0.107	0.108	1.181
2.229	2.108	68.502	67.509	68.6	11.343	4.85	869577.2	0.104	0.108	1.181
2.228	2.137	68.463	67.517	68.604	11.368	4.92	871437.7	0.107	0.109	1.181
2.223	2.166	68.473	67.486	68.591	11.332	4.944	868768.6	0.106	0.109	1.181
2.236	2.19	68.459	67.43	68.596	11.325	5.261	868419.3	0.108	0.108	1.181
2.219	2.209	68.446	67.47	68.565	11.354	4.822	870558.1	0.105	0.108	1.181
2.227	2.228	68.455	67.217	68.461	11.357	5.131	871555.2	0.102	0.108	1.182
2.223	2.227	68.462	67.419	68.615	11.408	5.016	874795.3	0.105	0.106	1.181
2.23	2.227	68.469	67.4	68.594	11.312	5.103	867507.2	0.107	0.106	1.181
2.225	2.226	68.422	67.43	68.501	11.361	4.767	871213.0	0.108	0.106	1.181
2.226	2.226	68.442	67.422	68.566	11.389	4.947	873380.1	0.106	0.106	1.181
2.228	2.226	68.544	67.495	68.594	11.378	4.851	872264.2	0.106	0.106	1.181
2.223	2.226	68.565	67.422	68.562	11.369	5.036	871862.1	0.106	0.106	1.181
2.226	2.226	68.659	67.469	68.577	11.367	5.269	871538.6	0.104	0.105	1.181
2.227	2.226	68.546	67.402	68.529	11.434	5.044	876875.4	0.105	0.105	1.181
2.223	2.226	68.713	67.467	68.618	11.334	5.102	869014.5	0.106	0.106	1.181
2.235	2.226	68.646	67.513	68.533	11.346	4.843	869817.6	0.112	0.106	1.181
2.224	2.227	68.603	67.405	68.539	11.336	4.803	869345.0	0.104	0.106	1.181
2.229	2.227	68.597	67.513	68.56	11.383	5.095	872640.8	0.107	0.106	1.181
2.228	2.227	68.562	67.456	68.507	11.343	5.127	869739.3	0.105	0.106	1.181

2.22	2.227	68.595	67.434	68.6	11.394	4.996	873677.5	0.105	0.106	1.181
2.224	2.227	68.648	67.517	68.585	11.358	5.237	870676.1	0.107	0.106	1.181
2.214	2.226	68.589	67.439	68.571	11.356	5.053	870787.5	0.106	0.106	1.181
2.227	2.226	68.613	67.484	68.595	11.373	5.034	871977.1	0.106	0.106	1.181
2.224	2.226	68.575	67.454	68.594	11.325	5.143	868391.9	0.106	0.106	1.181
2.224	2.226	68.496	67.497	68.57	11.408	5.104	874602	0.105	0.106	1.181
2.234	2.226	68.52	67.463	68.587	11.361	5.206	871057.1	0.107	0.106	1.181
2.215	2.226	68.502	67.483	68.584	11.325	5.171	868255.5	0.105	0.106	1.181
2.233	2.226	68.556	67.484	68.61	11.353	4.928	870383.1	0.108	0.106	1.181
2.232	2.226	68.492	67.357	68.57	11.322	5.003	868389.9	0.106	0.106	1.181
2.225	2.226	68.734	67.462	68.611	11.291	4.941	865747.1	0.104	0.106	1.181
2.231	2.226	68.685	67.385	68.627	11.344	4.938	870003.2	0.11	0.106	1.181
2.23	2.226	68.763	67.44	68.614	11.385	5.235	873001.4	0.103	0.106	1.181
2.227	2.226	68.661	67.374	68.601	11.385	5.047	873176.9	0.105	0.106	1.181
2.229	2.226	68.688	67.438	68.616	11.342	4.908	869745.4	0.104	0.106	1.181
2.218	2.226	68.509	67.427	68.542	11.362	5.067	871270.8	0.104	0.106	1.181
2.23	2.226	68.52	67.378	68.554	11.426	5.006	876347.8	0.106	0.106	1.181
2.222	2.226	68.642	67.452	68.642	11.403	4.782	874376.7	0.104	0.106	1.181
2.224	2.226	68.709	67.489	68.616	11.347	4.985	869947.8	0.104	0.106	1.181
2.215	2.226	68.62	67.396	68.617	10.249	19.622	786010.8	0.125	0.106	1.181
1.462	2.2	68.607	67.463	68.596	5.098	19.912	390894.2	0.114	0.107	1.181
1.483	2.175	68.61	67.669	68.587	1.295	31.953	99188.5	0.172	0.109	1.18
1.367	2.147	68.666	68.05	68.661	1.545	10.398	118200.6	0.148	0.11	1.179
1.411	2.119	68.636	68.2	68.626	1.655	10.388	126574.8	0.146	0.112	1.179
1.361	2.091	68.629	68.214	68.536	1.186	14.965	90666.2	0.119	0.112	1.179
1.362	2.062	68.605	68.223	68.539	0.748	12.924	57206.4	0.105	0.112	1.179
1.36	2.033	68.676	68.154	68.583	0.503	11.454	38493.2	0.101	0.112	1.179
1.358	2.004	68.746	68.26	68.632	0.428	7.636	32724.1	0.1	0.112	1.179
1.358	1.975	68.693	68.2	68.602	0.375	13.79	28669.5	0.099	0.111	1.179
1.358	1.946	68.643	68.201	68.587	0.272	6.94	20789.5	0.099	0.111	1.179
1.356	1.917	68.657	68.277	68.609	0.225	15.107	17205.7	0.099	0.111	1.179
1.357	1.888	68.426	68.124	68.561	0.183	2.949	14030.8	0.099	0.111	1.179
1.358	1.86	68.535	68.269	68.569	0.17	5.987	12962.8	0.098	0.11	1.179
1.356	1.831	68.523	68.4	68.59	0.163	3.426	12459.0	0.098	0.11	1.179
1.355	1.802	68.632	68.41	68.633	0.165	2.888	12588.3	0.098	0.11	1.179
1.358	1.773	68.701	68.54	68.647	0.163	2.8	12422.5	0.098	0.11	1.178
1.358	1.744	68.642	68.465	68.613	0.164	2.75	12526.4	0.099	0.109	1.178
1.356	1.715	68.585	68.481	68.58	0.162	2.773	12388.2	0.098	0.109	1.178
1.357	1.686	68.738	68.881	68.64	0.163	2.794	12407.0	0.098	0.109	1.177
1.356	1.657	68.815	69.231	68.639	0.164	2.783	12501.7	0.099	0.109	1.177
1.358	1.628	68.819	69.664	68.656	0.165	2.762	12549.1	0.099	0.108	1.175
1.357	1.599	68.803	69.868	68.722	0.165	2.822	12544.6	0.099	0.108	1.175
1.356	1.569	68.767	69.917	68.689	0.165	2.783	12532.1	0.099	0.108	1.175
1.358	1.54	68.738	69.765	68.685	0.164	2.765	12478.3	0.099	0.108	1.175
1.357	1.511	68.715	69.664	68.638	0.165	2.787	12527.3	0.098	0.108	1.175
1.356	1.483	68.702	69.424	68.651	0.164	2.782	12521.1	0.099	0.107	1.176
1.357	1.454	68.776	69.449	68.648	0.165	2.77	12527.9	0.1	0.107	1.176
1.357	1.425	68.67	69.393	68.638	0.164	2.797	12514.8	0.099	0.107	1.176
1.357	1.396	68.656	69.41	68.672	0.165	2.824	12563.9	0.098	0.107	1.176
1.358	1.367	68.575	69.422	68.645	0.164	2.702	12464.3	0.098	0.106	1.176
1.357	1.364	68.558	69.431	68.64	0.164	2.81	12480.1	0.099	0.105	1.176
1.358	1.36	68.63	69.462	68.627	0.164	2.779	12484.5	0.099	0.103	1.176
1.356	1.359	68.556	69.563	68.653	0.164	2.773	12502.8	0.099	0.101	1.176
1.356	1.357	68.385	69.621	68.622	0.165	2.765	12545.0	0.099	0.1	1.176
1.357	1.357	68.437	69.78	68.636	0.165	2.855	12547.8	0.098	0.099	1.175
1.357	1.357	68.421	69.827	68.641	0.164	2.759	12490.5	0.099	0.099	1.175
1.358	1.357	68.635	69.881	68.648	0.164	2.769	12497.0	0.099	0.099	1.175
1.357	1.357	68.67	69.891	68.653	0.164	2.81	12496.4	0.099	0.099	1.175
1.355	1.357	68.566	69.699	68.65	0.164	2.826	12443.1	0.097	0.099	1.175
1.357	1.357	68.569	69.723	68.611	0.163	2.805	12423.8	0.1	0.099	1.175
1.356	1.357	68.585	69.701	68.639	0.164	2.793	12437.6	0.099	0.099	1.175
1.356	1.357	68.776	69.792	68.656	0.164	2.797	12451.3	0.099	0.099	1.175
1.356	1.357	68.878	69.829	68.685	0.164	2.798	12445.3	0.098	0.099	1.175
1.356	1.357	68.712	69.483	68.592	0.163	2.774	12381.5	0.099	0.099	1.176
1.357	1.357	68.69	69.256	68.582	0.163	2.818	12410.1	0.098	0.099	1.176
1.356	1.357	68.61	69.207	68.612	0.162	2.861	12339.4	0.098	0.099	1.177
1.357	1.357	68.684	69.074	68.624	0.162	2.872	12326.3	0.098	0.099	1.177
1.357	1.357	68.729	69.163	68.592	0.162	2.84	12328.6	0.099	0.099	1.177

1.357	1.357	68.581	69.059	68.585	0.161	2.775	12286.2	0.098	0.099	1.177
1.358	1.357	68.473	69.099	68.604	0.161	2.823	12288.3	0.098	0.099	1.177
1.357	1.357	68.415	69.041	68.577	0.161	2.793	12275.2	0.099	0.099	1.177
1.358	1.357	68.5	69.161	68.633	0.161	2.858	12296.8	0.099	0.099	1.177
1.359	1.357	68.517	69.311	68.614	0.162	2.791	12352.3	0.099	0.099	1.176
1.358	1.357	68.435	69.256	68.619	0.162	2.842	12322.4	0.099	0.099	1.176
1.358	1.357	68.411	69.22	68.539	0.161	2.841	12248.5	0.099	0.099	1.177
1.358	1.357	68.276	68.978	68.494	0.161	2.805	12288.7	0.099	0.099	1.177
1.358	1.357	68.52	68.978	68.51	0.161	2.818	12292.1	0.099	0.099	1.177
1.358	1.357	68.491	68.902	68.489	0.162	2.792	12331.2	0.098	0.099	1.177
1.442	1.36	68.481	68.145	68.511	2.065	89.602	157938.5	0.126	0.1	1.179
1.664	1.37	68.581	67.503	68.587	7.4	3.405	567293.1	0.124	0.1	1.181
1.995	1.391	68.576	67.606	68.603	11.552	17.602	885266.8	0.165	0.103	1.181
2.306	1.423	68.486	67.579	68.609	12.821	1.627	982667.0	0.106	0.103	1.181
2.218	1.452	68.8	67.699	68.628	12.582	3.177	963874	0.109	0.103	1.18
2.19	1.48	68.571	67.611	68.647	11.941	1.098	915087.8	0.11	0.104	1.181
2.14	1.506	68.773	67.784	68.68	11.959	1.073	915933.6	0.11	0.104	1.18
2.164	1.533	68.533	67.742	68.596	11.977	1.102	917402.6	0.11	0.104	1.18
2.162	1.559	68.481	67.662	68.589	11.959	1.043	916280.1	0.111	0.105	1.18
2.16	1.586	68.49	67.628	68.633	11.966	1.084	916928.4	0.109	0.105	1.18
2.159	1.613	68.494	67.718	68.639	11.944	1.103	914999.5	0.11	0.106	1.18
2.162	1.64	68.373	67.667	68.623	11.961	1.157	916390.1	0.111	0.106	1.18
2.159	1.667	68.397	67.683	68.618	11.964	1.058	916625	0.11	0.106	1.18
2.159	1.693	68.355	67.709	68.668	11.965	1.158	916611.8	0.11	0.107	1.18
2.165	1.72	68.402	67.693	68.653	11.948	1.247	915322.8	0.114	0.107	1.18
2.158	1.747	68.397	67.665	68.675	11.95	1.07	915563.4	0.111	0.108	1.18
2.161	1.774	68.411	67.715	68.645	11.974	1.053	917269	0.109	0.108	1.18
2.155	1.8	68.452	67.681	68.653	11.926	1.119	913697.3	0.11	0.108	1.18
2.158	1.827	68.494	67.597	68.643	11.938	1.136	914902.0	0.11	0.109	1.181
2.156	1.854	68.447	67.636	68.672	11.932	1.095	914273.3	0.107	0.109	1.18
2.161	1.881	68.489	67.667	68.642	11.959	1.138	916254.1	0.11	0.109	1.18
2.163	1.907	68.451	67.681	68.624	11.973	1.143	917306.3	0.112	0.11	1.18
2.161	1.934	68.435	67.639	68.64	11.955	1.137	916097.0	0.109	0.11	1.18
2.162	1.961	68.567	67.721	68.628	11.957	1.144	915961.8	0.111	0.111	1.18
2.161	1.988	68.416	67.661	68.551	11.962	1.122	916505.6	0.11	0.111	1.18
2.16	2.015	68.378	67.683	68.588	11.965	1.115	916667.6	0.11	0.111	1.18
2.163	2.041	68.49	67.638	68.563	11.96	1.124	916420.8	0.111	0.112	1.18
2.16	2.068	68.531	67.719	68.606	11.963	1.075	916380.3	0.109	0.112	1.18
2.164	2.095	68.721	67.723	68.626	11.962	1.119	916299.3	0.111	0.112	1.18
2.159	2.122	68.56	67.762	68.578	11.956	1.141	915742.5	0.112	0.113	1.18
2.159	2.146	68.537	67.626	68.665	11.941	1.11	915027	0.109	0.112	1.181
2.155	2.162	68.618	67.743	68.618	11.958	1.084	915917.5	0.109	0.112	1.18
2.163	2.167	68.541	67.658	68.599	11.97	1.107	917173.2	0.112	0.11	1.18
2.157	2.162	68.529	67.676	68.568	11.959	1.086	916243.1	0.11	0.11	1.18
2.16	2.161	68.612	67.626	68.616	11.957	1.074	916225.7	0.111	0.11	1.181
2.157	2.159	68.642	67.695	68.629	11.958	1.193	916136.5	0.11	0.11	1.18
2.159	2.16	68.615	67.652	68.57	11.96	1.126	916416.4	0.11	0.11	1.18
2.159	2.16	68.562	67.688	68.591	11.957	1.135	916028.6	0.11	0.11	1.18
2.159	2.16	68.56	67.658	68.573	11.957	1.053	916183.5	0.109	0.11	1.18
2.16	2.16	68.642	67.653	68.603	11.963	1.041	916623.3	0.109	0.11	1.18
2.159	2.16	68.678	67.731	68.647	11.95	1.061	915410.3	0.11	0.11	1.18
2.156	2.16	68.422	67.593	68.595	11.925	0.946	913890.8	0.11	0.11	1.181
2.163	2.16	68.657	67.667	68.678	11.961	1.08	916436.7	0.112	0.11	1.18
2.157	2.16	68.738	67.722	68.663	11.965	1.016	916561.1	0.11	0.11	1.18
2.164	2.16	68.658	67.643	68.602	11.977	1.042	917714.9	0.11	0.11	1.18
2.159	2.16	68.717	67.639	68.638	11.951	0.986	915737.4	0.109	0.11	1.18
2.16	2.16	68.842	67.646	68.603	11.97	1.011	917150.2	0.11	0.11	1.18
2.159	2.16	68.677	67.656	68.615	11.953	0.952	915872.1	0.109	0.11	1.18
2.159	2.16	68.633	67.553	68.597	11.938	1.008	915048.3	0.109	0.11	1.181
2.16	2.16	68.688	67.616	68.677	11.97	0.971	917277.3	0.108	0.11	1.181
2.16	2.16	68.855	67.718	68.772	11.951	1.051	915496.1	0.111	0.11	1.18
2.163	2.16	68.729	67.716	68.752	11.998	1.183	919073.5	0.111	0.11	1.18
2.19	2.161	68.787	67.579	68.726	12.329	1.098	944916.0	0.11	0.11	1.181
2.183	2.162	68.795	67.699	68.701	12.336	0.973	945076.8	0.109	0.11	1.18
2.188	2.162	68.717	67.641	68.641	12.334	1.225	945099.6	0.111	0.11	1.18
2.304	2.167	68.842	67.464	68.689	12.054	9.022	924220.3	0.112	0.11	1.181
2.312	2.172	68.823	66.914	68.654	11.611	11.537	891971.5	0.117	0.11	1.182
2.336	2.178	68.714	66.858	68.638	11.769	12.01	904300.8	0.106	0.11	1.182

2.345	2.184	68.648	66.962	68.692	11.754	11.034	902854.6	0.109	0.11	1.182
2.317	2.189	68.694	67.04	68.615	11.562	11.757	887805.2	0.113	0.11	1.182
2.324	2.195	68.683	67.121	68.721	11.585	11.536	889355.9	0.117	0.11	1.182
2.338	2.201	68.711	67.265	68.716	11.754	12.957	901842.1	0.112	0.11	1.181
2.325	2.206	68.772	67.268	68.69	11.582	11.925	888650.5	0.112	0.11	1.181
2.333	2.212	68.621	67.369	68.628	11.504	11.164	882373.8	0.113	0.111	1.181
2.331	2.218	68.643	67.387	68.615	11.626	11.713	891656.5	0.11	0.111	1.181
2.31	2.223	68.855	67.458	68.66	11.301	10.902	866530.6	0.117	0.111	1.181
2.351	2.229	68.806	67.601	68.654	11.835	12.072	906975.4	0.11	0.111	1.181
2.317	2.235	68.63	67.619	68.698	11.719	11.569	898017	0.119	0.111	1.181
2.344	2.241	68.678	67.736	68.672	11.638	11.258	891471	0.123	0.112	1.18
2.315	2.246	68.544	67.715	68.63	11.545	10.675	884440.6	0.114	0.112	1.18
2.297	2.251	68.645	67.806	68.706	11.477	11.398	878893.9	0.108	0.112	1.18
2.334	2.257	68.649	67.906	68.666	11.893	10.183	910475.5	0.111	0.112	1.18
2.334	2.262	68.925	67.928	68.687	11.611	11.708	888776.3	0.108	0.112	1.18
2.332	2.268	68.765	68.055	68.688	11.581	11.343	886106.6	0.111	0.112	1.179
2.321	2.273	68.694	68.017	68.655	11.614	11.164	888738.4	0.112	0.112	1.18
2.324	2.279	68.743	68.113	68.667	11.748	12.02	898723.9	0.111	0.112	1.179
2.316	2.284	68.668	68.159	68.633	11.619	11.847	888679.8	0.11	0.112	1.179
2.345	2.29	68.636	68.177	68.593	11.728	11.236	896988.8	0.117	0.112	1.179
2.317	2.296	68.639	68.178	68.652	11.703	12.529	895027.8	0.11	0.112	1.179
2.33	2.301	68.679	68.247	68.679	11.568	11.226	884518.4	0.11	0.112	1.179
2.319	2.307	68.758	68.261	68.698	11.755	10.792	898714.8	0.111	0.112	1.179
2.321	2.312	68.711	68.356	68.664	11.682	12.13	892896.3	0.114	0.112	1.179
2.324	2.316	68.683	68.393	68.645	11.654	12.014	890619.4	0.124	0.113	1.179
2.305	2.32	68.722	68.333	68.687	11.561	10.794	883704.8	0.115	0.113	1.179
2.335	2.325	68.669	68.433	68.66	11.673	10.524	891902	0.115	0.113	1.179
2.326	2.326	68.443	68.397	68.623	11.754	10.859	898263.6	0.112	0.113	1.179
2.333	2.327	68.581	68.476	68.606	11.872	11.311	907018.3	0.111	0.113	1.178
2.306	2.326	68.65	68.45	68.631	11.574	11.968	884300.6	0.112	0.113	1.178
2.311	2.324	68.638	68.551	68.587	11.533	11.219	880893.4	0.12	0.113	1.178
2.314	2.324	68.666	68.529	68.611	11.616	12.222	887309.5	0.112	0.113	1.178
2.318	2.324	68.837	68.616	68.67	11.667	10.783	890888	0.114	0.113	1.178
2.327	2.324	68.789	68.634	68.614	11.699	11.745	893285.1	0.117	0.113	1.178
2.317	2.324	68.708	68.593	68.631	11.823	11.824	902887.3	0.113	0.114	1.178
2.311	2.323	68.84	68.683	68.668	11.84	11.964	903865.5	0.109	0.113	1.178
2.319	2.322	68.951	68.843	68.662	11.618	11.631	886439.5	0.112	0.113	1.177
2.341	2.323	68.922	68.734	68.643	11.864	11.445	905591.6	0.107	0.113	1.178
2.302	2.322	68.844	68.737	68.705	11.549	10.892	881475.1	0.11	0.113	1.178
2.315	2.322	68.861	68.803	68.665	11.643	11.749	888467.6	0.111	0.113	1.178
2.314	2.321	68.866	68.833	68.679	11.732	11.565	895201.2	0.107	0.112	1.178
2.312	2.321	68.851	68.873	68.703	11.538	12.003	880243.8	0.11	0.112	1.177
2.331	2.322	68.837	68.944	68.645	11.591	12.144	884070.6	0.115	0.112	1.177
2.309	2.321	68.966	68.908	68.633	11.702	11.17	892618.1	0.11	0.112	1.177
2.33	2.321	68.937	68.907	68.621	11.596	11.337	884597.9	0.105	0.112	1.177
2.327	2.321	68.951	68.978	68.587	11.644	12.006	887981.2	0.11	0.112	1.177
2.315	2.32	68.924	68.944	68.606	11.724	10.608	894229.8	0.107	0.112	1.177
2.29	2.319	68.943	69.006	68.656	11.656	11.365	888814.5	0.11	0.112	1.177
2.333	2.32	68.916	69.046	68.626	11.653	12.229	888445.5	0.113	0.112	1.177
2.298	2.318	68.748	68.959	68.604	11.658	11.752	889106.0	0.107	0.112	1.177
2.332	2.319	68.855	69.134	68.605	11.81	10.605	900146.6	0.11	0.112	1.177
2.329	2.319	68.874	69.065	68.567	11.68	11.908	890455.1	0.111	0.112	1.177
2.318	2.319	68.905	69.114	68.567	11.584	11.594	883006.6	0.11	0.112	1.177
2.303	2.318	68.877	69.154	68.641	11.685	11.362	890578.2	0.107	0.112	1.177
2.329	2.318	68.827	68.801	68.63	11.832	11.453	902941.8	0.11	0.111	1.178
2.396	2.321	68.84	68.198	68.614	12.421	11.043	949921.3	0.103	0.111	1.179
2.396	2.323	68.885	67.877	68.642	12.679	9.867	970691.9	0.101	0.11	1.18
2.302	2.323	69.281	67.883	68.721	12.686	6.749	971245.1	0.101	0.11	1.18
2.143	2.316	69.117	67.708	68.639	11.949	0.966	915344.1	0.105	0.11	1.18
2.161	2.311	69.093	67.605	68.609	11.936	1.079	914743.1	0.106	0.109	1.181
2.151	2.306	69.025	67.614	68.617	11.953	1.021	915966.1	0.106	0.109	1.181
2.151	2.301	69.054	67.566	68.69	11.929	1.08	914288.6	0.107	0.109	1.181
2.147	2.295	69.029	67.664	68.646	11.959	0.976	916260.5	0.105	0.109	1.18
2.149	2.289	69.038	67.548	68.666	11.939	0.999	915149.1	0.106	0.108	1.181
2.148	2.283	69.014	67.578	68.7	11.951	1.003	915983.4	0.106	0.108	1.181
2.152	2.278	69.038	67.5	68.646	11.937	1.062	915136.9	0.107	0.108	1.181
2.151	2.272	69.065	67.585	68.667	11.955	1.034	916226.9	0.108	0.108	1.181
2.151	2.266	69.017	67.453	68.689	11.936	0.986	915191.8	0.108	0.108	1.181

2.151	2.261	69.064	67.481	68.715	11.948	0.958	916007.3	0.106	0.108	1.181
2.15	2.256	69.051	67.51	68.646	11.947	0.985	915893.2	0.106	0.107	1.181
2.153	2.25	69.141	67.424	68.673	11.945	0.976	915962	0.107	0.107	1.181
2.153	2.245	68.982	67.477	68.63	11.943	1.028	915639.0	0.106	0.107	1.181
2.156	2.239	69.009	67.367	68.726	11.933	1.085	915291.7	0.107	0.107	1.181
2.158	2.234	69.042	67.498	68.724	11.957	0.961	916652.1	0.108	0.107	1.181
2.154	2.228	68.908	67.418	68.688	11.924	1.005	914425.8	0.11	0.107	1.181
2.154	2.223	69.037	67.452	68.751	11.945	0.99	915863.4	0.109	0.107	1.181
2.156	2.217	69.037	67.567	68.709	11.95	0.982	915922.0	0.108	0.107	1.181
2.156	2.213	68.971	67.415	68.702	11.927	0.947	914625.6	0.108	0.107	1.181
2.154	2.207	69.069	67.539	68.72	11.961	0.964	916816.3	0.107	0.107	1.181
2.155	2.202	69.147	67.555	68.75	11.944	1.138	915514.3	0.109	0.107	1.181
2.157	2.196	69.153	67.485	68.722	11.953	0.979	916438.3	0.108	0.107	1.181
2.152	2.19	69.138	67.557	68.707	11.952	0.973	916113.6	0.107	0.107	1.181
2.153	2.185	69.066	67.451	68.706	11.951	0.985	916351.8	0.106	0.107	1.181
2.155	2.18	69.039	67.537	68.712	11.937	1.022	915020.8	0.108	0.107	1.181
2.154	2.174	68.98	67.481	68.683	11.952	1.045	916344.2	0.111	0.107	1.181
2.154	2.166	68.982	67.436	68.704	11.937	1.049	915324.5	0.109	0.107	1.181
2.157	2.158	69.051	67.495	68.76	11.948	1.097	915981.3	0.111	0.107	1.181
2.157	2.153	69.028	67.489	68.761	11.962	0.982	917052	0.108	0.107	1.181
2.152	2.153	69.055	67.451	68.795	11.946	0.973	915981.3	0.107	0.107	1.181
2.154	2.153	69.148	67.541	68.74	11.938	0.972	915045	0.109	0.108	1.181
2.157	2.153	69.176	67.439	68.734	11.947	1.039	916078.5	0.109	0.108	1.181
2.154	2.154	69.138	67.535	68.78	11.949	1.005	915964.1	0.109	0.108	1.181
2.154	2.154	69.03	67.351	68.731	11.926	1.046	914776.2	0.11	0.108	1.181
2.153	2.154	69.194	67.495	68.696	11.968	0.964	917499.1	0.108	0.108	1.181
2.155	2.154	69.104	67.356	68.736	11.937	0.97	915610.6	0.108	0.108	1.181
2.157	2.154	69.185	67.495	68.751	11.957	1.057	916663.1	0.11	0.108	1.181
2.155	2.154	69.109	67.454	68.736	11.95	0.978	916297.9	0.107	0.108	1.181
2.152	2.154	69.087	67.482	68.804	11.939	0.957	915345.6	0.107	0.108	1.181
2.155	2.155	69.019	67.522	68.753	11.944	1.093	915604.3	0.108	0.108	1.181
2.152	2.155	68.944	67.579	68.698	11.945	0.967	915461	0.108	0.108	1.181
2.151	2.155	68.921	67.455	68.7	11.931	1.038	914830.9	0.109	0.108	1.181
2.156	2.155	69.19	67.688	68.782	11.976	1.178	917542.5	0.114	0.108	1.18
2.154	2.155	69.083	67.48	68.801	11.944	1.051	915765.4	0.109	0.109	1.181
2.15	2.154	69.055	67.583	68.749	11.939	1.069	914996.4	0.108	0.109	1.181
2.153	2.154	69.017	67.513	68.73	11.945	0.958	915705	0.108	0.108	1.181
2.154	2.154	69.015	67.495	68.766	11.951	1.022	916229.4	0.108	0.108	1.181
2.155	2.154	68.959	67.559	68.732	11.955	1.015	916328.5	0.108	0.108	1.181
2.153	2.154	68.963	67.479	68.75	11.923	1.043	914089.5	0.11	0.109	1.181
2.159	2.154	69.024	67.618	68.777	11.959	1.09	916442.6	0.111	0.109	1.181
2.158	2.154	68.993	67.531	68.741	11.955	1.004	916404	0.108	0.109	1.181
1.649	2.138	68.979	67.52	68.73	6.545	8.001	501716.0	0.134	0.109	1.181
1.378	2.112	69.031	67.843	68.728	1.499	46.51	114790.7	0.177	0.112	1.18
1.438	2.088	69.007	68.292	68.7	1.739	8.272	132926.3	0.149	0.113	1.179
1.383	2.062	69.26	68.44	68.764	1.664	14.124	127126.5	0.141	0.114	1.178
1.366	2.036	69.049	68.443	68.718	0.846	19.684	64608.5	0.11	0.114	1.178
1.361	2.009	69.11	68.441	68.706	0.582	18.895	44476.8	0.103	0.114	1.178
1.359	1.983	69.191	68.507	68.72	0.465	13.995	35507.0	0.101	0.114	1.178
1.358	1.956	69.033	68.555	68.738	0.301	20.881	22997.8	0.1	0.113	1.178
1.359	1.93	68.943	68.516	68.75	0.283	12.526	21633.1	0.101	0.113	1.178
1.357	1.903	68.936	68.522	68.743	0.22	4.381	16783.9	0.1	0.113	1.178
1.357	1.877	68.957	68.51	68.777	0.228	6.949	17391.6	0.099	0.113	1.178
1.355	1.85	68.937	68.532	68.678	0.2	8.444	15302.0	0.098	0.112	1.178
1.353	1.823	69.053	68.479	68.722	0.192	5.305	14652.6	0.099	0.112	1.178
1.355	1.797	69.374	68.615	68.753	0.205	6.535	15653.6	0.099	0.112	1.178
1.355	1.77	69.28	68.453	68.653	0.18	4.04	13729.1	0.098	0.111	1.178
1.355	1.743	69.286	68.47	68.73	0.169	2.65	12922.1	0.098	0.111	1.178
1.354	1.716	69.144	68.537	68.756	0.168	2.322	12819.0	0.098	0.111	1.178
1.355	1.69	69.079	68.459	68.739	0.164	2.546	12503.3	0.098	0.11	1.178
1.355	1.663	69.039	68.642	68.7	0.162	2.347	12401.9	0.098	0.11	1.178
1.356	1.637	69.009	68.66	68.668	0.163	2.38	12417.0	0.098	0.11	1.178
1.352	1.61	69.001	68.798	68.746	0.162	2.315	12380.3	0.098	0.109	1.178
1.355	1.583	69.047	69.095	68.745	0.163	2.388	12415.5	0.098	0.109	1.177
1.355	1.557	69.094	69.216	68.736	0.163	2.339	12410.2	0.098	0.108	1.177
1.355	1.53	69.039	69.442	68.762	0.164	2.386	12457.4	0.098	0.108	1.176
1.354	1.504	69.032	69.456	68.691	0.164	2.355	12473.5	0.098	0.108	1.176
1.355	1.477	69.064	69.409	68.757	0.164	2.349	12495.7	0.098	0.108	1.176

1.354	1.45	68.902	69.321	68.735	0.164	2.384	12512.6	0.099	0.107	1.176
1.355	1.424	68.89	69.251	68.79	0.164	2.362	12492.1	0.098	0.107	1.176
1.354	1.397	68.945	69.344	68.743	0.163	2.343	12445.0	0.098	0.106	1.176
1.354	1.37	68.84	69.454	68.718	0.164	2.369	12455.9	0.098	0.106	1.176
1.356	1.36	68.998	69.367	68.726	0.163	2.354	12422.7	0.098	0.105	1.176
1.355	1.36	69.073	69.254	68.728	0.161	2.362	12290.3	0.098	0.102	1.176
1.355	1.357	68.918	69.026	68.754	0.162	2.31	12356.0	0.098	0.101	1.177
1.355	1.356	68.928	68.961	68.77	0.163	2.364	12435.8	0.098	0.099	1.177
1.355	1.355	68.799	68.874	68.708	0.163	2.34	12454.2	0.098	0.099	1.177
1.354	1.355	69.088	68.978	68.742	0.163	2.33	12404.9	0.098	0.099	1.177
1.355	1.355	69.12	68.936	68.728	0.162	2.339	12374.6	0.098	0.098	1.177
1.355	1.355	69.107	68.978	68.745	0.162	2.359	12335.9	0.098	0.098	1.177
1.355	1.355	69.075	68.879	68.721	0.161	2.367	12275.5	0.098	0.098	1.177
1.356	1.355	69.176	69.043	68.749	0.161	2.461	12286.5	0.098	0.098	1.177
1.356	1.355	69.246	69.114	68.754	0.161	2.339	12303.5	0.098	0.098	1.177
1.357	1.355	68.969	69.167	68.706	0.162	2.333	12327.0	0.099	0.098	1.177
1.356	1.355	68.828	69.263	68.695	0.162	2.327	12356.8	0.099	0.098	1.176
1.355	1.355	68.787	69.244	68.679	0.162	2.355	12335.6	0.098	0.098	1.177
1.356	1.355	68.892	69.213	68.798	0.161	2.39	12302.9	0.098	0.098	1.177
1.355	1.355	68.889	69.176	68.762	0.161	2.334	12262.0	0.098	0.098	1.177
1.355	1.355	68.874	69.097	68.737	0.161	2.378	12256.8	0.098	0.098	1.177
1.355	1.355	69.057	68.95	68.692	0.161	2.382	12252.7	0.098	0.098	1.177
1.355	1.355	68.887	68.834	68.633	0.16	2.349	12230.2	0.098	0.098	1.178
1.355	1.355	68.951	68.906	68.684	0.16	2.375	12221.9	0.098	0.098	1.177
1.354	1.355	69.073	68.931	68.702	0.16	2.341	12215.6	0.098	0.098	1.177
1.355	1.355	69.401	68.992	68.725	0.16	2.366	12204.6	0.098	0.098	1.177
1.355	1.355	69.22	68.912	68.69	0.161	2.407	12291.7	0.098	0.098	1.177
1.355	1.355	69.052	68.752	68.683	0.16	2.356	12238.4	0.098	0.098	1.178
1.356	1.355	69.157	68.888	68.754	0.161	2.42	12267.6	0.099	0.098	1.177
1.356	1.355	68.943	68.864	68.722	0.161	2.381	12288.1	0.098	0.098	1.177
1.355	1.355	68.863	68.724	68.754	0.161	2.393	12306.3	0.099	0.098	1.178
1.356	1.355	69.072	68.912	68.715	0.162	2.369	12335.4	0.098	0.098	1.177
1.357	1.355	69.025	68.816	68.663	0.161	2.397	12247.3	0.098	0.098	1.178
1.358	1.355	68.937	68.765	68.649	0.161	2.387	12262.5	0.099	0.098	1.178
1.355	1.355	68.949	68.777	68.673	0.16	2.31	12227.1	0.098	0.098	1.178
1.355	1.355	69.043	68.853	68.689	0.16	2.413	12239.2	0.098	0.098	1.177
1.355	1.355	68.942	68.793	68.682	0.161	2.39	12300.9	0.098	0.098	1.178
1.355	1.355	68.998	68.733	68.686	0.161	2.382	12279.3	0.098	0.098	1.178
1.354	1.355	69.133	68.898	68.625	0.161	2.395	12288.5	0.098	0.098	1.177
1.354	1.355	69.028	68.796	68.65	0.16	2.378	12238.5	0.098	0.098	1.178
1.355	1.355	69.129	68.964	68.669	0.161	2.539	12264.4	0.098	0.098	1.177
1.547	1.362	69.173	67.92	68.692	4.49	44.95	343713.5	0.152	0.1	1.18
1.659	1.372	69.138	67.664	68.701	7.527	1.25	576738.6	0.105	0.1	1.18
2.053	1.395	69.042	67.67	68.699	11.925	14.82	913648.5	0.166	0.102	1.18
2.3	1.427	69.051	67.487	68.572	12.793	1.54	980815.7	0.105	0.103	1.181
2.213	1.455	68.874	67.542	68.663	12.506	3.349	958616.2	0.11	0.103	1.181
2.187	1.483	68.782	67.693	68.663	11.93	1.041	913994	0.112	0.103	1.18
2.153	1.509	68.645	67.586	68.695	11.935	1.03	914688.5	0.11	0.104	1.181
2.158	1.536	68.715	67.697	68.684	11.941	0.957	914768.4	0.109	0.104	1.18
2.156	1.563	68.678	67.649	68.693	11.93	1.019	914110.2	0.108	0.105	1.18
2.154	1.589	68.821	67.689	68.681	11.941	0.989	914856.8	0.109	0.105	1.18
2.154	1.616	68.672	67.624	68.65	11.933	1.002	914436.6	0.109	0.105	1.181
2.158	1.643	68.643	67.667	68.679	11.949	1.069	915473.3	0.111	0.106	1.18
2.156	1.67	68.783	67.792	68.692	11.976	0.942	917157.9	0.108	0.106	1.18
2.157	1.696	68.749	67.686	68.644	11.94	1.041	914778.7	0.111	0.106	1.18
2.154	1.723	68.697	67.664	68.726	11.935	0.974	914477.8	0.109	0.107	1.18
2.157	1.75	68.688	67.721	68.707	11.958	1.015	916003.2	0.11	0.107	1.18
2.151	1.776	68.672	67.666	68.653	11.941	0.968	914898.9	0.109	0.108	1.18
2.152	1.803	68.677	67.703	68.675	11.949	0.948	915398.8	0.108	0.108	1.18
2.158	1.829	68.727	67.638	68.725	11.94	1.042	914911.3	0.109	0.108	1.18
2.156	1.856	68.714	67.755	68.714	11.971	0.959	916880.6	0.108	0.109	1.18
2.155	1.883	68.776	67.635	68.749	11.941	0.997	915003.5	0.108	0.109	1.18
2.157	1.909	68.791	67.741	68.739	11.955	0.942	915751.5	0.109	0.109	1.18
2.157	1.936	68.732	67.717	68.677	11.964	1.022	916461.9	0.109	0.11	1.18
2.157	1.963	68.73	67.651	68.744	11.944	1.069	915166.0	0.112	0.11	1.18
2.157	1.99	68.777	67.764	68.689	11.943	1.027	914733.5	0.11	0.11	1.18
2.153	2.016	68.829	67.707	68.703	11.948	0.978	915295.3	0.109	0.111	1.18
2.155	2.043	68.646	67.65	68.656	11.942	0.975	915060.2	0.109	0.111	1.18

2.156	2.07	68.881	67.73	68.762	11.942	1.077	914755.6	0.108	0.112	1.18
2.157	2.096	68.831	67.791	68.708	11.962	1.147	916083.6	0.11	0.112	1.18
2.159	2.123	68.671	67.772	68.647	11.968	1.071	916652.3	0.111	0.112	1.18
2.159	2.144	68.715	67.766	68.678	11.946	0.998	914969.5	0.11	0.111	1.18
2.157	2.16	68.77	67.838	68.665	11.962	1.095	915976	0.109	0.111	1.18
2.153	2.163	68.637	67.813	68.661	11.938	0.996	914198.6	0.109	0.109	1.18
2.156	2.159	68.688	67.884	68.678	11.948	1.028	914706.6	0.109	0.109	1.18
2.154	2.157	68.917	67.979	68.769	11.956	1.019	915000	0.11	0.109	1.18
2.154	2.156	68.851	67.979	68.675	11.97	1.005	916120.0	0.108	0.109	1.18
2.156	2.156	68.762	67.934	68.719	11.958	1.012	915335.2	0.109	0.109	1.18
2.155	2.156	68.772	67.962	68.761	11.954	1.015	914936.3	0.108	0.109	1.18
2.154	2.156	68.747	68.087	68.765	11.964	1.086	915311.8	0.109	0.109	1.179
2.155	2.156	68.818	67.999	68.764	11.945	1.087	914122.8	0.108	0.109	1.18
2.154	2.156	68.951	68.095	68.789	11.945	0.963	913798.3	0.11	0.109	1.179
2.16	2.156	68.9	68.043	68.699	11.962	0.971	915296.5	0.109	0.109	1.179
2.162	2.156	68.852	68.178	68.72	11.963	1.068	914902	0.11	0.109	1.179
2.157	2.156	68.856	68.127	68.689	11.966	1.071	915355.8	0.111	0.109	1.179
2.154	2.156	68.943	68.173	68.718	11.94	1.033	913183.8	0.109	0.109	1.179
2.159	2.156	69.114	68.228	68.798	11.944	0.996	913339.9	0.109	0.109	1.179
2.153	2.156	68.925	68.286	68.745	11.958	0.965	914213.8	0.108	0.109	1.179
2.155	2.156	68.876	68.191	68.72	11.955	0.999	914299.1	0.108	0.109	1.179
2.154	2.156	68.734	68.241	68.681	11.956	1.01	914194.6	0.108	0.109	1.179
2.157	2.156	68.808	68.221	68.748	11.965	1.032	914905.4	0.11	0.109	1.179
2.153	2.156	68.795	68.263	68.702	11.959	0.948	914380.1	0.108	0.109	1.179
2.154	2.156	68.828	68.336	68.749	11.942	0.982	912776.1	0.107	0.109	1.179
2.155	2.156	68.749	68.272	68.686	11.949	0.961	913566.3	0.107	0.109	1.179
2.155	2.156	68.787	68.344	68.685	11.962	0.966	914293.1	0.109	0.109	1.179
2.156	2.156	68.751	68.328	68.645	11.962	1.006	914337.7	0.109	0.109	1.179
2.156	2.156	68.795	68.332	68.669	11.958	1.05	914020	0.107	0.109	1.179
2.154	2.156	69.108	68.51	68.857	11.979	1.002	915095.6	0.107	0.109	1.178
2.131	2.155	68.982	68.509	68.734	10.596	19.884	809389.1	0.13	0.11	1.178
1.511	2.133	68.952	68.286	68.686	6.655	1.094	508756.8	0.101	0.109	1.179
1.621	2.115	68.925	68.335	68.744	6.652	1.091	508433.0	0.094	0.109	1.179
1.562	2.096	68.856	68.458	68.767	6.666	1.214	509290.6	0.095	0.108	1.178
1.582	2.076	68.885	68.465	68.758	6.647	1.175	507840.0	0.095	0.108	1.178
1.582	2.057	68.825	68.508	68.711	6.663	1.043	508986.5	0.094	0.107	1.178
1.581	2.038	68.928	68.524	68.754	6.65	1.135	507957.6	0.095	0.107	1.178
1.581	2.019	68.978	68.593	68.798	6.661	1.176	508646.5	0.095	0.106	1.178
1.578	2	68.883	68.612	68.793	6.642	1.108	507170.4	0.095	0.106	1.178
1.58	1.981	68.991	68.622	68.782	6.649	1.156	507748.0	0.095	0.105	1.178
1.584	1.962	68.941	68.648	68.753	6.666	1.148	508961.5	0.095	0.105	1.178
1.581	1.943	68.951	68.594	68.74	6.653	1.19	508067.6	0.096	0.104	1.178
1.577	1.923	68.959	68.628	68.772	6.653	1.152	507981.7	0.096	0.104	1.178
1.583	1.904	68.745	68.587	68.692	6.657	1.13	508369.7	0.094	0.103	1.178
1.579	1.885	68.78	68.55	68.74	6.643	1.154	507393.7	0.094	0.103	1.178
1.581	1.866	68.957	68.628	68.736	6.646	1.178	507493.1	0.095	0.102	1.178
1.578	1.846	68.912	68.634	68.752	6.651	1.071	507871.9	0.095	0.102	1.178
1.578	1.827	68.878	68.615	68.785	6.654	1.123	508082.5	0.095	0.101	1.178
1.58	1.808	69.015	68.674	68.761	6.663	1.108	508725.5	0.095	0.101	1.178
1.581	1.789	68.931	68.63	68.723	6.644	1.179	507321.3	0.094	0.101	1.178
1.58	1.769	68.923	68.584	68.756	6.65	1.177	507879.7	0.094	0.1	1.178
1.582	1.75	68.955	68.697	68.78	6.664	1.082	508718.5	0.095	0.1	1.178
1.58	1.731	69.078	68.65	68.762	6.655	1.173	508132.0	0.095	0.099	1.178
1.582	1.712	69.124	68.69	68.789	6.645	1.139	507249.2	0.095	0.099	1.178
1.579	1.693	69.06	68.64	68.766	6.649	1.172	507717.7	0.095	0.098	1.178
1.583	1.674	69.069	68.628	68.769	6.67	1.095	509339.8	0.096	0.098	1.178
1.582	1.655	69.147	68.683	68.787	6.653	1.065	507875.0	0.095	0.097	1.178
1.578	1.636	69.058	68.624	68.78	6.656	1.072	508260.0	0.094	0.097	1.178
1.579	1.616	68.974	68.723	68.791	6.653	1.174	507802.5	0.094	0.097	1.178
1.581	1.597	68.966	68.626	68.784	6.642	1.171	507193.9	0.095	0.096	1.178
1.581	1.579	69.007	68.657	68.79	6.653	1.168	507944.5	0.096	0.095	1.178
1.579	1.581	68.943	68.671	68.835	6.656	1.076	508156.1	0.094	0.095	1.178
1.577	1.58	69.102	68.694	68.793	6.66	1.118	508389.2	0.094	0.095	1.178
1.579	1.58	69.139	68.706	68.785	6.648	1.112	507454.5	0.095	0.095	1.178
1.582	1.58	69.116	68.639	68.819	6.67	1.136	509304.7	0.094	0.095	1.178
1.581	1.58	69.072	68.595	68.768	6.647	1.175	507627.4	0.094	0.095	1.178
1.581	1.58	69.113	68.662	68.824	6.66	1.111	508461.8	0.095	0.095	1.178
1.577	1.58	69.018	68.643	68.758	6.643	1.255	507208.8	0.094	0.095	1.178

1.581	1.58	69.043	68.658	68.749	6.673	1.215	509466.1	0.095	0.095	1.178
1.581	1.58	69.029	68.594	68.781	6.669	1.139	509287.1	0.095	0.095	1.178
1.578	1.58	69.167	68.663	68.801	6.633	1.175	506383.4	0.095	0.095	1.178
1.581	1.58	69.057	68.659	68.756	6.659	1.187	508406.5	0.095	0.095	1.178
1.581	1.58	68.977	68.602	68.78	6.651	1.306	507874.0	0.095	0.095	1.178
1.579	1.58	69.058	68.663	68.775	6.66	1.138	508455.2	0.095	0.095	1.178
1.58	1.58	69.168	68.692	68.798	6.666	1.155	508904.8	0.095	0.095	1.178
1.579	1.58	69.162	68.639	68.837	6.65	1.166	507787.8	0.095	0.095	1.178
1.58	1.58	69.176	68.704	68.835	6.672	1.147	509342.3	0.096	0.095	1.178
1.583	1.58	69.169	68.748	68.757	6.666	1.131	508803.8	0.094	0.095	1.178
1.578	1.58	69.149	68.692	68.789	6.653	1.128	507879.5	0.094	0.095	1.178
1.579	1.58	69.122	68.741	68.794	6.654	1.136	507913.9	0.095	0.095	1.178
1.579	1.58	69.138	68.771	68.753	6.668	1.164	508886.4	0.094	0.095	1.178
1.579	1.58	69.072	68.741	68.831	6.661	1.206	508384.4	0.095	0.095	1.178
1.581	1.58	69.184	68.787	68.841	6.66	1.23	508286.5	0.095	0.095	1.178
1.581	1.58	69.131	68.827	68.78	6.668	1.101	508804.7	0.095	0.095	1.178
1.579	1.58	69.157	68.702	68.799	6.662	1.13	508582.4	0.094	0.095	1.178
1.58	1.58	69.229	68.812	68.836	6.665	1.127	508603.7	0.094	0.095	1.178
1.58	1.58	69.226	68.825	68.865	6.659	1.128	508072.9	0.094	0.095	1.178
1.581	1.58	68.971	68.695	68.746	6.651	1.227	507758.7	0.095	0.095	1.178
1.58	1.58	69.006	68.772	68.748	6.652	1.093	507672.0	0.094	0.095	1.178
1.579	1.58	69.013	68.71	68.752	6.656	1.112	508087.2	0.094	0.095	1.178
1.58	1.58	68.939	68.679	68.727	6.666	1.139	508873.5	0.094	0.095	1.178
1.542	1.579	69.076	68.655	68.717	5.362	19.684	409395.1	0.109	0.095	1.178
1.423	1.573	69.143	68.679	68.798	1.424	25.991	108746.2	0.173	0.098	1.178
1.399	1.567	69.117	68.743	68.84	1.591	11.953	121447.2	0.147	0.099	1.178
1.398	1.561	69.144	68.764	68.787	1.703	11.215	130003.9	0.146	0.101	1.178
1.383	1.555	69.174	68.85	68.787	1.349	14.664	102946.3	0.129	0.102	1.177
1.361	1.547	69.169	68.81	68.798	0.787	22.439	60045.6	0.106	0.103	1.178
1.361	1.54	69.04	68.746	68.799	0.614	17.011	46856.6	0.101	0.103	1.178
1.357	1.533	69.175	68.739	68.833	0.412	12.584	31480.1	0.1	0.103	1.178
1.357	1.525	69.06	68.742	68.779	0.294	12.606	22426.4	0.099	0.103	1.178
1.356	1.518	69.037	68.678	68.774	0.245	11.145	18709.0	0.099	0.103	1.178
1.356	1.51	69.014	68.709	68.789	0.239	6.894	18221.5	0.099	0.104	1.178
1.357	1.503	69.019	68.659	68.788	0.228	16.23	17423.5	0.099	0.104	1.178
1.356	1.495	69.061	68.626	68.818	0.217	10.317	16535.3	0.099	0.104	1.178
1.355	1.488	69.036	68.646	68.878	0.199	5.386	15178.6	0.098	0.104	1.178
1.353	1.48	69.047	68.581	68.873	0.186	5.43	14170.0	0.098	0.104	1.178
1.355	1.473	69.109	68.644	68.807	0.179	2.561	13631.8	0.098	0.104	1.178
1.355	1.465	69.028	68.655	68.803	0.168	2.538	12838.2	0.098	0.104	1.178
1.355	1.458	69.083	68.731	68.818	0.164	2.467	12551.3	0.098	0.104	1.178
1.356	1.45	68.903	68.752	68.739	0.162	2.399	12391.9	0.098	0.104	1.178
1.355	1.443	68.945	68.861	68.76	0.163	2.421	12431.2	0.098	0.105	1.177
1.354	1.435	69.068	68.966	68.75	0.163	2.45	12455.5	0.098	0.105	1.177
1.353	1.428	69.221	69.19	68.79	0.164	2.463	12522.9	0.099	0.105	1.177
1.355	1.42	69.064	69.146	68.804	0.165	2.409	12582.2	0.098	0.105	1.177
1.355	1.413	69.132	69.29	68.821	0.166	2.48	12613.3	0.098	0.105	1.176
1.356	1.405	69.071	69.317	68.82	0.165	2.438	12582.4	0.098	0.105	1.176
1.355	1.398	69.226	69.516	68.832	0.165	2.403	12582.0	0.098	0.105	1.176
1.355	1.39	69.443	69.535	68.78	0.165	2.45	12533.9	0.098	0.105	1.176
1.353	1.383	69.5	69.527	68.813	0.164	2.424	12509.5	0.098	0.105	1.176
1.354	1.375	69.465	69.615	68.845	0.165	2.43	12519.3	0.098	0.106	1.176
1.355	1.368	69.377	69.553	68.738	0.165	2.415	12535.9	0.099	0.106	1.176
1.353	1.361	69.25	69.451	68.829	0.165	2.506	12569.2	0.098	0.105	1.176
1.356	1.359	69.199	69.533	68.819	0.167	2.556	12748.6	0.099	0.103	1.176
1.353	1.358	69.17	69.487	68.84	0.164	2.437	12462.1	0.098	0.101	1.176
1.355	1.356	69.142	69.532	68.852	0.164	2.47	12454.1	0.098	0.1	1.176
1.356	1.355	69.09	69.599	68.863	0.164	2.442	12516.3	0.098	0.099	1.176
1.355	1.355	69.022	69.494	68.847	0.164	2.436	12447.3	0.098	0.098	1.176
1.355	1.355	69.098	69.406	68.821	0.163	2.388	12390.7	0.097	0.098	1.176
1.354	1.355	69.147	69.354	68.767	0.162	2.369	12314.3	0.098	0.098	1.176
1.353	1.355	69.081	69.333	68.797	0.161	2.425	12285.4	0.098	0.098	1.176
1.354	1.355	69.014	69.459	68.79	0.162	2.481	12297.8	0.098	0.098	1.176
1.354	1.355	69.05	69.484	68.761	0.162	2.376	12307.7	0.098	0.098	1.176
1.354	1.355	69.208	69.611	68.769	0.162	2.331	12323.3	0.098	0.098	1.176
1.355	1.354	69.175	69.653	68.766	0.162	2.391	12331.2	0.097	0.098	1.176
1.355	1.354	69.262	69.738	68.843	0.162	2.391	12340.3	0.098	0.098	1.175
1.356	1.355	69.212	69.639	68.888	0.162	2.423	12302.3	0.097	0.098	1.176

1.356	1.355	69.008	69.555	68.805	0.162	2.376	12293.2	0.098	0.098	1.176
1.355	1.355	68.89	69.388	68.784	0.161	2.422	12287.0	0.098	0.098	1.176
1.355	1.355	69.076	69.371	68.811	0.162	2.389	12313.4	0.098	0.098	1.176
1.355	1.355	69.173	69.509	68.804	0.162	2.381	12321.0	0.098	0.098	1.176
1.355	1.355	69.016	69.326	68.749	0.161	2.377	12297.7	0.098	0.098	1.176
1.354	1.355	69.065	69.29	68.755	0.161	2.394	12289.8	0.098	0.098	1.176
1.353	1.355	69.131	69.315	68.767	0.161	2.38	12292.9	0.098	0.098	1.176
1.354	1.355	69.159	69.18	68.757	0.161	2.384	12277.5	0.098	0.098	1.177
1.354	1.355	69.296	69.178	68.828	0.161	2.46	12300.0	0.098	0.098	1.177

Average values for each setting depicted in Figure A.1.

Capacitec	Voltage	TC-1	TC-2	TC-3	Velocity	Tu%	Rex	Transducer	Voltage	Density
1.355745	1.42377	68.7878	69.159	68.652	0.16836	3.0854	12830.7	0.098344	0.101521	1.17671
1.581172	1.67770	68.8713	68.22	68.692	6.65726	1.1818	509036.1	0.095236	0.098290	1.17903
2.157178	2.06977	68.6999	67.607	68.644	11.9538	1.0660	916075.8	0.109428	0.108952	1.18044
2.225943	2.09850	68.4999	67.453	68.587	11.3592	5.0400	870981.8	0.105679	0.106264	1.18101
2.321666	2.29591	68.7611	68.378	68.647	11.6594	11.468	891072.4	0.112083	0.112208	1.17862
0.225426								-0.003108		
0.801432								0.011083		
0.870197								0.007334		
0.965920								0.013738		

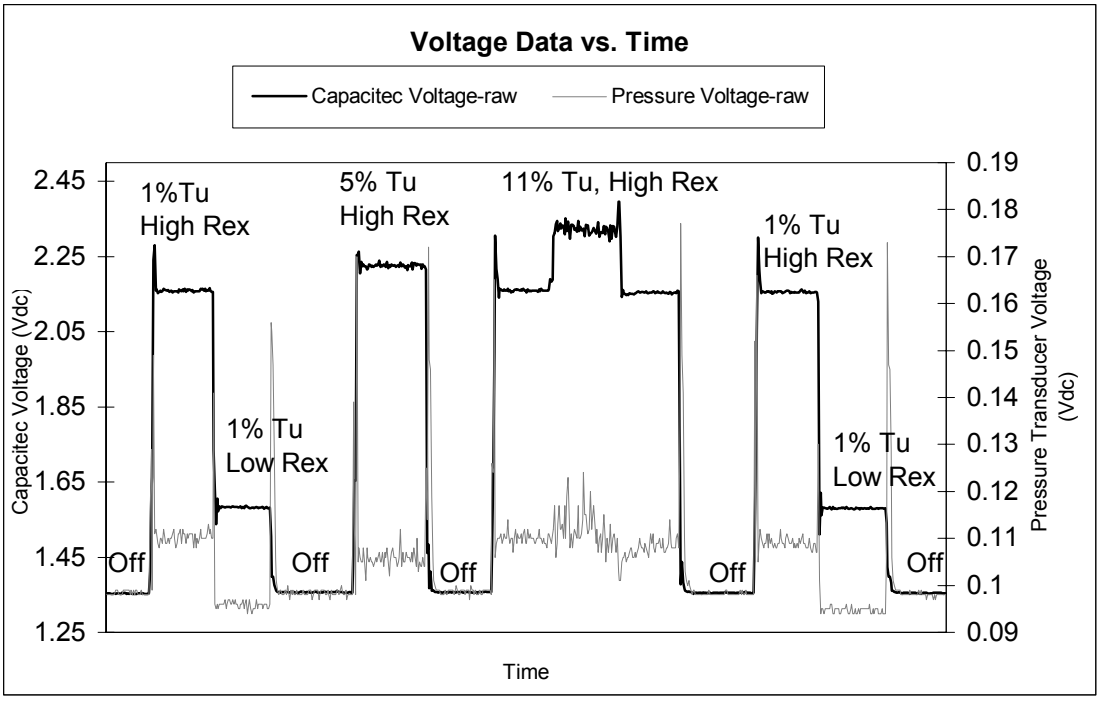

Figure A.1 Example Plot of Skin Friction Data

Appendix B: Error Analysis Data

	Precision Error	
Panel	**Re=500,000**	**Re=900,000**
Smooth	±10.58%	±12.51%
Erosion #1	±1.56%	±3.02%
Erosion #2	±7.95%	±9.13%
Fuel Deposits	±4.14%	±1.82%
Pitted	±0.96%	±1.78%
KS Erosion #2	±2.76%	±4.83%
TBC	±1.03%	±4.14%
TBCop	±1.58%	±3.31%

		Cf-new		(w*Cf-new)^2	
Source of Error	**Uncertainty,w**	**Re=500,000**	**Re=900,000**	**Re=500,000**	**Re=900,000**
Area-top	±0.50%	0.003310	0.003251	2.699E-10	2.604E-10
Area-side	±6.46%	0.003372	0.003277	4.742E-08	4.478E-08
Slope-Capacitec	±2.42%	0.003264	0.003193	6.241E-09	5.972E-09
Slope-Pressure Transducer	±0.25%	0.003328	0.003268	6.923E-11	6.673E-11
Hotwire	±0.05%	0.003322	0.003262	2.758E-12	2.661E-12
Capacitec	±0.01%	0.003327	0.003267	1.107E-13	1.068E-13
		Sum=		5.400E-08	5.108E-08
		Sqrt(sum)=		0.000232	0.000226
		Actual Readings=		0.003327	0.003267
		Bias Error=		**±6.9856%**	**±6.9176%**

Appendix C: Varying Statistical Parameters vs. Adjusted k_s

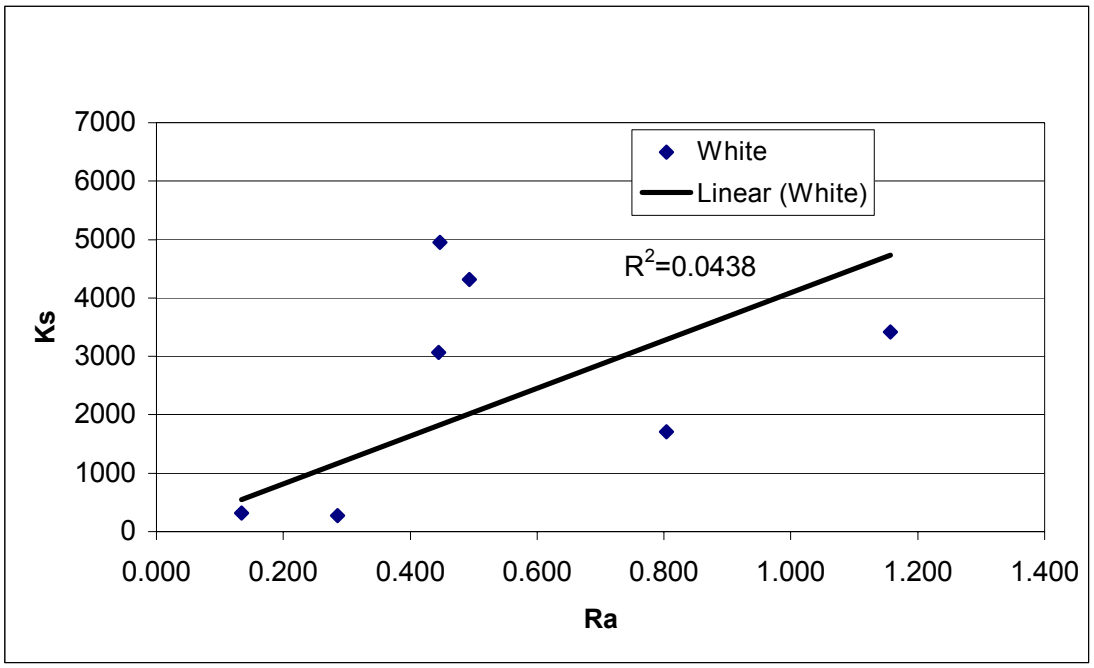

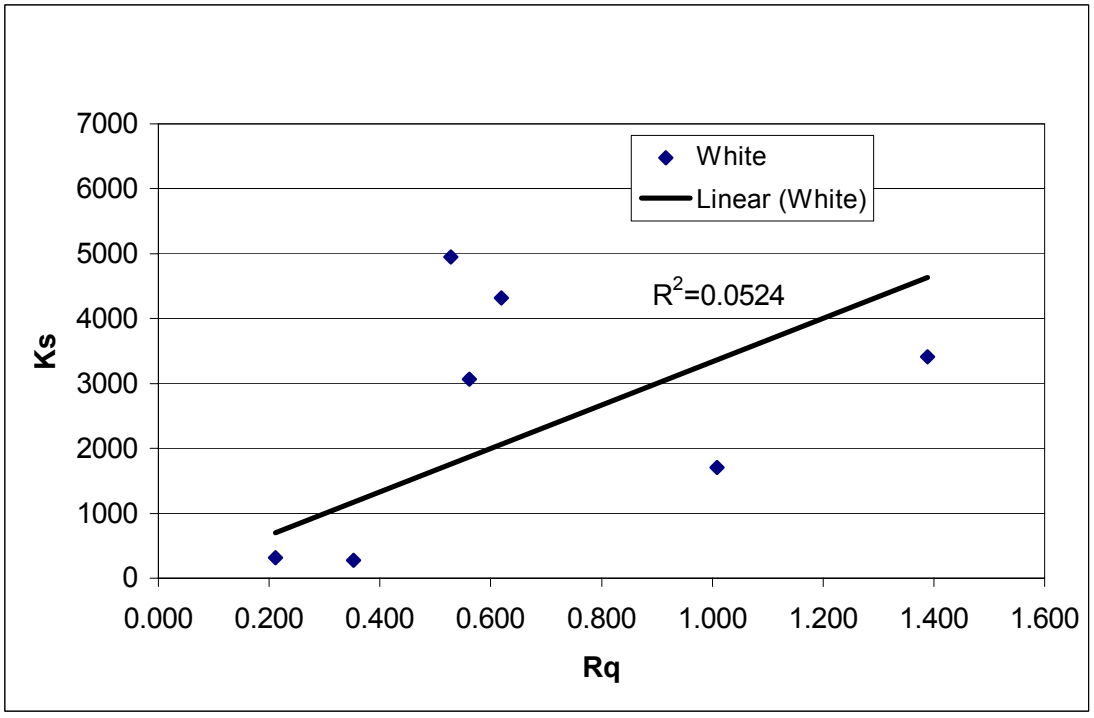

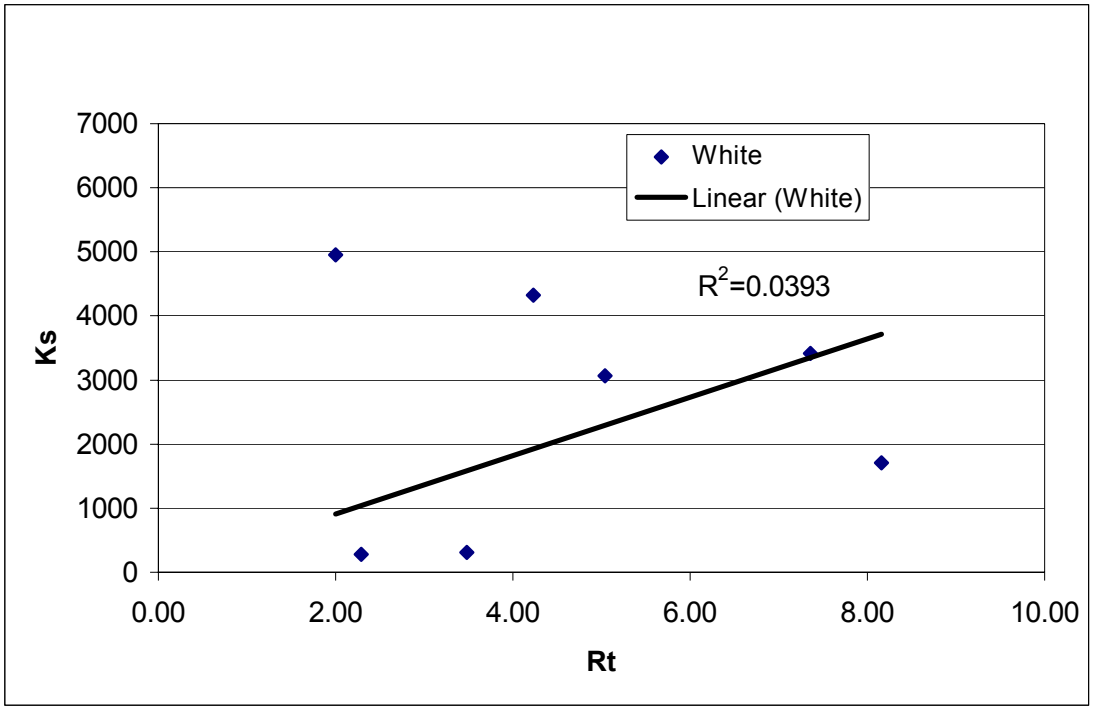
7000
6000
5000
4000
3000
2000
1000
0
Ks
0.00
2.00
4.00
6.00
8.00
10.00
Rt
White
Linear (White)
R2=0.0393

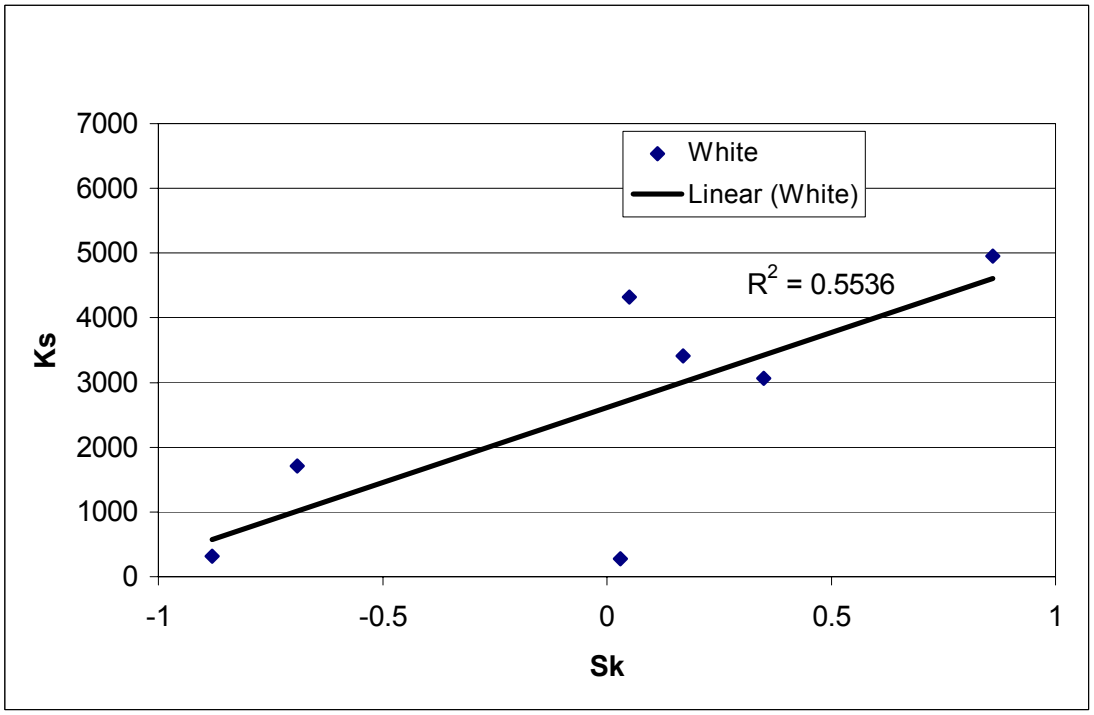
7000
6000
5000
4000
3000
2000
1000
0
Ks
-1
-0.5
0
0.5
1
Sk
White
Linear (White)
R2 = 0.5536

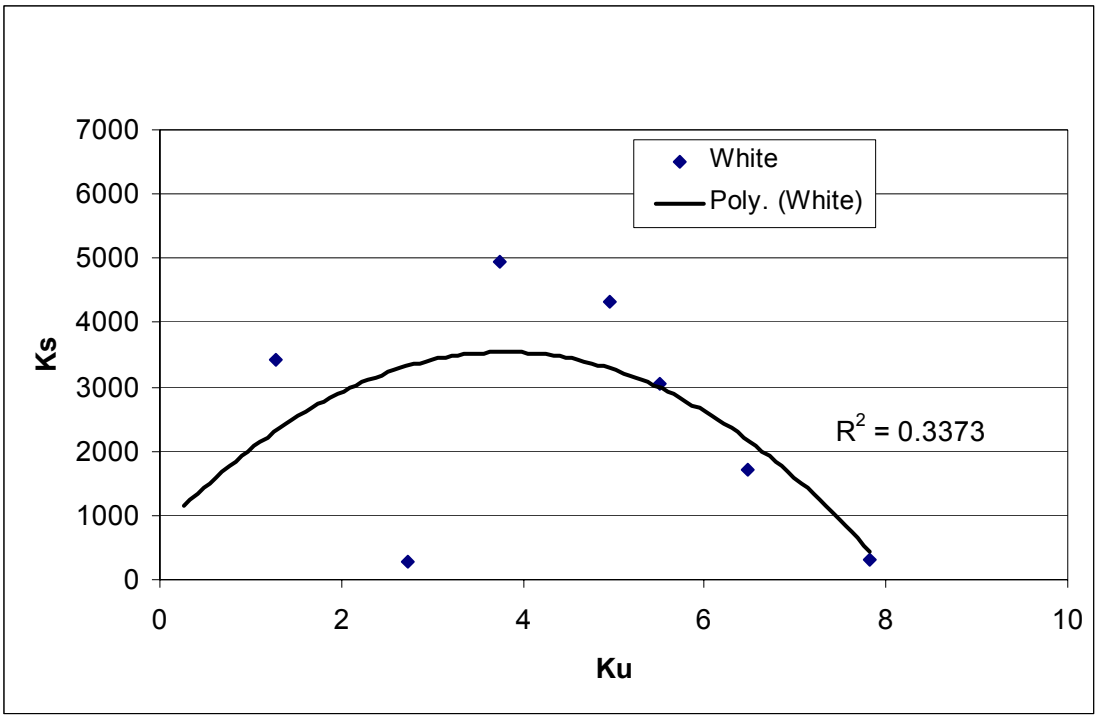
7000
6000
5000
4000
3000
2000
1000
0
Ks
0
2
4
6
8
10
Ku
White
Poly. (White)
R2 = 0.3373

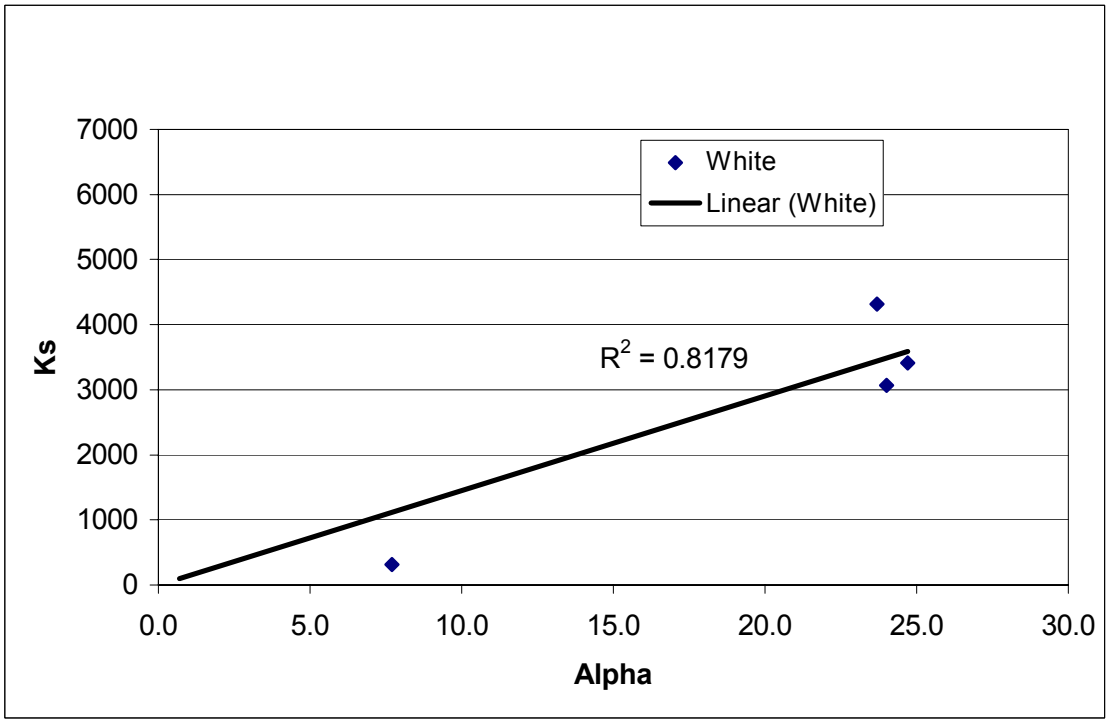
7000
6000
5000
4000
3000
2000
1000
0
Ks
0.0
5.0
10.0
15.0
20.0
25.0
30.0
Alpha
White
Linear (White)
R2 = 0.8179

Bibliography

Acharya, M., J. Bornstein, and M.P. Escudier. "Turbulent Boundary Layers on Rough Surfaces," *Experiments in Fluids*, 4: 33-47 (Spring-Summer 1986).

Bennett, Jean M. and Lars Mattsson. *Introduction to Surface Roughness and Scattering*. Washington DC: Optical Society of America, 1989.

Bogard, D. G., D. L. Schmidt, and M. Tabbita. "Characterization and Laboratory Simulation of Turbine Airfoil Surface Roughness and Associated Heat Transfer," *Journal of Turbomachinery*, 120:337-342 (April 1998).

Bons, Jeffrey P., Robert P. Taylor, Stephen T. McClain, and Richard B. River. "The Many Faces of Turbine Surface Roughness," *Journal of Turbomachinery*, 123:739-747 (October 2001).

Drab, Jess W. *Turbine Blade Surface Roughness Effects on Shear Drag and Heat Transfer*. MS Thesis, AFIT/GAE/ENY/01M-01. School of Aeronautical and Astronautical Engineering, Air Force Institute of Technology (AU), Wright-Patterson AFB, OH, March 2001 (AD-A390595).

Maciejewski, P. K. and R. J. Moffat. "Heat Transfer With Very High Free-Stream Turbulence: Part 1-Experimental Data," *Journal of Heat Transfer*, 114: 827-833 (November 1992).

Mathieu, Jean and Julian Scott. *An Introduction to Turbulent Flow*. Cambridge: Cambridge University Press, 2000.

Mills, Anthony F. *Heat Transfer*. New York: Irwin Press, 1992.

Pedisius, A. A., P. –V. A. Kazimekas, and A. A. Slanciauskas. "Heat Transfer from a Plate to a High-Turbulence Air Flow," *Heat Transfer-Soviet Research*, 11-5: 125-133 (September-October 1979).

Schlichting, Hermann. *Boundary Layer Theory* (7th Edition). New York: McGraw-Hill, 1979

Wheeler, Anthony J. and Ahmad R. Ganji. *Introduction to Engineering Experimentation*. New Jersey: Prentice Hall, 1996.

White, Frank M. *Viscous Fluid Flow* (2nd Edition). New York: McGraw-Hill, 1991.

Vita

2nd Lieutenant Christine P. Ellering was born and raised in Saint Cloud, MN. Upon graduating from Technical High School she entered undergraduate studies at the United States Air Force Academy in Colorado Springs, CO. She graduated in the top 15% of her class on 31 May 2000 with a Bachelor of Science in Mechanical Engineering and a Reserve Commission in the United States Air Force.

Her first assignment brought her to the Graduate Aeronautical Engineering program at the Air Force Institute of Technology, Wright-Patterson AFB, OH. Upon graduation she will be assigned to the National Air Intelligence Center, Wright-Patterson AFB, OH.

REPORT DOCUMENTATION PAGE

Form Approved
OMB No. 074-0188

1. REPORT DATE *(DD-MM-YYYY)*	2. REPORT TYPE	3. DATES COVERED *(From – To)*
26-03-2002	Master's Thesis	August 2000 – March 2002

4. TITLE AND SUBTITLE

THE COMBINED EFFECTS OF FREESTREAM TURBULENCE, PRESSURE GRADIENTS, AND SURFACE ROUGHNESS ON TURBINE AERODYNAMICS

5a. CONTRACT NUMBER

5b. GRANT NUMBER

5c. PROGRAM ELEMENT NUMBER

6. AUTHOR(S)

Ellering, Christine P., 2nd Lieutenant, USAF

5d. PROJECT NUMBER

5e. TASK NUMBER

5f. WORK UNIT NUMBER

7. PERFORMING ORGANIZATION NAMES(S) AND ADDRESS(S)

Air Force Institute of Technology
Graduate School of Engineering and Management (AFIT/ENY)
2950 P Street, Building 640
WPAFB OH 45433-7765

8. PERFORMING ORGANIZATION REPORT NUMBER

AFIT/GAE/ENY/02-5

9. SPONSORING/MONITORING AGENCY NAME(S) AND ADDRESS(ES)

Department of Energy, South Carolina Institute for Energy Studies (SCIES)
Attn: Dr. Richard A. Wenglarz
Advanced Gas Turbine Systems Research
386-2 College Avenue
Clemson, SC 29634-5711 (864) 656-2267

10. SPONSOR/MONITOR'S ACRONYM(S)

DOE

11. SPONSOR/MONITOR'S REPORT NUMBER(S)

12. DISTRIBUTION/AVAILABILITY STATEMENT

APPROVED FOR PUBLIC RELEASE; DISTRIBUTION UNLIMITED.

13. SUPPLEMENTARY NOTES

.

14. ABSTRACT

This work used scaled facsimiles of real turbine blade surfaces to characterize correlations between turbine blade roughness, freestream turbulence, pressure gradients and skin friction (C_f). Addition of roughness caused C_f to increase: up to 300% for the roughest surface. Addition of freestream turbulence resulted in 125% increase for the same surface. The combined effects showed increases up to 380%. Although decreasing roughness, freestream turbulence, and Reynolds number resulted in less dramatic results, it was concluded that the C_f increases due to combined effects were consistently higher than their corresponding sum of the parts. The combined effects of roughness and pressure gradients yielded inconclusive results, however, limited observations seem to corroborate the trends seen during zero pressure gradient tests.

15. SUBJECT TERMS

Skin Friction, Roughness, Freestream Turbulence, Pressure Gradients, Bulk Drag, Heat Transfer

16. SECURITY CLASSIFICATION OF:			17. LIMITATION OF ABSTRACT	18. NUMBER OF PAGES	19a. NAME OF RESPONSIBLE PERSON
a. REPORT	b. ABSTRACT	c. THIS PAGE	UU	99	Maj Jeffrey P. Bons, ENY
U	U	U			19b. TELEPHONE NUMBER *(Include area code)* (937) 255-3636, ext 4327

Standard Form 298 (Rev. 8-98)
Prescribed by ANSI Std. Z39-18

Form Approved
OMB No. 074-0188